Dynamometer Testing of Hydraulic Fluids in an Axial Piston Pump Under Simulated Backhoe Loader Trenching Conditions

by

Malik, Muhammad Hassan Mansoor

A Report Submitted to the Faculty of the

Milwaukee School of Engineering

in Partial Fulfillment of the

Requirements for the Degree of

Master of Science in Engineering

Milwaukee, Wisconsin

July 2022

Abstract

This report describes a Milwaukee School of Engineering (MSOE) Master of Science in Engineering (MSE) capstone project. This capstone project is part of an on-going investigation at MSOE's Fluid Power Institute (FPI) involving a dynamometer assembly that simulates the trenching duty cycle of an off-highway machine—in this case, a backhoe loader. The investigation was focused on testing the hypothesis that polymer enhanced hydraulic fluids mitigate deviations in system control, thereby improving the overall efficiency of the system. MSOE FPI is engaged in several investigations to understand the tribological aspects associated with the polymer enhancement of hydraulic fluids and its effects on system performance. These investigations include dynamic duty cycle tests, step tests, and ISO 4409 testing, which is the international standard for steady state testing as defined by the International Organization of Standardization (ISO). The investigations additionally feature ISO 8426 testing and Toet method testing – which determine the derived capacity of hydraulic fluid powered positive displacement pumps under steady-state conditions. Several hydraulic fluids, with different polymer compositions, were tested in the dynamometer assembly. The results of these tests solidified the repeatability and consistency of the test methods. Efficiency numbers from the dynamic tests were compared to the efficiency of the system in steady-state condition using ISO 4409 test methods. The results revealed that most of the system's response was determined by activity at the pump inlet. Further investigations were then focused on the pump's inlet. Some of the results suggested that the hydraulic fluid's viscosity and density play a role in determining the system's response. Moving forward, FPI plans to create and study RLC (resistance, inductance, capacitance) models of the pump's inlet in order to understand how the fluid properties effect the system's response.

Acknowledgments

This project would not have been possible without the help and guidance of the following individuals. Dr. Subha Kumpaty, the Program Director of the Milwaukee School of Engineering's (MSOE) Master of Science in Engineering (MSE) program. Dr. Kumpaty served as one of the co-advisors for this project. Dr. Kumpaty has been very accommodating with respect to the author's needs and was a great resource of information through the several courses he has taught in the author's MSE course of study. Paul Michael, the Manager of Tribology in MSOE's Fluid Power Institute (FPI). Paul has been a supervisor, an advisor, and a teammate to the author and has treated this capstone project as one of his own. Paul's knowledge in Fluid Power technologies and his expert guidance have been key to the completion of this project. Gary Shimek, Director of the MSOE Library. Gary served as a catalyst in helping the author finish the writing phase of this capstone project. Gary has been a wonderful resource of information to the author, providing expert guidance on how to structure the report, literature review, and with editorial and proofreading work. Lucas Garcia, Advanced Technologies Engineer at FPI. Lucas's technological expertise is second to none, and he has been a great help to the author, providing help with programming and troubleshooting problems in the dynamometer control. Dr. Mehdat Khalil, the Director of Professional Education and Research Development (PERD), and Tim Kerrigan, the Director of Fluid Power Institute, for teaching certificate courses on hydraulic fluid power that helped the author understand the fundamentals of hydraulic fluid power technology. Professor Kim Stelson, founding Director of the Center for Compact and Efficient Fluid Power (CCEFP), and Dr. Daniel Williams, Associate Professor in the Mechanical Engineering department at MSOE, for their assistance with the inlet modeling. Terry McCart, the Lab Manager at FPI. Terry has helped

set up the test stand used for this project and assisted the author with understanding the physical workings of the dynamometer. Moreover, Terry made working at FPI a pleasant and joyful experience. The author's colleagues at FPI, Jazil bin Shahid, Sean Kwasny, and Shriya Kalijaveedu. Finally, the author's friends and family, who have been an anchor of support throughout the project's journey.

The author would also like to pay tribute to Thomas Wanke, the Director of Fluid Power Industrial Consortium and Industrial Relations, who sadly passed away in June 2022. Tom personally invited the author to several fluid power conferences hosted by the National Fluid Power Association (NFPA), which aided the author with learning about and realizing the importance of advancing fluid power technologies.

Table of Contents

List of Figures

List of Tables

Nomenclature

C_n – Constant, where n is an integer (0,1,2,3…)

dt – Change in time

dx – Change in variable, where ‘x’ is any variable

D – Pipe Diameter

K – Bulk Modulus

L – Pipe Length

p – Pressure

Q – Flow

T – Torque

V_i – Displacement

β – Bulk Modulus

δ OR Δ – Change in

μ – Viscosity

ρ – Density

τ or Tc – Time Constant

ω – Rotational speed

Abbreviations

cc – Cubic Capacity

cSt – Centistoke

CFD – Computational Fluid Dynamics

f-OCP – Functionalized Olefin Co-Polymer

FPI – Fluid Power Institute

HP – Horsepower

ISO – International Organization of Standardization

LPM – Liters per Minute

mph – Miles per hour

MP or MP Dist. – Matrix Profile Distance Analysis

MSE – Master of Science in Engineering

MSOE – Milwaukee School of Engineering

N-m – Newton-meter

Nil – No Polymer Added

OCP – Olefin Co-Polymer

PAO – Polyalphaolefin

PIB – Polyisobutylene

PLC – Programmable Logic Control

PPE – Personal Protective Equipment

RPM – Revolutions per Minute

s – seconds (unit of time)

SB – Styrene Butadiene

VM – Viscosity Modifier

Introduction

The Milwaukee School of Engineering (MSOE) Master of Science in Engineering (MSE) capstone design project described in this report concerns the use of several compositions of polymer-enhanced hydraulic fluids in a dynamometer assembly that simulates the working of a backhoe loader, in its trenching and side-loading operations, at MSOE's Fluid Power Institute [1] (FPI) facility. The Fluid Power Institute is a research facility that has laboratories at the MSOE campus and at Chase Commerce Center on the south side of Milwaukee. These facilities are equipped with testing cells that include a wide variety of hydraulic components that are capable of operating under high pressure and flow conditions, allowing for in-depth testing and analysis solutions under expert supervision.

At the heart of this project is the dynamometer assembly, located in the on-campus research center laboratory at MSOE. A dynamometer is a device that is used for measuring the torque and braking power that is required for the running of driven machinery, i.e., a machine that provides energy to a fluid. There are two types of dynamometers [2]:

- Power Absorption Dynamometer: Power absorption dynamometers are the type of dynamometers that absorb and measure the output power of the engine that is coupled with the machine. The power that is absorbed is dissipated as heat energy.
- Power Transmission Dynamometers: Power transmission dynamometers transmit controlled power to the load that is coupled with the engine. Torque meters are typically used to control the power transmission.

Of the various types of power absorption dynamometers, the dynamometer assembly at FPI is a hydraulic dynamometer, which means that it uses hydraulic oils as a means of providing the driving force and power to the dynamometer. Hydraulic oils are used as the conventional industry standard fluid for hydraulic systems, as compared to water, which was used in early machines. This is because hydraulic oils are capable of performing at higher efficiency rates when compared to water. This is due to the viscosity of water being much lower than that of hydraulic fluids. A lower viscosity means that systems that use water as the driving force are more prone to leakage through the gap heights [3]. Moreover, water cannot be used for testing at high temperatures as it can introduce steam into the system. Steam being a form of gas, which is a compressible fluid, lowers the driving power of the system and can also cause turbulence in the system along with other barriers like cavitation, corrosion and lack of lubrication. Leakage and turbulence are sources of inefficiency in systems that use fluids to provide power.

While using fluids with higher viscosity reduces leakage, after a certain viscosity threshold, high viscosity fluids are inefficient at maneuvering through elbows and bends in the hydraulic line(s), creating turbulence. To tackle the problem with fluid motion in the hydraulic line and to analyze its effect on system efficiency, fluids formulated using polymer additives, also known as Viscosity Modifiers (VM's) were used for this project. Viscosity modifiers change the physical properties of the fluids in critical shearing zones [4] within the system by changing the molecular formation of the fluid. The combination of hydraulic oils and viscosity modifiers used for this project are listed in the background section of this report along with the physical properties of the fluids. Figure 1 shows the difference between using formulated fluids in comparison to non-formulated fluids in the system.

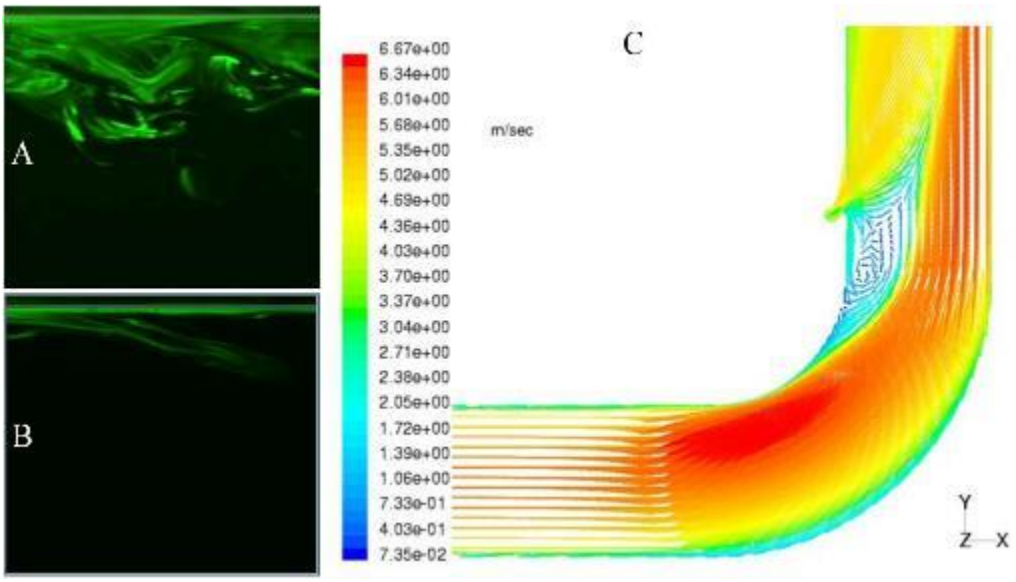

Figure 1 - Viscosity Modifier Effect on Fluid Flow in Pipes [5].

In Figure 1,

(A) Turbulent mixing along the pipe wall;

(B) Drag reduction by polymer additives;

(C) Computational Fluid Dynamics (CFD) model showing how secondary flows create restrictions in elbows and bends.

Turbulence in fluid flow can also cause cavitation, which is the formation of bubbles in the liquid. This phenomenon can result in accelerated wear and tear of the machinery and is highly undesirable [6]. Polymer induction in fluids increases the continuity of the flowing liquid, making the flow more laminar, which reduces one of many sources of cavitation in the system and increases machine life. This methodology is also being used in industry where fluid flow is fundamental.

Pressure ripples in fluid flow are another form of turbulence which is being studied by industry and research academics to understand its negative effects on hydraulic system efficiency [7, 8]. Pressure ripples are disadvantageous to the machine as they cause vibrations and fluid noise, which can add mechanical stresses to the pump components in the dynamometer assembly.

The dynamometer assembly used for this project consists of a variable displacement axial piston pump which uses a precision-controlled swashplate. A variable displacement swashplate varies its position (angle) to control the displacement (pushing of) of the fluid, as per test requirements using sensors. Testing is controlled by setting various system parameters to simulate the working of backhoe loader duty cycle. The duty cycle characterization was accomplished using Matrix Profile Distance (MP Dist.) analysis [9].

Matrix Profile analysis of the backhoe loader trenching and side loading operation allowed the simulation of the duty cycle under dynamic conditions in a laboratory setting. This process was key to this project as most of the documented testing procedures define testing under steady state conditions. Therefore, a comparison of dynamic and steady state test results was made possible.

A unique aspect of this test assembly was that viscosity and density sensors were installed in the inlet line of the dynamometer pump. This, to the author's knowledge and research, has not been practiced in other research work or in the industry. The data collected from the sensors gave valuable information about the response of the system, which will be explained further in this report.

The Venn diagram in Figure 2 shows the scope of this capstone design project, which features three areas, including Fluid Formulations, Dynamic and Steady-State Duty Cycle Testing,

and Inlet Line Influence. In order to analyze the response of the dynamometer system to the various fluid formulations under dynamic and steady-state test conditions and identifying the inlet's influence on system response, a significant level of expert knowledge and technical expertise in the fields mentioned was required. The research team at FPI along with professors at MSOE were a valuable resource for the completion of this project.

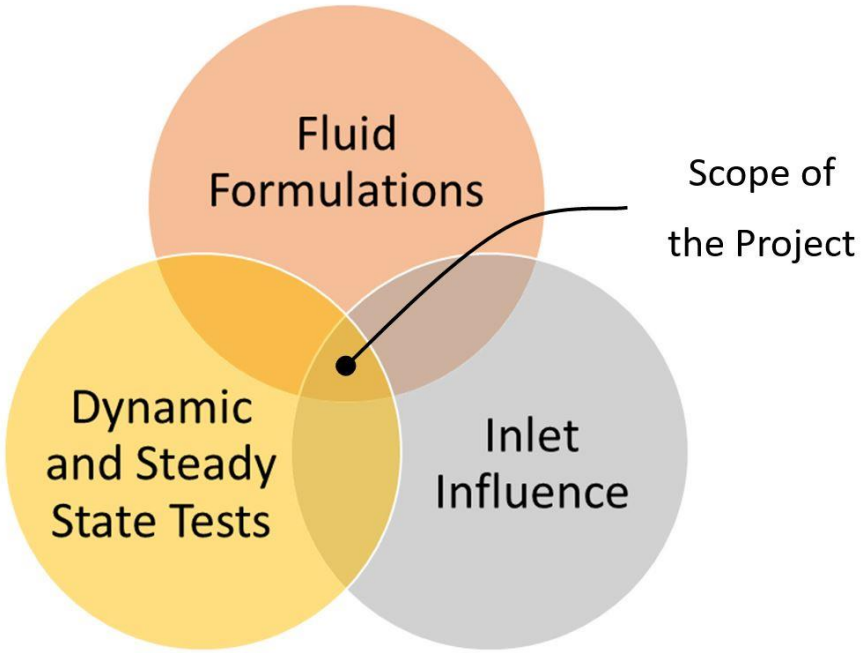

Figure 2 - Scope and Focus of this Project.

The remainder of this capstone project report is organized as follows. In the Background section, the motivation and justification for carrying out this research is provided in detail. Moreover, the backhoe loader and its trenching duty cycle simulated in the dynamometer and the algorithm used for the characterization of the dynamic duty cycle is described. Furthermore,

technical information on the dynamometer assembly, the variable displacement axial piston pump with precision swashplate, and the polymer-enhanced fluids used in testing for this project are discussed. The Background section is followed by the Methods and Methodology section of the report, which explains how the testing was conducted. Technical details about the testing methods used are offered, which include dynamic and steady-state Duty Cycle tests, Toet tests, Step Response tests, as well as the simulation of the inlet line, which was done in MATLAB Simulink. Next, the Results and Discussion section details the key findings from the data analysis of the test results. Finally, the Conclusions and Recommendations for future work are outlined.

Background

Project Motivation and Justification

The Environmental Protection Agency (EPA) provides information about fuel economy in passenger vehicles using data collected from the driving duty cycles on city roads, highways, as well as in rural areas [10]. When comparing passenger vehicle gas mileages on city roads to mileages on the highway, it is evident that the fuel economy on highways is much greater than that on city roads. Figure 3 and Figure 4 show speed versus time graphs for the driving duty cycle that the EPA uses to calculate the average mileage a vehicle achieves on city roads and on highways, respectively.

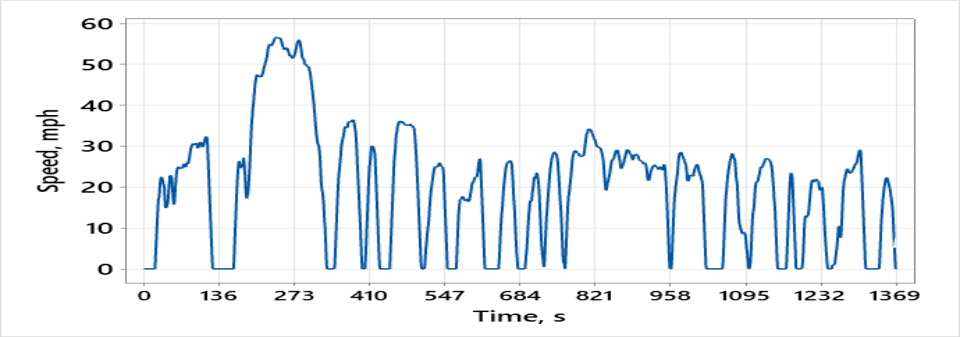

Figure 3 - City Driving Cycle Used by the EPA [10].

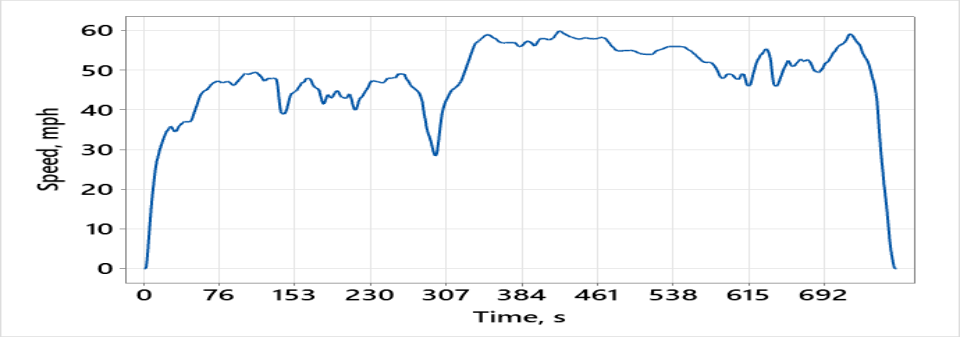

Figure 4 - Highway Driving Cycle Used by the EPA [10].

Figure 5 shows a comparison of two average consumer vehicles of the same make and model, differing in engine size. The vehicles used for the comparison were a 2022 Chevrolet Malibu, one having a 1.5-liter engine, while the other having a 2.0-liter engine. Both vehicles had a turbo engine, four cylinders, and automatic transmission. From this comparison, it can be approximated that, with respect to gas mileage, the engine performance is up to 24 to 50% more efficient on highways than on city roads. This efficiency range is subject to the author's research, which involved the comparison of several vehicles of different makes and models from the EPA database.

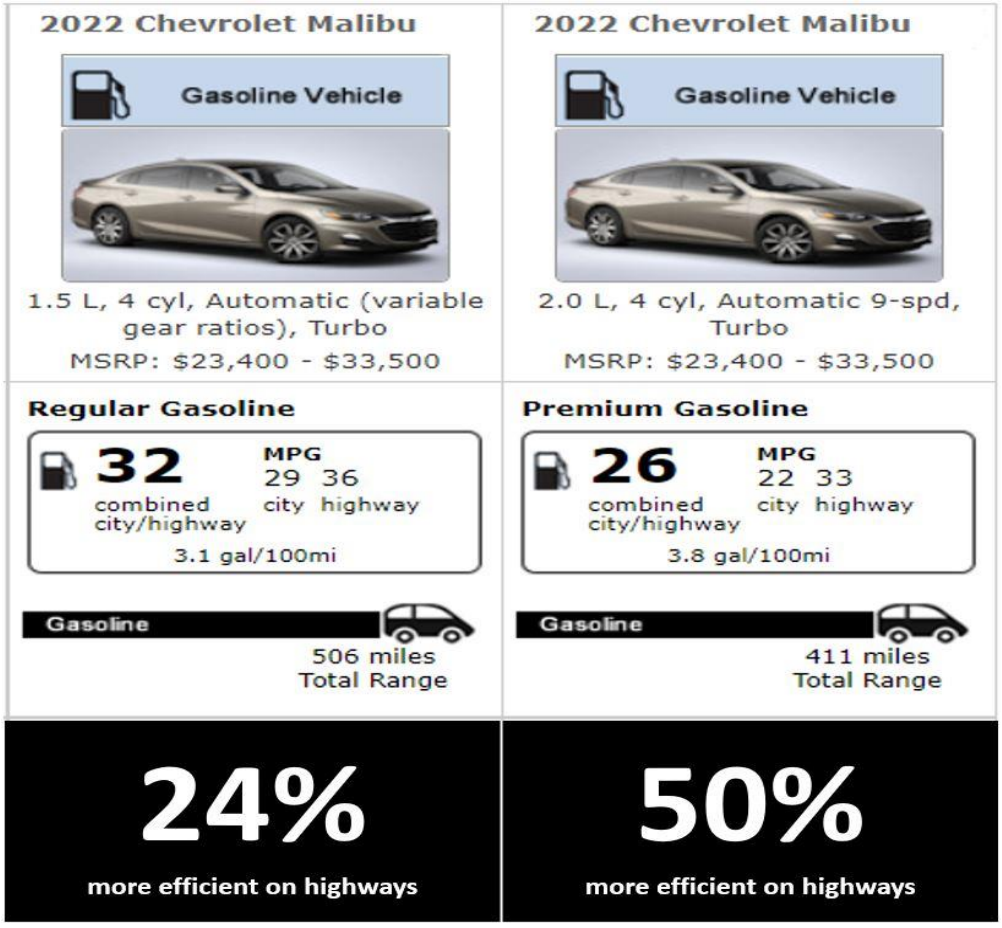

Figure 5 - Comparison of Two Average Consumer Vehicle Gas Mileages [10].

The difference in fuel economy, along with factors such as air resistance and road conditions, is mostly due to the frequent braking and accelerating of the vehicle in heavy traffic, at stop signs, and at traffic lights, which is common on city roads [11]. In contrast, highway driving is steadier, with little variations in speed and longer durations of travel at constant speeds. This comparison served as an analogy to study the difference between dynamic and steady-state tests performed on the dynamometer. It was hypothesized that the difference in efficiencies between dynamic and steady-state tests would be comparable to the difference in engine performance between city and highway driving duty cycles, with respect to gas mileages.

The current International Organization for Standardizations (ISO) test methods are only defined for steady-state testing. Therefore, the aim of this project was to investigate ways in which the overall efficiency of an industrial hydraulic machine performing under dynamic testing conditions can be analyzed. Real-world operations are dynamic in nature and much more complicated to study as a whole. This study attempts to build a bridge between dynamic and steady state data sets and compare them side by side in order to find patterns which present opportunities for potential improvement.

To execute this study, the trenching and side loading operation of a backhoe loader, shown in Figure 6, was used. A typical backhoe loader duty cycle, digging a 4-foot deep, 2-foot wide, trench spread over a length of 50 feet, was analyzed using Matrix Profile (MP) analysis. Matrix Profile analysis [9] is a state-of-the-art method for finding patterns in the time series data of industrial machines and features the use of data mining to create a profile for the duty cycle of the machine.

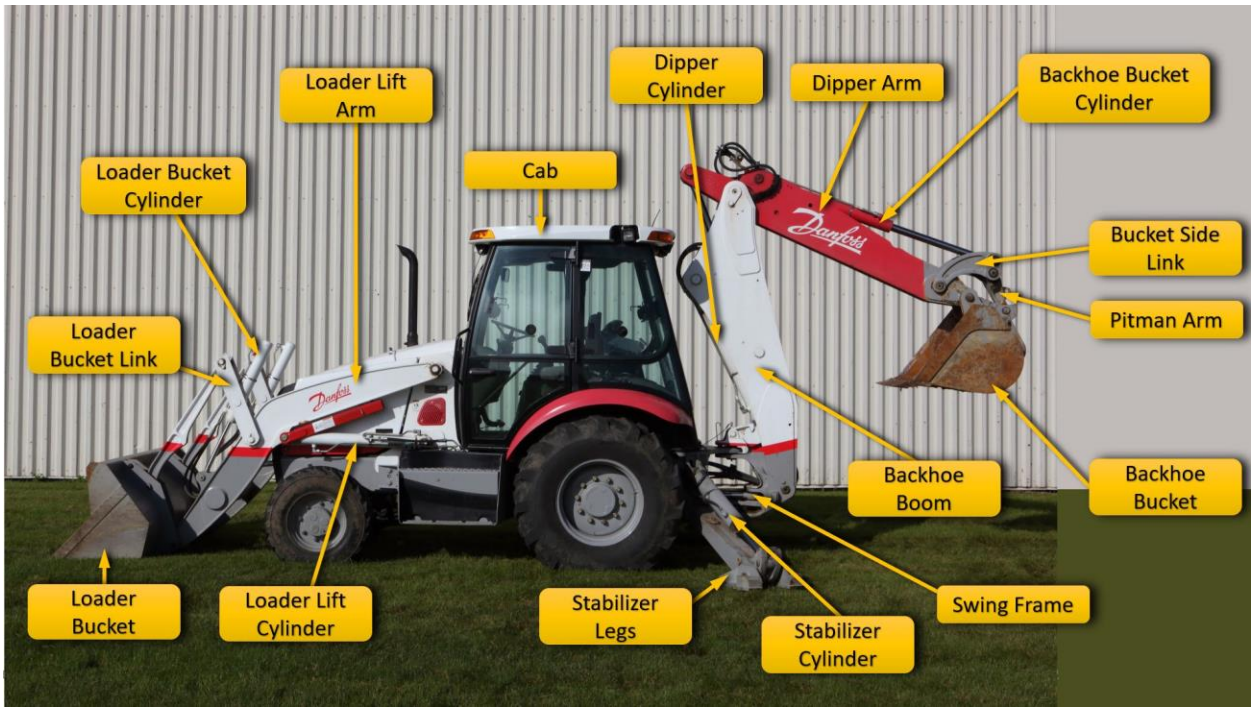

Figure 6 - Backhoe Loader Used for Trenching and Side Loading Operations [12].

MP analysis recognized patterns in the trenching operation and resulted in three 12-second characteristic curves for the dynamic performance of the motor speed, pump displacement, and pump outlet pressure. The use of MP analysis was ideal for this project as the pattern recognition algorithm used for this method mitigates the loss of data to curve smoothing. This is because the algorithm does not characterize small variations in the curve as noise, allowing for a more accurate replication of the dynamic duty cycle. Figure 7 shows the characteristic curves for speed, displacement, and pressure, obtained using MP analysis.

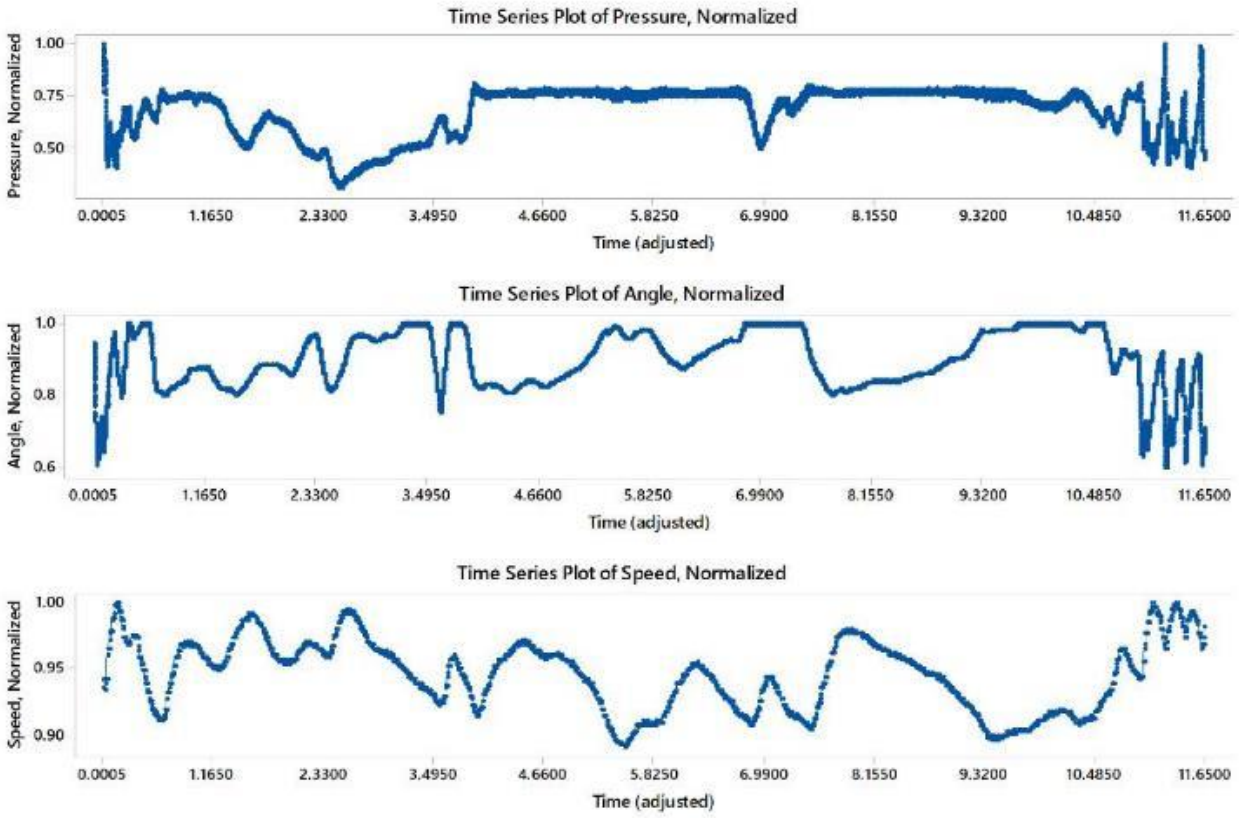

Figure 7 - 12-second Characteristic Profiles of Speed, Displacement, and Pressure.

The fluctuations recorded at the beginning the of displacement curve represent the initial movement of the bucket to dig the soil from the ground, while the fluctuations at the end of the displacement curve represent the bucket shake for the disposing of the collected soil. These patterns were recognized to identify one complete cycle of the trenching operation.

The characteristic profiles of speed, displacement, and pressure were used to program the dynamometer assembly, shown in Figure 8. The dynamic testing conducted on this test stand is a robust representation of a typical 12-second trenching duty cycle of the backhoe loader. Moreover,

the dynamometer can be programmed to perform test-point steady-state tests, step response tests and other test methods that require manual input commands by the test conductor.

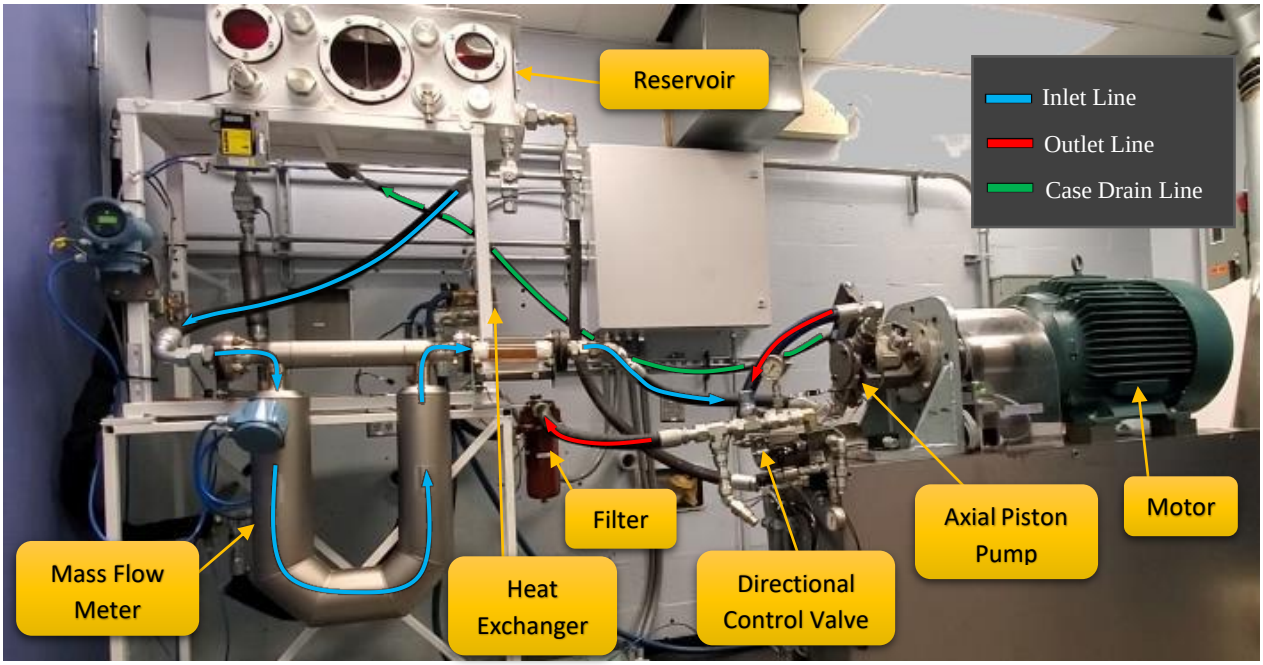

Figure 8 - Dynamometer Test Stand Assembly Used for Testing.

Figure 9 illustrates the circuit schematic of the test stand assembly. The dynamometer assembly was built in accordance with the standards set by ISO 4409 [13]. ISO 4409, “Hydraulic Fluid Power – Positive Displacement Pumps, Motors, and Integral Transmissions – Methods of Testing and Presenting Basic Steady State Performance”, is the international standard method defined by the ISO for assembly, testing of, and calculation of the efficiency of hydraulic equipment. Steady-state performance is assessed by measuring input torque and outlet flow at constant speed, displacement, temperature, and differential pressure.

As can be seen in the circuit schematic, the test assembly has measured and controlled variables. The controlled variables (shown in green) are speed, inlet temperature, pump displacement, and outlet pressure. The measured variables (shown in blue) are torque, inlet pressure, pump outlet temperature, outlet flowrate, case drain flowrate and mass flowrate.

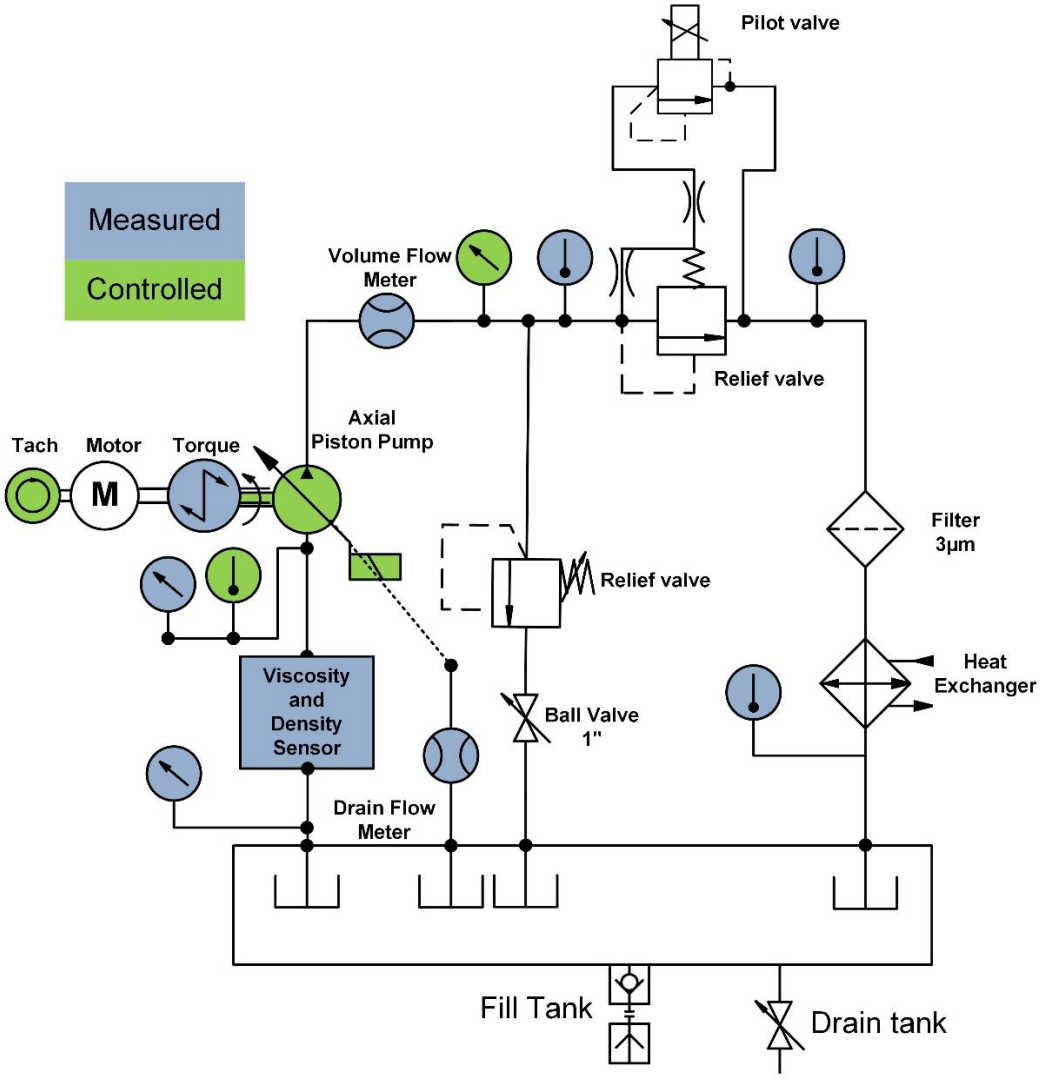

Figure 9 - Circuit Schematic of the Dynamometer Assembly.

The dynamometer consists of a 46cc variable displacement axial piston pump with an electronic swashplate control as shown in Figure 10.

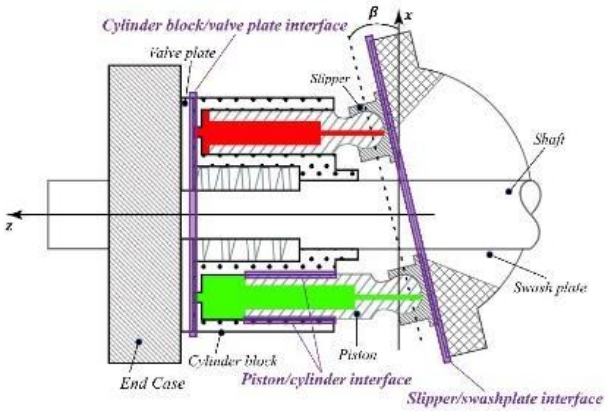

Figure 10 - Axial Piston Pump with Swashplate [14].

A swashplate piston pump is used to translate the motion of a rotating shaft into the reciprocating motion of a piston. The position and angle of the swashplate determine the movement of the pistons in the cylinder block, the fluid intake at the inlet, and the fluid deposited at the outlet.

The pump assembly has some lubricating gaps where frictional losses can be observed at certain shear rate ranges of hydraulic fluids. As Panwar *et al.* observe, "For hydraulic fluids formulated with polymer additives, the critical shear rate is a function of the molecular weight and concentration of the polymers" [15]. Mainly, friction occurs in the gaps which exist in the following interfaces (highlighted in purple in Figure 10):

- Piston/Cylinder Interface
- Slipper/Swashplate Interface

- Cylinder block/Valve plate Interface

The lubricating gaps in these areas of the axial piston pump are the main source of power loss in machines run with this axial piston pump [16]. Table 1 shows the gap heights and the shear rate ranges measured at these lubricating gaps:

Table 1 - Gap Heights and Shear Rate Ranges at Lubricating Gaps [15].

Lubricating Gaps	**Gap Height** [μm]	**Shear Rate Range [1/s]**
Piston/Cylinder	5.0-8.0	$9 * 10^4 \ to \ 5 * 10^5$
Slipper/Swash plate	7.0-25.0	$8 * 10^4 \ to \ 1 * 10^6$
Cylinder/Valve plate	0.9-2.1	$1 * 10^6 \ to \ 9 * 10^6$

It can be concluded that the critical shear rate range in the pump is 10^4 to 10^7 1/s. A tool has been developed for formulating hydraulic fluids that predict the critical shear rate of the oil based on the polymer molecular weight and base oil composition.

Each formulation of the fluid has a different concentration and type of Viscosity Modifier (VM) in its molecular chemistry. These VMs result in varying performance factors in the machine. PIB (polyisobutylene), PAO (polyalphaolefin), f-OCP (functionalized olefin co-polymer), OCP (olefin co-polymer), and SB (styrene-butadiene) polymers were used to formulate the fluids selected for this study. The selected formulations enable the effect of fluid viscosity to be isolated and show very low viscosity losses [15].

Table 2 shows the polymers used for the formulations of the hydraulic fluids, along with their physical properties.

Table 2 - Polymer Enhanced Fluids Used for Testing with Their Physical Properties.

Fluid ID	46	75	100	125
Base Oil Type	Mineral	PAO	Mineral	Mineral
Base Oil Group	II	IV	III	II
Polymer	f-OCP	PIB	OCP	SB
Viscosity Index	102	184	161	162
Kin Vis 40 °C, cSt	45.4	76.8	99.9	125.7
Sheared Vis 40 °C, cSt	44.2	73.1	77.1	76.9
Vis Loss, %	2.64	4.90	22.84	38.81
Density, g/ml 15 °C	0.8669	0.8328	0.8510	0.8622

Fluid identification numbers (46, 75, 100, and 125) have been assigned to the tested fluids in accordance with their kinematic viscosity measured at 40 °C. The kinematic viscosity of a fluid is described as the ratio of the shear stress to shear strain, divided by the density of the fluid. ISO 3104, “Petroleum products — Transparent and Opaque Liquids — Determination of Kinematic

Viscosity and Calculation of Dynamic Viscosity", defines the international standard to determine the kinematic viscosity of oils and states that the calculation is to be conducted at 40 °C [17].

The sheared viscosity of the fluids was also measured using the ISO 3104 standard. Sheared viscosity refers to the calculation of the fluid's viscosity after running the fluid through one or multiple break-in procedure(s). The break-in procedure is performed at maximum displacement of the pump at high pressure and speed settings for several hours, which applies high shear stresses on the fluids. Under high shear stress, the molecular structure of the fluid polymers is stretched, resulting in reversible and irreversible viscosity loss. Irreversible or permanent viscosity loss, also known as shear thinning, occurs when the polymer structure breaks due to the high shear stress. After a certain point, further shear thinning is no longer observed in the fluids. Fluids are then considered to have reached shear stability. Figure 11 shows the viscosities of the test fluids in their initial states and after reaching shear stability.

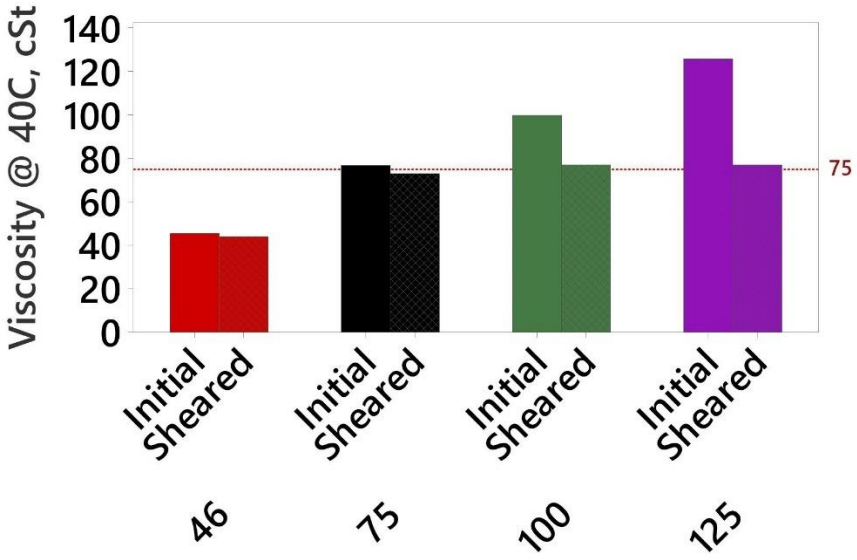

Figure 11 - Initial and Sheared Viscosities of the Test Fluids.

Fluids 46 and 75 show very little shear thinning with a viscosity loss of 2.64 and 4.90%, respectively. Fluids 100 and 125, on the other hand, exhibited a higher level of permanent viscosity loss. Fluid 100 reached shear stability after a viscosity loss of 22.84%, while Fluid 125 reached shear stability after a viscosity loss of 38.81%. It can be concluded that Fluids 46 and 75 have high shear stability in their initial states, while Fluids 100 and 125 do not. Moreover, Fluids 75, 100, and 125 reach shear stability at approximately the same level of viscosity, 75 cSt. The selection of these fluids was made in order to allow for a more comparable analysis of the test procedures.

The following section of the report explains how the testing was conducted. Technical details about the testing methods used are offered, which include dynamic and steady-state Duty Cycle tests, Toet tests, Step Response tests, as well as the simulation of the inlet line, which uses RLC (Resistance, Inductance, Capacitance) analysis, and is modeled using MATLAB Simulink. The theoretical models used for the inlet modeling are also detailed in the next section.

Methods and Materials

Testing conducted at FPI is performed under expert supervision. FPI employees must undergo annual safety training, such as Lock Out/ Tag Out (LOTO), and they are provided with a video catalogue that highlights the importance of safety protocols in the workplace. Along with safety training, Personal Protective Equipment, such as goggles, earmuffs and safety boots are supplied to students working for FPI before they are authorized to conduct testing in the laboratory. PPEs were worn by the author to ensure that safety requirements are met while the following tests were being carried out.

Calculating the Derived Displacement of the Pump

ISO 8426 Method

The ISO 8426 test method, "Hydraulic fluid power — Positive displacement pumps and motors — Determination of derived capacity" [18], is a quick method that provides reasonably useful results. It is a successor to the ISO standard method that was introduced and championed by Jim Bollinger in 1988 and withdrawn in 2007 [19]. According to the ISO 8426 method, the derived displacement can be found by calculating the ratio of the actual flow in the machine and the shaft revolution speed at which it is run. This method neglects the effects of cross-port leakages and some other factors to allow the flow and speed to have a linear relationship. This linearity then makes it feasible for testing to be held at a single speed while changes are made to pressure.

The tests were run at two different speeds, 1800RPM and 2400RPM, at 50°C and 80°C, giving four sets of data. Each set was tested at 11 different pressure settings ranging from 1000 to

3000 psi. The value of the derived displacement is defined to be the y-intercept of the pressure versus flow volume per revolution.

Toet Method

The Toet Method [19, 20, 21] was developed by Professor Gijsbert Toet from Eindhoven Technological University, Eindhoven, to find the derived displacement of the pump. The Toet Method takes into account the Couette effect in hydraulic fluids. The Couette effect [22] is defined as the shearing effect created by the flow of viscous fluid in the gaps between two surfaces in the machine which are moving at a tangent to one another. This effect was not taken into consideration in earlier methods before the introduction of the Toet Method. These gaps hold an importance as the friction-reducing lubricating film, within the pressure gaps, reduce wear in machine parts and increase the longevity of the machine. According to the Toet Method, the relationship between the shaft speed of a motor or pump has a high level of linearity with the effective flow volumetric flow rate. However, due to the Couette effect, the relation between flow and pressure results in a curved line in comparison to the completely linear relation suggested by ISO 8426 method, which takes a simplistic approach. This means that the derivative, with respect to shaft speed, of the volumetric flow rate should result in a constant, showing linearity [23]. The Toet Method requires the testing of pumps at five different shaft speeds, at different pressure conditions and at a constant temperature.

This study used the Toet Method tests to analyze the dynamometer at two different temperature settings, 50°C and 80°C.

Appendix A shows examples the command settings used for ISO 8426 and Toet test at 50 ℃ and 80 °C, as well as the tabulated results obtained from the test. Moreover, the command pressure and speed inputs used in the dynamometer assembly at both temperature settings are shown.

Dynamic Duty Cycle and Steady State

As mentioned in the background section of the report, the dynamometer assembly is programmed to perform several test methods, including dynamic duty cycle tests, step response tests, and test point steady state tests.

Instantaneous data recorded for these tests include the output power, torque, motor speed, case drain flowrate, mass flow rate, pump flow rate, outlet pressure, inlet pressure, fluid density, displacement, tank pressure, and temperature at the inlet and outlet of the pump.

Motor speed and torque are used to calculate the input power of the pump. The ratio of the output and input power is used to calculate the overall efficiency of the pump. Moreover, the derived displacement of the pump found by using the ISO 8246 and Toet methods are used to calculate the volumetric efficiency of the pump. Furthermore, the hydromechanical efficiency of the pump is calculated by dividing the overall efficiency with the volumetric efficiency.

A comparison of pump efficiencies obtained for dynamic and steady-state duty cycles is presented in the results section of this report.

Dynamic Duty Cycle Tests

The 12-second time series characteristic, developed through MP analysis, was split into 2397 data points at 0.005s intervals. The 0.005s time interval between test points allowed for a precise replication of the dynamic duty cycle with minimum data loss. The motor's rotational frequency, swashplate angle of displacement, and pump pressure served as input commands for the dynamometer to simulate the dynamic duty cycle.

Testing was conducted at two separate temperature settings, 50 °C and 80 °C. Therefore, it is necessary to warm up the test stand to run at each temperature setting. The warm-up procedure took about 20 minutes to reach the set temperature. Each dynamic duty cycle test resulted in 20 replications of the 12-second characteristic duty cycle.

Test Point Steady-State Tests

Steady-state testing was carried out by breaking the dynamic duty cycle into 583 data points. Each data point represents an instance of the 12-second operation and was run in the dynamometer for 15s at 0.005s intervals. The input command for each instance was held constant, allowing the dynamometer to stabilize at that setting. Data recorded for each test point consist of 2997 rows of data. Data collected for each instance was averaged out and plotted to represent the characterized trenching duty cycle under steady state.

Step Tests

A series of step tests were performed on the dynamometer to obtain a better understanding of the dynamic response of the pump. Step-up (zero to max) and step-down (max to zero) tests for

the pump pressure, motor speed, and swashplate displacement were performed. Similar to the other test methods mentioned above, step tests were conducted at 50 °C and 80 °C.

Two seconds of data were recorded for a single step response run. One complete test required five replications of the step response command in the dynamometer, resulting in 30 runs for each of the following tests:

- Pressure step up
- Pressure step down
- Speed step up
- Speed step down
- Swash step up
- Swash step down

The pump outlet flowrate and the input torque for these step tests were measured to determine the time constants for the machine components with each test fluid. Time constant is defined as the time taken for a step to reach 63.2% of its final position. This information is used to assess how quickly the system components respond to the input commands. For simplicity, the step response was studied as a first order control system [24].

Models for torque and flow were created for the purpose of studying the response of the dynamometer assembly. Models for both toque and flow were developed using the Latin Hypercube Sampling Method [25].

The torque model is represented by the following equation [25]:

$$T = C_o + C_1 \frac{(V_i)p}{2\pi} + C_2 \mu\omega(V_i) + C_3 \frac{\rho(V_i)^{\frac{5}{3}}}{4\pi}\omega^2 , \quad (1)$$

where

$$\frac{(V_i)p}{2\pi} \quad (2)$$

is the theoretical torque,

$$\mu\omega(V_i) \quad (3)$$

are the laminar losses, and

$$\frac{\rho(V_i)^{\frac{5}{3}}}{4\pi}\omega^2 \quad (4)$$

are the turbulent losses.

Figure 12 shows a comparison of the torque's response under standard steady-state conditions and under dynamic conditions. It is noteworthy that the dynamic response of the torque model follows the torque trend seen in the results for the steady state tests.

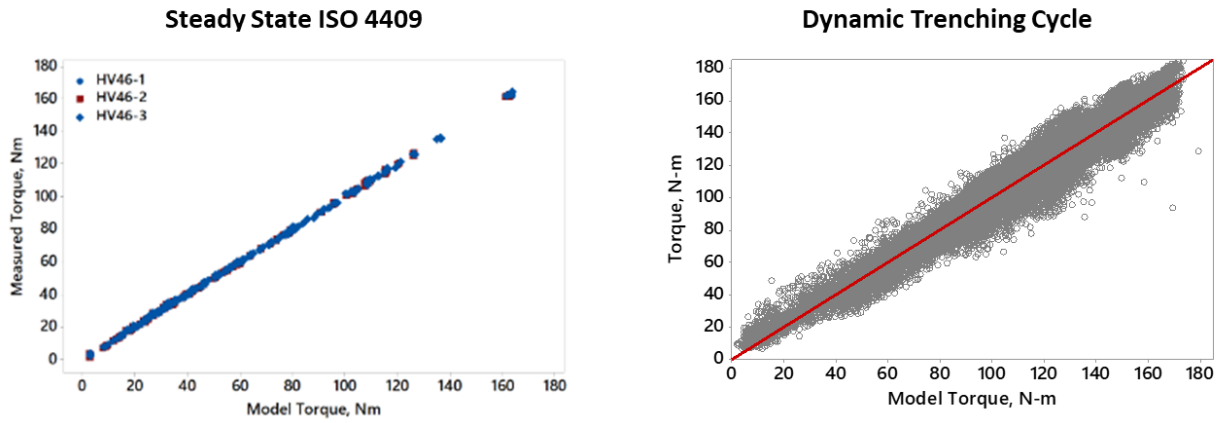

Figure 12 - Comparison of the Torque Model's Response Under Dynamic and Steady-State Conditions [25].

The flow model is represented by the following equation [25]:

$$Q = C_o + C_1(V_i\omega) + C_2\left(\frac{\omega(\delta p)}{K}\right) + C_3\left(\frac{\delta p}{\mu\omega}\right), \quad (5)$$

where

$$V_i\omega \quad (6)$$

is the theoretical flow,

$$\frac{\omega(\delta p)}{K} \quad (7)$$

are the compressibility losses, and

$$\frac{\delta p}{\mu\omega} \quad (8)$$

are the pressure-driven losses.

Figure 13 shows a comparison of the flow's response under dynamic and standard steady-state conditions. When compared to the torque's response, the dynamic response of flow does not follow the trend observed in steady state.

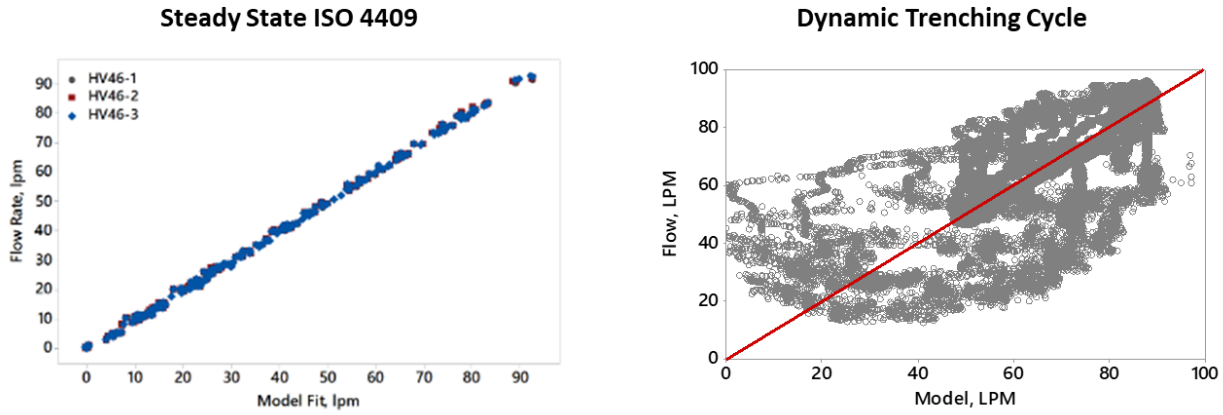

Figure 13 - Comparison of the Flow Model's Response Under Dynamic and Steady-State Conditions [23].

A first-order transfer function, $tf = \frac{1}{\tau s+1}$, with the time constant, $\tau = 65ms$, was applied to the dynamic model for flow. This approach helped improve the dynamic response of flow. The result of this application is shown in Figure 14.

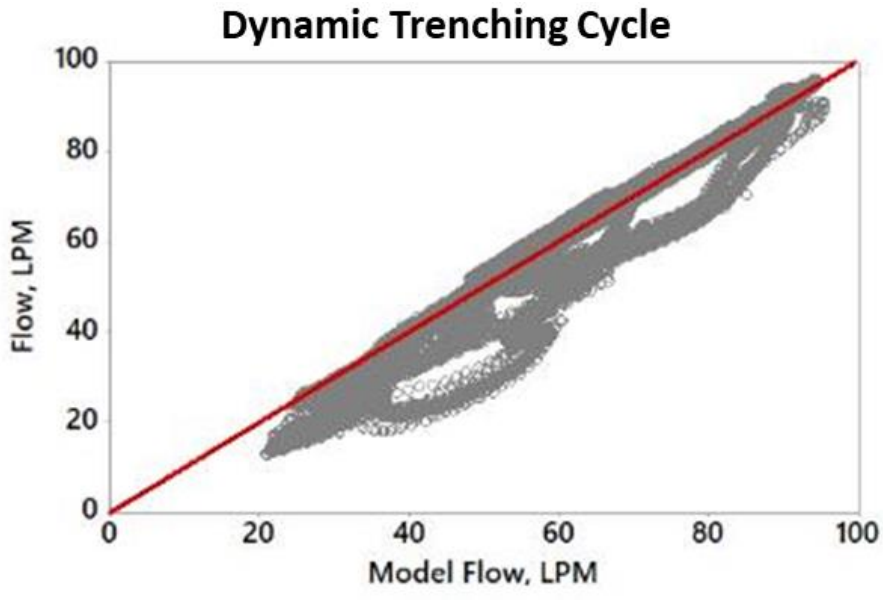

Figure 14 - Dynamic Flow Response After First-Order Time Constant Application [23].

The torque and flow models were used to characterize the step response tests conducted for this project. Furthermore, the pump outlet pressure, pump inlet pressure, and the pump outlet flowrate were measured to analyze the influence of the inlet line on the response of the system. The results of this analysis were used to build a model of the inlet line for further study.

Inlet Modeling

The following description of the methods used for modeling the inlet of the dynamometer is taken from a research paper submitted for approval to the American Society of Mechanical Engineers, for a symposium in the University of Bath, United Kingdom (ASME/BATH). The equations mentioned in this description were developed by Kim Stelson, Founding Director of the Center for Compact and Efficient Fluid Power (CCEFP), and co-author of the research paper [26].

In hydraulic circuit analysis, line losses are typically analyzed in steady state conditions, focusing on the relationship between flow and pressure drop. This analysis is useful for proper sizing of lines to avoid excessive power loss for the required flow. However, steady state analysis of lines does not provide insight into the dynamic effects hydraulic lines have on the transient nature of fluid power motion control systems. Under certain design and operating conditions, the dynamic pressure and flow responses are important factors that must be included in the analysis. Low pressure pump inlet lines, low flow load sense pressure lines, and large capacity power transmission lines are three examples where line dynamics are known to be important.

Lumped Model Approximation

In its most general form, a hydraulic line is a distributed system with time and position varying pressure and velocity. A detailed model can be constructed with Computational Fluid

Dynamics, CFD, but the resulting equations are computationally intensive. To facilitate understanding and simplify computations, a transmission line model is useful where the time varying flow and pressure is assumed to vary along the line length. This leads to an infinitely ordered system that can be described by transcendental transfer functions.

The modeling of transients in fluid lines for hydraulic power applications has been extensively studied [27]. To simplify the model, a lumped approximation may be used. In the simplest lumped approximation, fluid inertance I, fluid capacitance C, and fluid resistance R, are approximated for an entire line with the values $I = \frac{4\rho L}{\pi d2}$, $C = \frac{V}{\beta}$ and $R = \frac{128\,\mu\,L}{\pi\,d4}$, where μ is dynamic viscosity, L is length, d is diameter, ρ is density, β is bulk modulus and $V = pd2L/4$ is volume. I is constant. However, C or R may not be constant depending on whether or not the bulk modulus is constant in the case of C and whether or not the flow is Newtonian, laminar and fully developed in the case of R. Since viscosity is temperature dependent, the temperature must be fairly constant for the assumption to hold.

The model can be understood as an analog of an electrical circuit shown in Figure 15, where pressure replaces voltage as the effort variable and flow replaces current as the flow variable.

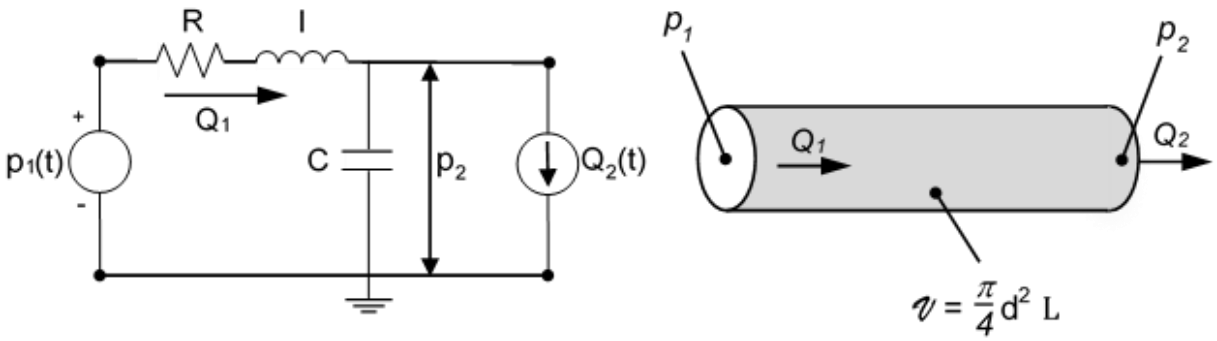

Figure 15 - Analogous Circuit for the Lumped Transmission Line Model [26].

Linear State Equations Model

The inputs to the model are the pressure p_1 on the left and the flow Q_2 on the right. The model is second order since there are two independent energy storage elements, *I* and *C*. Since the energy in *I* is a function of Q_1 and the energy in *C* is a function of p_2, Q_1 and p_2 are the states of the system.

A force balance on the fluid in the pipe gives the first state equation:

$$\frac{dQ_1}{dt} = \frac{1}{I}\,(p_1 - p_2 - RQ_1)\,. \tag{9}$$

The constitutive relation for the compliance gives the second state equation:

$$\frac{dp_2}{dt} = \frac{1}{C}\,(Q_1 - Q_2)\,. \tag{10}$$

The same equations can be derived from the analogous circuit using Kirchhoff's laws and the constitutive relations for *I*, *C* and *R*.

The state equations can be put in matrix form:

$$\begin{Bmatrix} \frac{dQ_1}{dt} \\ \frac{dp_2}{dt} \end{Bmatrix} = \begin{bmatrix} -\frac{R}{I} & -\frac{1}{I} \\ \frac{1}{C} & 0 \end{bmatrix} \begin{Bmatrix} Q_1 \\ p_2 \end{Bmatrix} + \begin{bmatrix} \frac{1}{I} & 0 \\ 0 & -\frac{1}{C} \end{bmatrix} \begin{Bmatrix} p_1 \\ Q_2 \end{Bmatrix}. \tag{11}$$

Using standard state-variable system analysis [28], this system yields four transfer functions between each of the two inputs and the two states. All of these transfer functions have the same denominator, the characteristic polynomial, $\Delta(s)$, given by

$$\Delta(s) = S^2 + \frac{I}{R}\,S + \frac{1}{IC}. \tag{12}$$

From the characteristic polynomial, the natural frequency, ω_n, and damping ratio, ζ, can be found:

$$\omega_n = \frac{1}{\sqrt{IC}}, \tag{13}$$

$$\zeta = \frac{R}{2}\sqrt{\frac{C}{I}}. \tag{14}$$

Nonlinear Models

In contrast to electrical circuits where the linearity assumption is accurate, nonlinearities can play an important role in hydraulic line dynamics. The line resistance might be linear or nonlinear, depending on the Reynolds number, and capacitance, existing as a function of the fluid bulk modulus, will generally not be constant. This is due to the way air in the liquid significantly influences how the effective bulk modulus changes with pressure.

For the purposes of numerical simulation, we can replace Equations (9) and (10) with nonlinear Equations (15) and (16):

$$\frac{dQ_1}{dt} = \frac{1}{I}\left(p_1 - p_2 - f(Q_1)\right), \tag{15}$$

$$\frac{dp_2}{dt} = g\,(Q_1 - Q_2)\,. \tag{16}$$

In Equation (15), the pressure loss term, RQ_1, is replaced with the nonlinear function $f(Q_1)$. In Equation (16) the capacitance term, $(Q_1\text{-}Q_2)/C$, is replaced with $g(Q_1 - Q_2)$. The resistance function, $f(Q_1)$, is generalized to include turbulent and transition flow conditions using the Moody chart [29], where the friction factor, f_D, is a function of Reynolds number. The friction factor is defined as:

$$\Delta p = f_D \frac{\rho V^2}{2}\frac{L}{D}\,. \tag{17}$$

For laminar flow, the friction factor is given by

$$f_D = \frac{64}{R_e}, \tag{18}$$

where the Reynolds number is given by

$$R_e = \frac{\rho V D}{\mu}\,. \tag{19}$$

Substituting Equation (19) into equation (18) gives the value of linear flow resistance, $R = 128\,\mu L/(\pi d^4)$.

In addition to the pressure loss in the line there are so-called minor losses due to flow transitions such as bends and fittings [30]. These are modeled using loss factors, which are a

generalization of the orifice equation for more complex shapes. Since the orifice equations neglect viscous loss, the minor loss equations will not include the influence of viscosity. The standard orifice equation [30]

$$V = C_d \sqrt{\frac{2\Delta p}{\rho}}, \tag{20}$$

where $V=Q/A_0$ is the average velocity across the exit of the orifice, Δp is the pressure drop, and C_D is the discharge coefficient.

Solving for Δp,

$$\Delta p = \frac{1}{C_d^2} \frac{\rho V^2}{2}. \tag{21}$$

Minor losses are modeled by replacing $1/(C_D)^2$ in Equation (21) with K, the so-called loss factor, where tables have been compiled of empirical loss factors for various transition shapes [30]. The resulting equation for Δp is

$$\Delta p = K \frac{\rho V^2}{2}. \tag{22}$$

Solving for Δp as a function of $Q_1 = VA_0$, where A_0 is the minimum area of the transition,

$$\Delta p = K \frac{\rho Q_1^2}{2A_0^2}. \tag{23}$$

Each of the minor losses can be summed to get the total loss. If there are flow reversals, Q_1 in Equation (23) must be replaced with $Q_1 sgn(Q_1)$ so that the sign of the pressure drop changes when the direction of flow changes.

There is extensive literature on effective bulk modulus theories where the influence of the compressibility of oil and air, and the expansion of the pipe are combined into a single parameter, the effective bulk modulus [31]. Including the air in the model is especially important in low-pressure studies. Assuming a rigid pipe, the function $g(Q_1 - Q_2)$ is formulated by replacing the constant bulk modulus in $C = \frac{V}{\beta}$ with the effective bulk modulus [30] using Equation (24):

$$\frac{1}{\beta_e} = \frac{1}{\beta} + \frac{V_g}{V}\frac{1}{\beta_g}, \tag{24}$$

where β_e is the effective bulk modulus, β is the liquid bulk modulus, β_g is the gas bulk modulus, V_g is the volume of gas, and V is the total volume. Since the transients are rapid, the gas is assumed to be ideal and adiabatic obeying the polytropic law, $p\ V_g^n$ = constant, with n = 1.4.

Following are the results and discussions for the test methods described.

Results and Discussion

ISO 8426 and Toet Method Tests

As mentioned in the previous section, the ISO 8246 and Toet Methods are used to find the derived displacement of the hydraulic pump. Table 3 shows the derived displacement obtained via the ISO 8426 method. The ISO 8426 method was carried out in two different motor speed settings, 1800 RPM and 2400 RPM. It is worth noting that the derived displacement at 50 °C, while the motor was running at 2400 RPM, was considerably lower than the values obtained at other test settings.

Table 3 - Derived Displacement of the Pump via ISO 8426 Method.

Temperature (°C)	50		80	
Speed (RPM)	1800	2400	1800	2400
Derived Displacement	47.17	40.39	47.29	45.43
	47.20	41.29	47.26	45.37

Table 4 illustrates the derived displacement of the pump calculated using the Toet Method. The Toet Method, in comparison to ISO 8426, tests the pump assembly at five different speed settings, 2400 RPM, 2000 RPM, 1600 RPM, 1200 RPM, and 1800 RPM, in the respective order. Moreover, the derived displacement was calculated using two methods that differed in their approach. Method 1 used the motor speed and pump pressure to obtain the derived displacement,

while Method 2 used motor speed, pump pressure, and the swashplate angle to determine the derived displacement of the pump.

Data recorded at 2400 RPM showed results that were inconsistent with the rest of the data. Therefore, outlier tests were performed on the collected data, resulting in the removal of five of the 100 test points in the dataset. The derived displacement for both, the unfiltered and filtered data, is shown in Table 4.

Table 4 - Derived Displacement of the Pump via Toet Method.

Temperature (°C)	50		80	
Test Point Count	100	95	100	95
Method 1	44.897	46.093	46.432	46.789
Method 2	44.951	45.822	46.314	46.466
Method 1	44.871	46.029	46.512	46.840
Method 2	44.873	45.750	46.411	46.533

The pump used in the dynamometer assembly is rated at 46CCs for fluid displacement. However, a more accurate representation of the pump displacement was required for the efficiency analysis of the dynamic and steady-state duty cycles. Using the results from the ISO 8426 testing and the Toet Method, a value of 45.786 was obtained for the derived displacement of the pump.

Plotted data used for the determination of the displacement with ISO 8426 testing and the Toet Method results are shown in Appendix A.

Dynamic Duty Cycle Tests

Dynamic duty cycle testing was performed on the four test fluids and the results were compared. Figure 16 and Figure 17 show the pump speed versus time and displacement versus time plots for the four fluids. Comparing the four fluids, it can be observed that all four fluids result in near identical traces for speed and displacement.

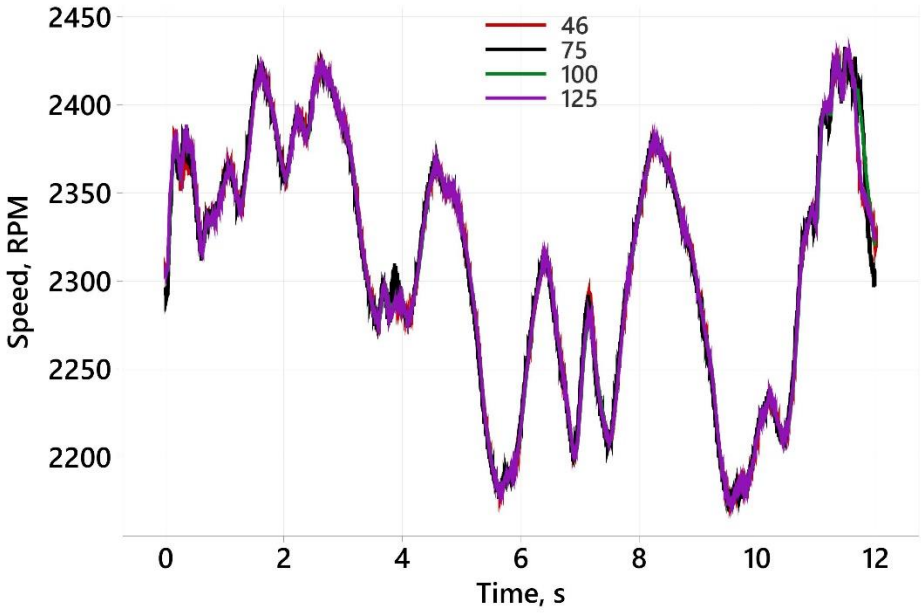

Figure 16 – 12-second Dynamic Speed Profiles for the Four Test Fluids.

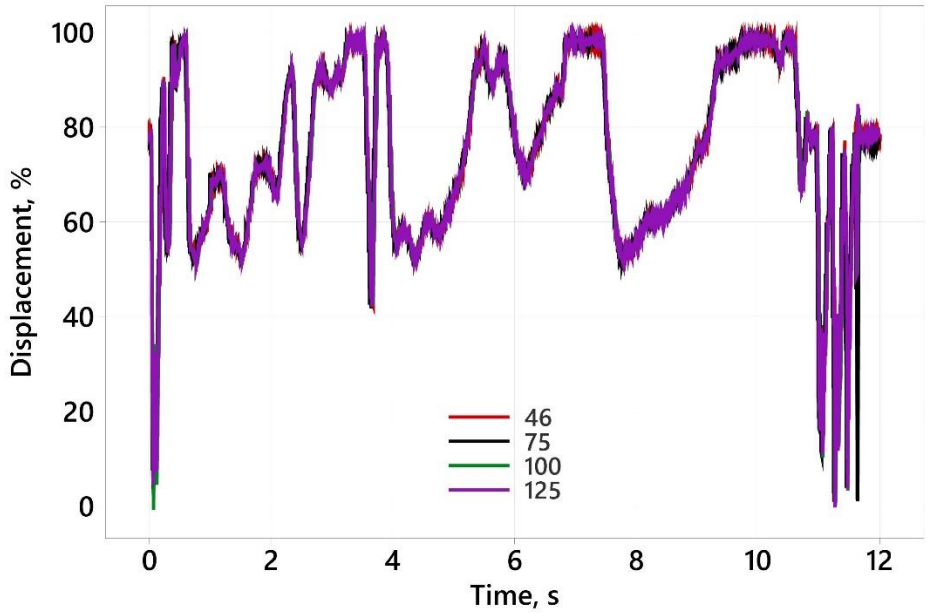

Figure 17 - 12-second Dynamic Displacement Profiles for the Four Test Fluids.

Figure 18 shows the outlet pressure versus time plot obtained through the duty cycle testing of the four fluids. The outlet pressure exhibited some variations, specifically towards the end of the duty cycle, when the dynamometer is simulating the bucket shake of the backhoe loader. In this region, pressure spikes of over the 300-bar range were recorded in both the dynamometer testing and in field tests. Overall, the pressure response of the four fluids showed similar results.

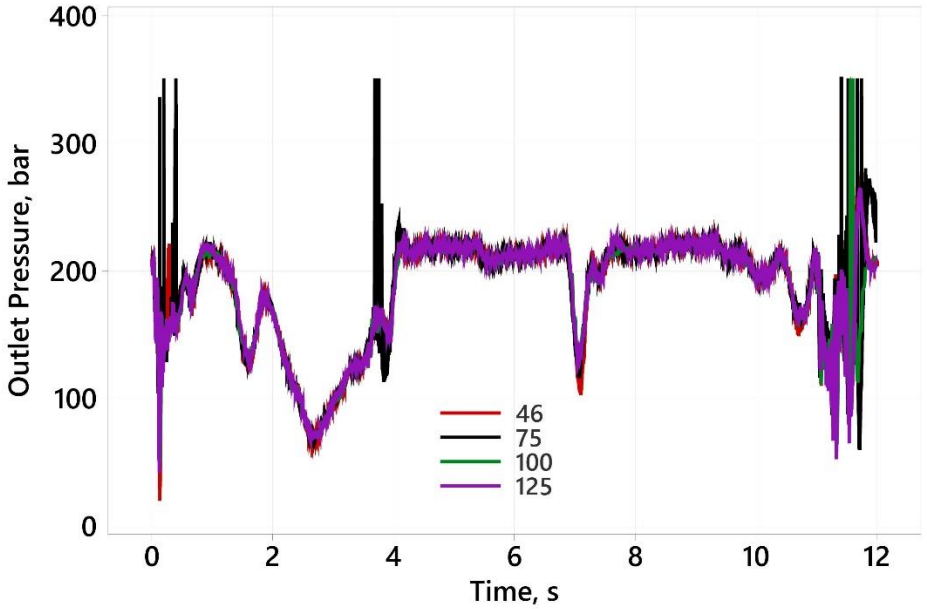

Figure 18 - 12-second Dynamic Outlet Pressure Profiles for the Four Test Fluids.

Figure 19 and Figure 20 show the plots for pump outlet flow and input torque, recorded during the duty cycle tests, respectively. It can be seen in Figure 19 that the flow profiles of the four fluids show good similarity. The torque measurements, on the other hand, despite following a similar trend, exhibited a lot of oscillations. While the pressure oscillations (see Figure 18) could be a factor that cause these effects, the torque ripples are more likely to be a result of the differences in the responsiveness of the torque and flow sensors. Overall, the torque and flow response showed similar trends for fluids that significantly varied in viscosity.

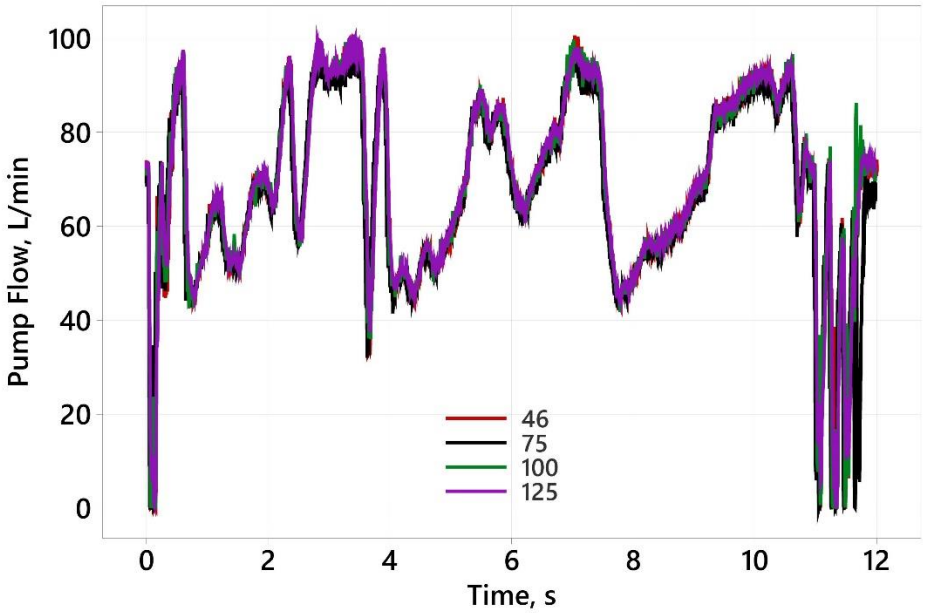

Figure 19 - 12-second Dynamic Outlet Flowrate Profiles for the Four Test Fluids.

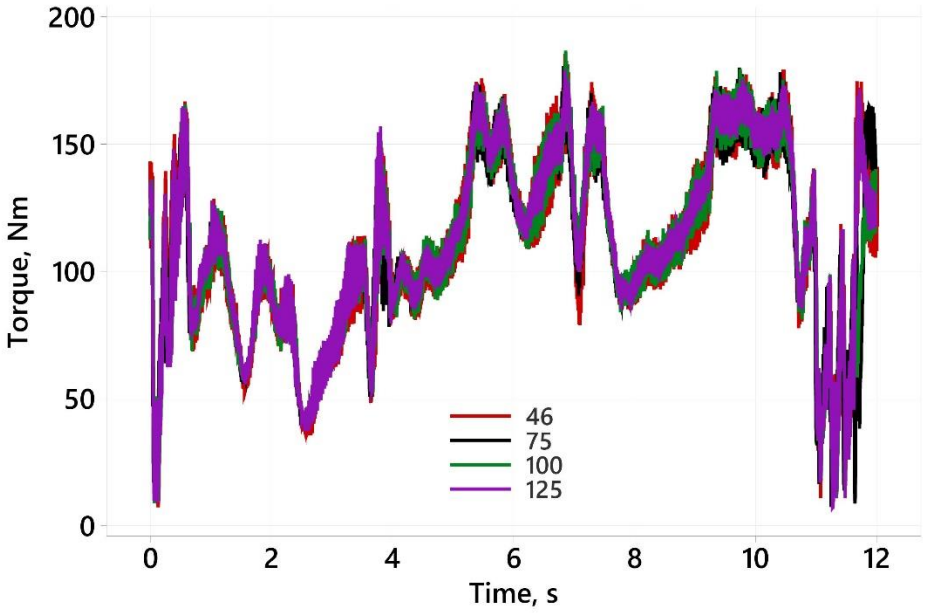

Figure 20 - 12-second Dynamic Torque Profiles for the Four Test Fluids.

Appendix B shows time series and interval plots of the results collected through dynamic duty cycle tests, including Power In, Power Out, Efficiency, Case Drain Flow Rate and Power Loss.

Comparison of Dynamic and Steady-State Duty Cycle

Tests conducted on the dynamometer under dynamic and steady-state conditions were compared. Figure 21 shows a comparison of the response of the motor under dynamic and steady-state test conditions. The plot shows that the dynamic response experiences overshoots which are due to the pump's response to the sudden changes in the command rotational frequency. Moreover, the dynamic response also exhibits some lag in several regions of the duty cycle. This lag is most evident near the ten-second mark, shown on the graph.

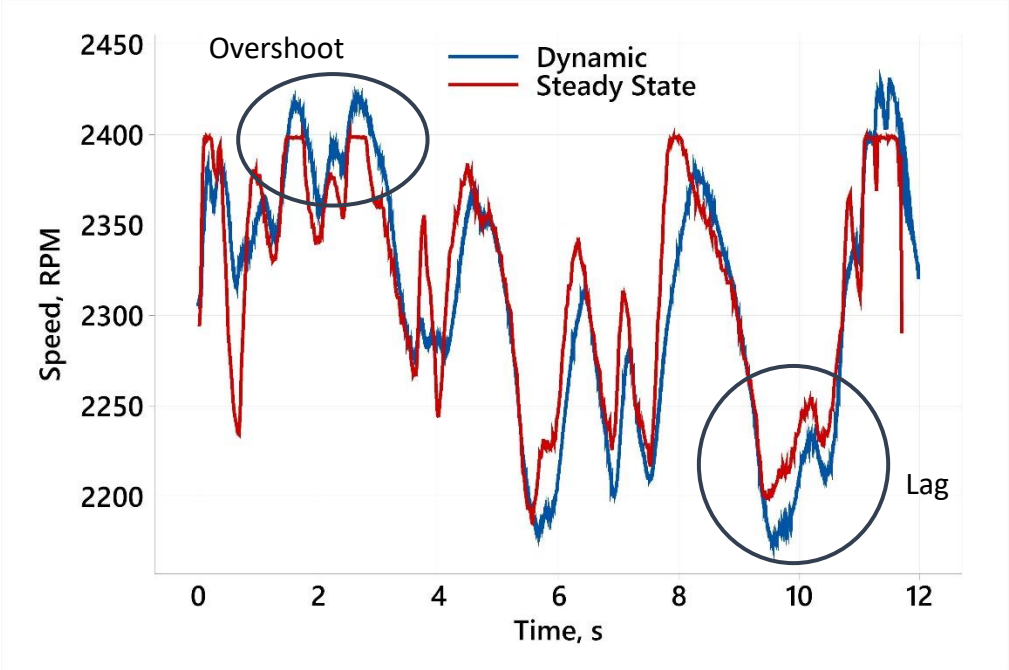

Figure 21 - Comparison of Pump Motor Speed Under Dynamic and Steady-State Test Conditions.

Figure 22 shows the flow rate under the two test conditions. It can be observed that the flow rates under dynamic and steady-state conditions closely follow a trend with little variations. However, at the beginning and end of the duty cycle, higher flow rates were observed in the steady-state test result. This was due to the quick changes in the pump displacement.

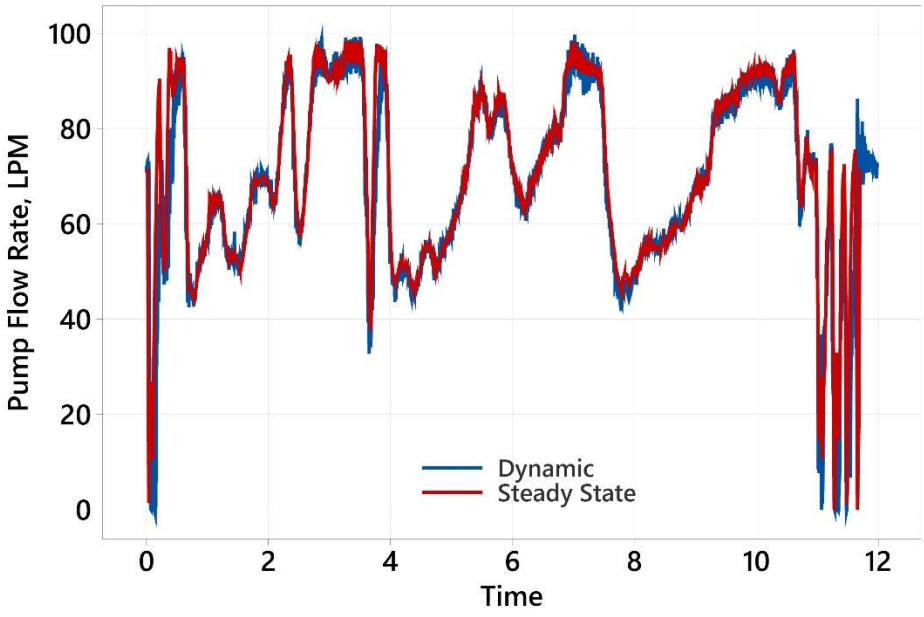

Figure 22 - Comparison of Pump Flow Rate Under Dynamic and Steady-State Test Conditions.

Figure 23 shows a comparison of input torque under dynamic and steady-state test conditions. From the plot, it can be seen that the torque response of the pump experienced some lag during the dynamic testing. This is most evident at the three-second mark of the duty cycle. Taking the lag in torque response into consideration, close examination of the flow response revealed that it experienced some lag as well. The cause for torque and flow lag were studied through step tests, which are discussed further in this report.

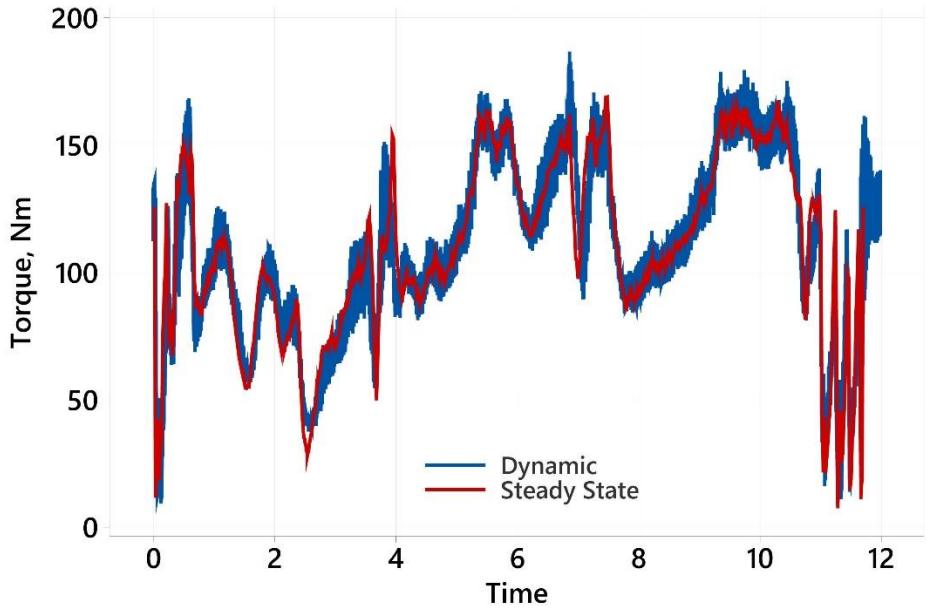

Figure 23 - Comparison of Pump Input Torque Under Dynamic and Steady-State Test Conditions.

Figure 24 shows a comparison of the apparent efficiency for the dynamometer under dynamic and steady-state conditions. It can be seen that the results for dynamic and steady-state efficiencies showed a similar pattern and magnitude. However, a greater degree of variation was observed in the dynamic duty cycle results. The apparent efficiency was calculated from the ratio of the output power to input power of the pump. Apparent efficiency for the dynamic duty cycle test, despite following a similar trend to the steady-state efficiency, is not the actual efficiency as this method ignores the energy stored in the system.

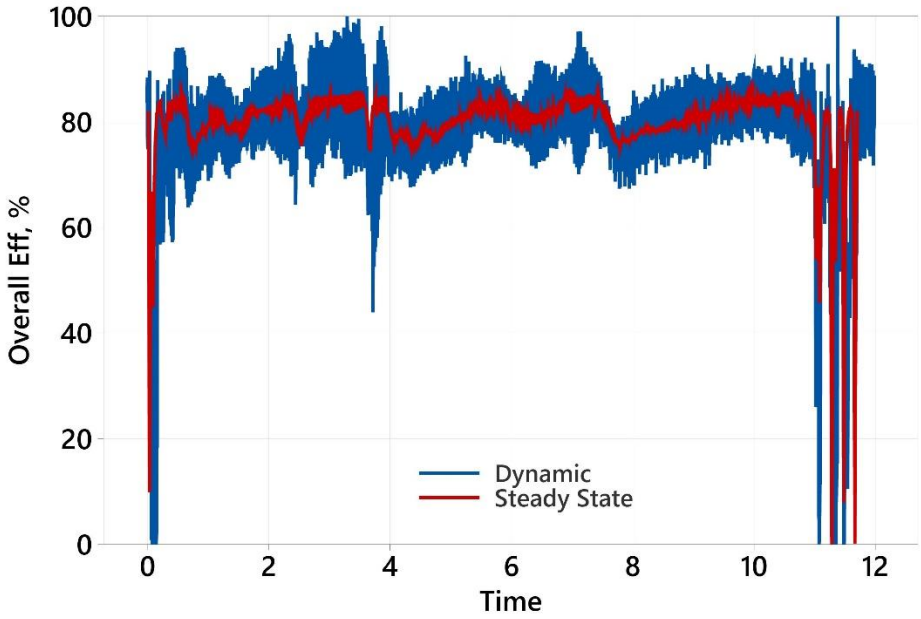

Figure 24 - Comparison of Pump Apparent Efficiency Under Dynamic and Steady-State Test Conditions.

The derived displacement found through the ISO 8426 and Toet methods was used to obtain a more accurate representation of system efficiency. This approach took into consideration the stored energy which was neglected in the calculation of the pump apparent efficiency. Several outliers in the results were introduced through the effects of stored energy. Minitab statistical analysis software was used to identify and remove the high and low outliers resulting in a cleaner dataset. The removal of these outliers was required due to the overshoots observed in the dynamic testing, particularly during the digging and bucket shake zones at the start and end of the characterized duty cycle. These overshoots result in an exaggerated evaluation of the dynamic efficiency of the dynamometer (see Figure C3 in Appendix C), which is not a true representation, hence, their removal is required.

Figure 25 shows an interval plot comparison of the volumetric, hydromechanical, and overall efficiency under dynamic and steady-state tests, with outliers removed and a 95% confidence interval. The mean volumetric efficiency of the pump tested at 50 °C and 80 °C was 1.9% to 2.5% higher under steady-state conditions than dynamic test results. Because the hydromechanical efficiency of the pump is statistically insignificant, results for the mean overall efficiency under steady state were found to be 1.6% to 1.9% higher than the dynamic test conditions. This difference in the range of efficiencies defies and is, at minimum, over 10 times smaller than, the hypothesized difference of the project. This finding, however, is potentially significant as it provides some justification for using composite duty cycles in hydraulic system design.

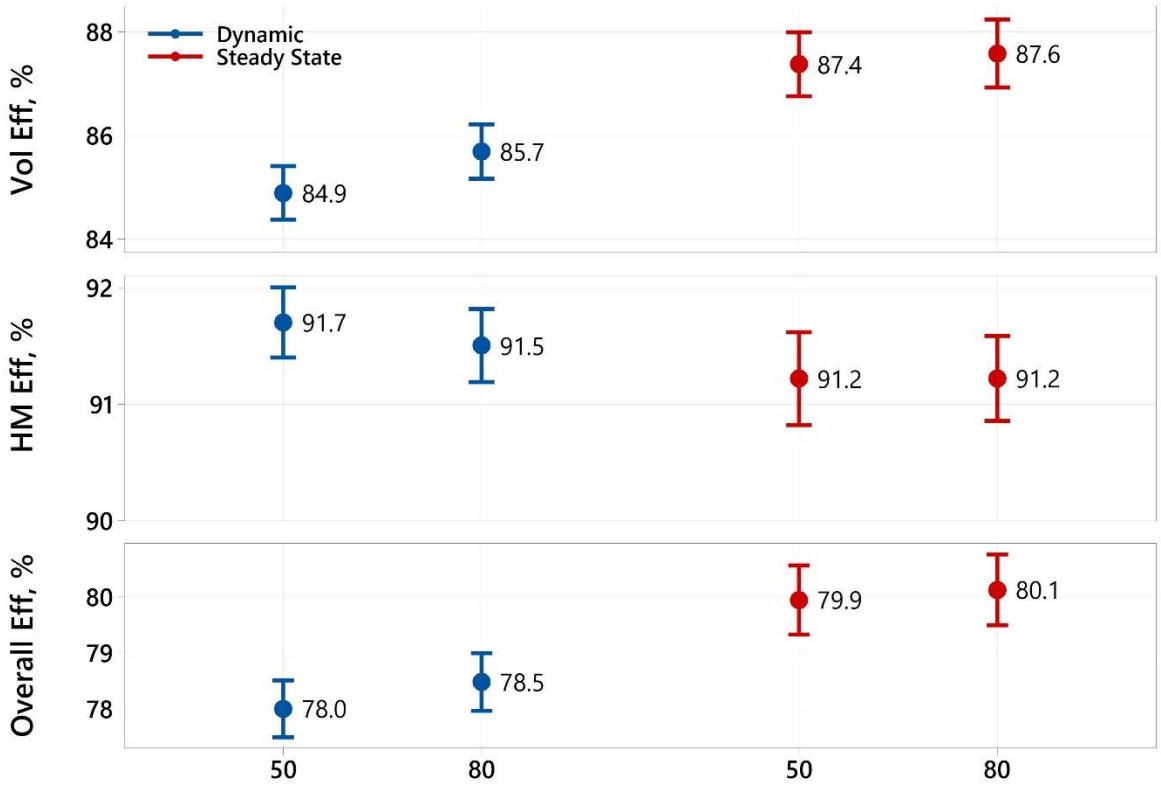

Figure 25 - Comparison of Volumetric, Hydromechanical, and Overall Efficiency Under Dynamic and Steady-State Test Conditions at 50 and 80 °C (Fluid 100).

Appendix C shows plots for the volumetric, hydromechanical, and overall efficiencies over the 12 second duty cycle, as well as the outliers that were removed using Minitab Statistical Software.

Various factors can have an effect on the flow response of the pump, causing it to act differently under dynamic conditions. Figure 26 shows a comparison of the inlet pressure of the pump under dynamic and steady-state conditions. The results make it evident that the dynamic tests saw pressure spikes at the beginning and end of the trenching duty cycle while the steady state did not.

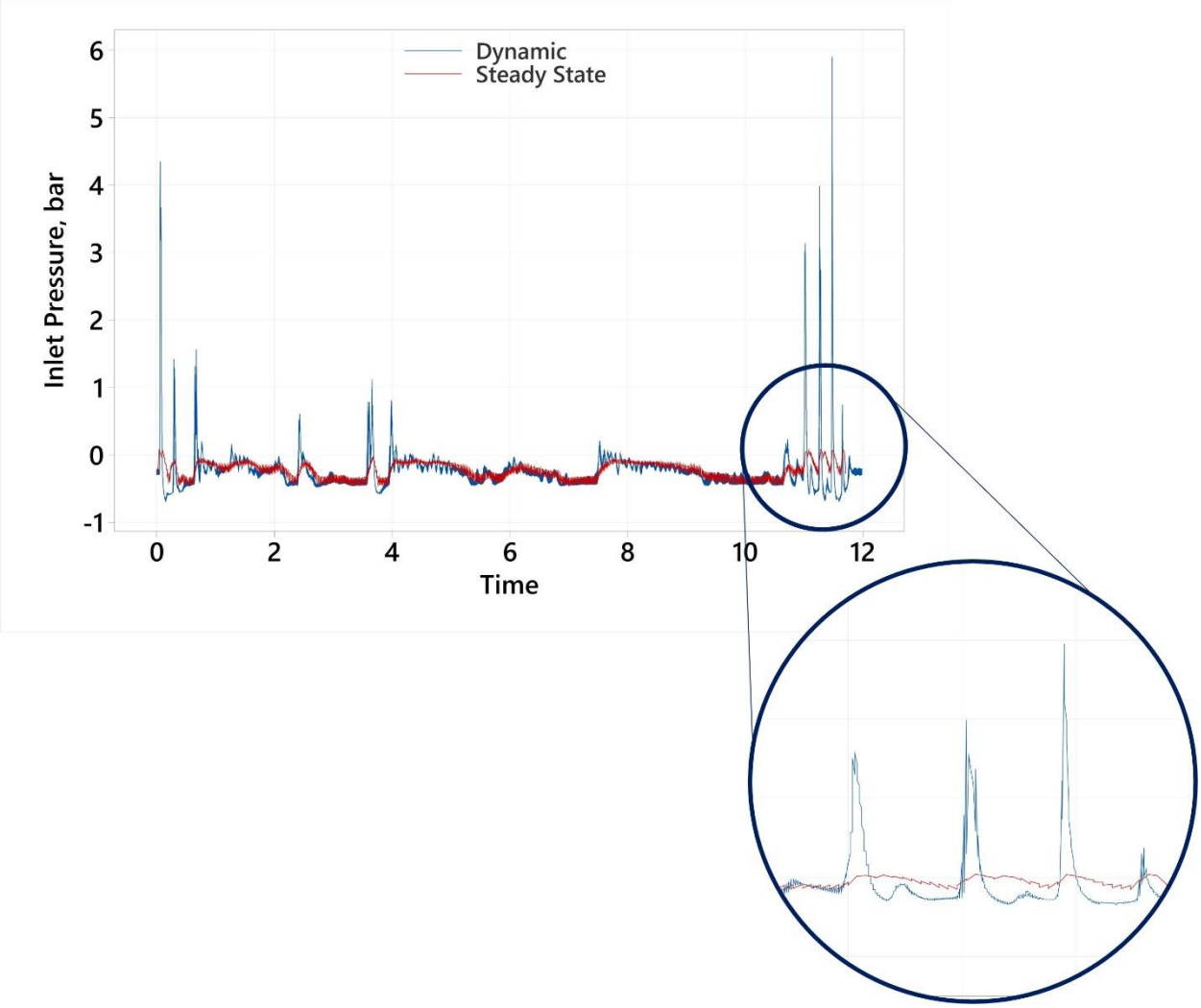

Figure 26 - Comparison of Pump Inlet Pressure Under Dynamic and Steady-State Test Conditions.

All test fluids exhibited near identical results for inlet pressure under dynamic conditions, as shown in Figure 27. Step tests were conducted to study the behavior of the inlet and its effect on system response.

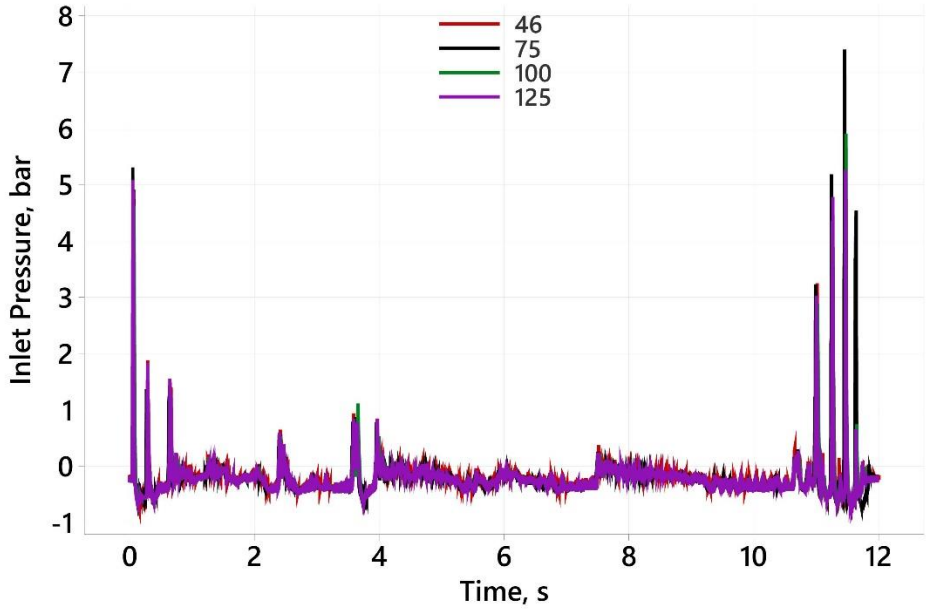

Figure 27 – Comparison of the Dynamic Inlet Pressure for the Four Test Fluids.

Step Tests

A study of the inlet line dynamics showed the torque's response to pressure step was quick. Torque response to pressure steps was consistent for both, step up and step down tests. Figure 28 and Figure 29 show the torque response for pressure step down and step up, respectively. It is worth noting that the torque response to pressure steps can be interpreted as first order, i.e., the increase or decrease in torque exhibits a linear relationship with time until it reaches steady state.

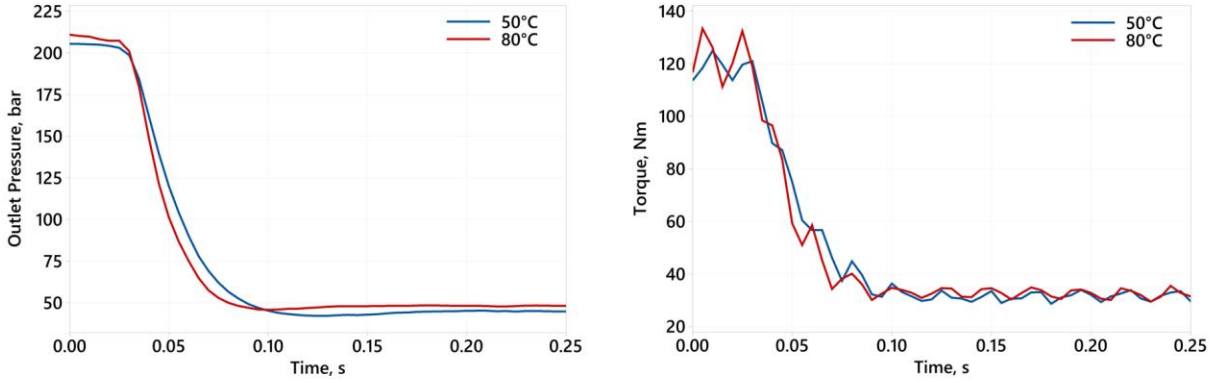

Figure 28 - Torque Response to Pressure Step Down.

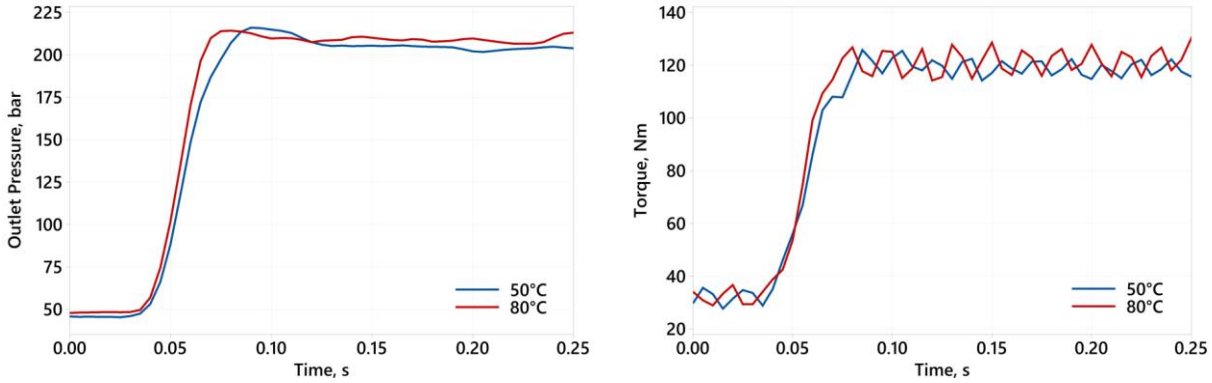

Figure 29 - Torque Response to Pressure Step Up.

Torque response to displacement steps, however, depended on whether it stepped up or down, as shown in Figure 30. The time constants evaluated for displacement step down show that the torque response is almost instantaneous. On the other hand, the response to displacement step up exhibited a lag of approximately 82ms.

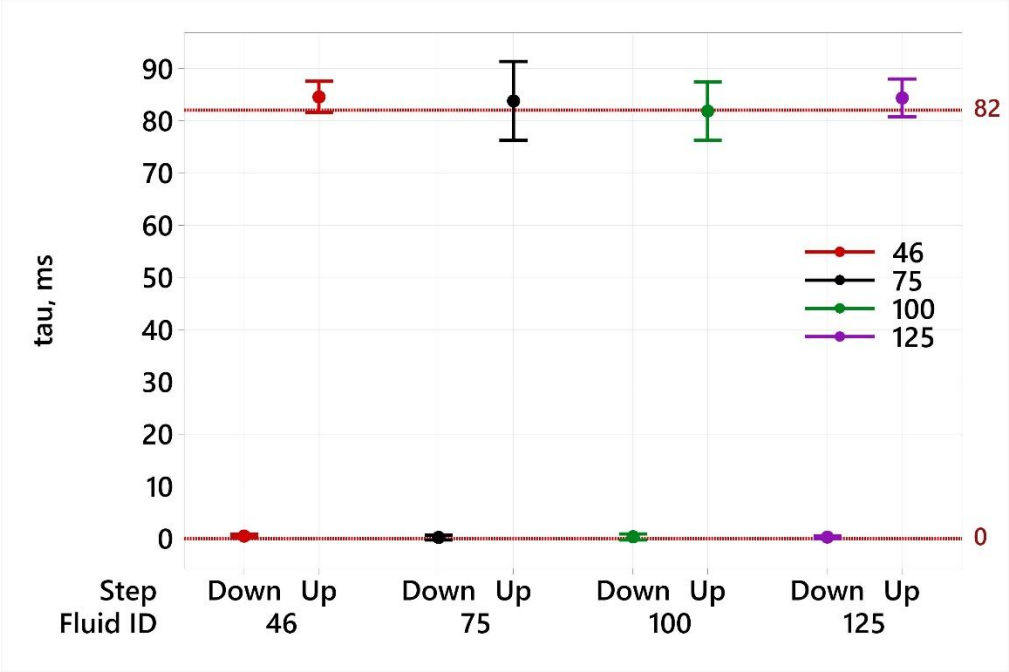

Figure 30 - Comparison of Torque Time Constants for the Four Test Fluids in Step Down and Step Up Tests.

Figure 31 and Figure 32 show the flow response to displacement step down and up, respectively. An interesting observation was made in the flow response when the displacement is stepped up. In contrast to the flow response to displacement step down, the step up results did not exhibit a first order response.

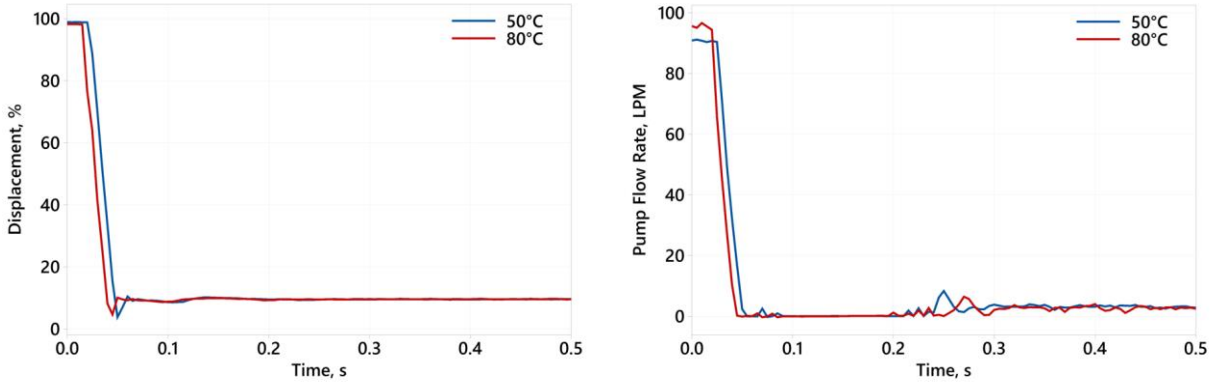

Figure 31 - Flow Rate Response to Swash Step Down.

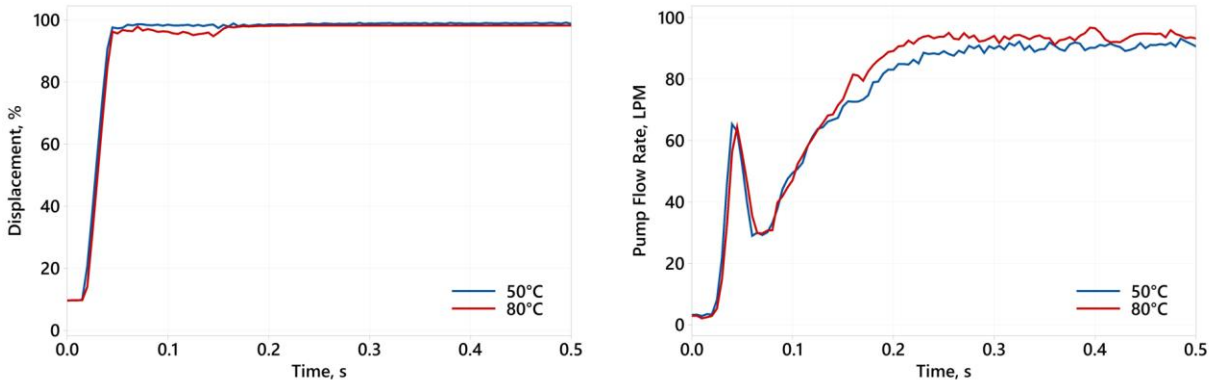

Figure 32 - Flow Rate Response to Swash Step Up.

Figure 33 shows the time constants for the flow response to the displacement stepped up and down. Similar to torque, the flow response to displacement step down was much quicker than step up. It is also noteworthy that the time constants for torque and flow in swash step up tests turned out to be the same. This observation is significant as it provides verification that sensor latency is not a contributor to the apparent lag in the response.

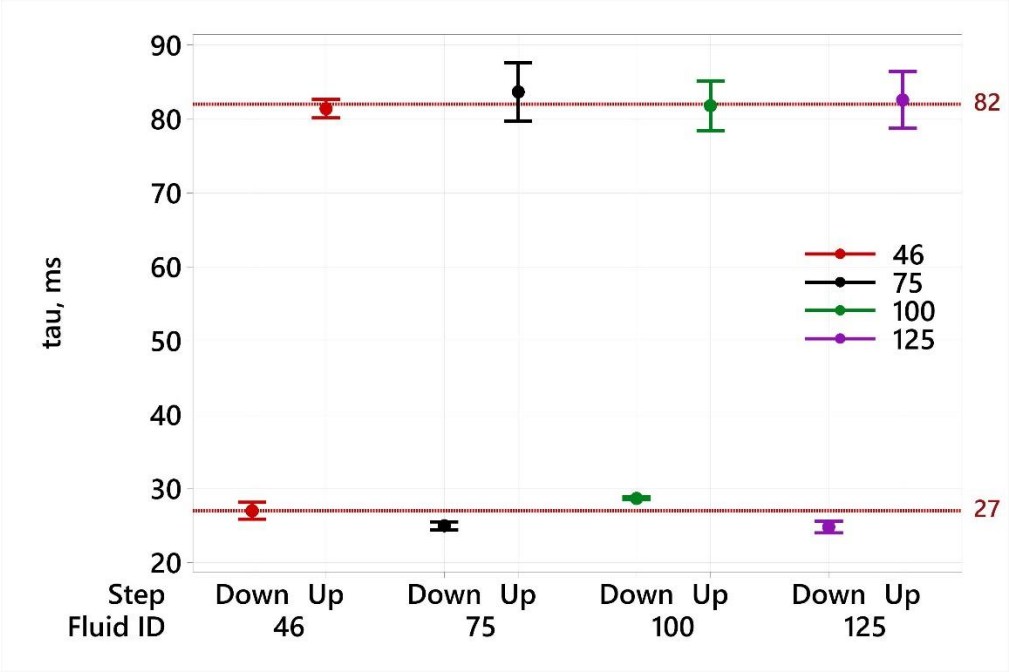

Figure 33 - Comparison of Flow Time Constants for the Four Test Fluids in Step Down and Step Up Tests.

Figure 34 shows the response of the pump inlet pressure, outlet flow, torque, and outlet pressure to the swashplate stepping up. As the swashplate is stepped up, there is a rapid drop in the inlet pressure. This is because all the fluid stored in the inlet is displaced into the system. This discharge of fluid from the inlet into the system exhibited a surge in the outlet flow, torque, and pressure responses. After the pressure drop in the inlet line, the inlet line pressure slowly increased beyond its minimum value. As the inlet pressure increased, a steady rise in outlet flow, torque, and pressure was observed. Similar trends were observed with all four fluids. Appendix D shows some plots that illustrate the dynamometers' response to pressure and speed steps, as well as swash up and swash down layouts (see Figure 34) of all test fluids.

Based upon these observations, it was hypothesized that the inlet line dominates the response of the pump. The findings led to the conclusion that the pressure losses in the inlet line were a contributing factor in the lower volumetric and overall efficiencies observed in the dynamic duty cycle.

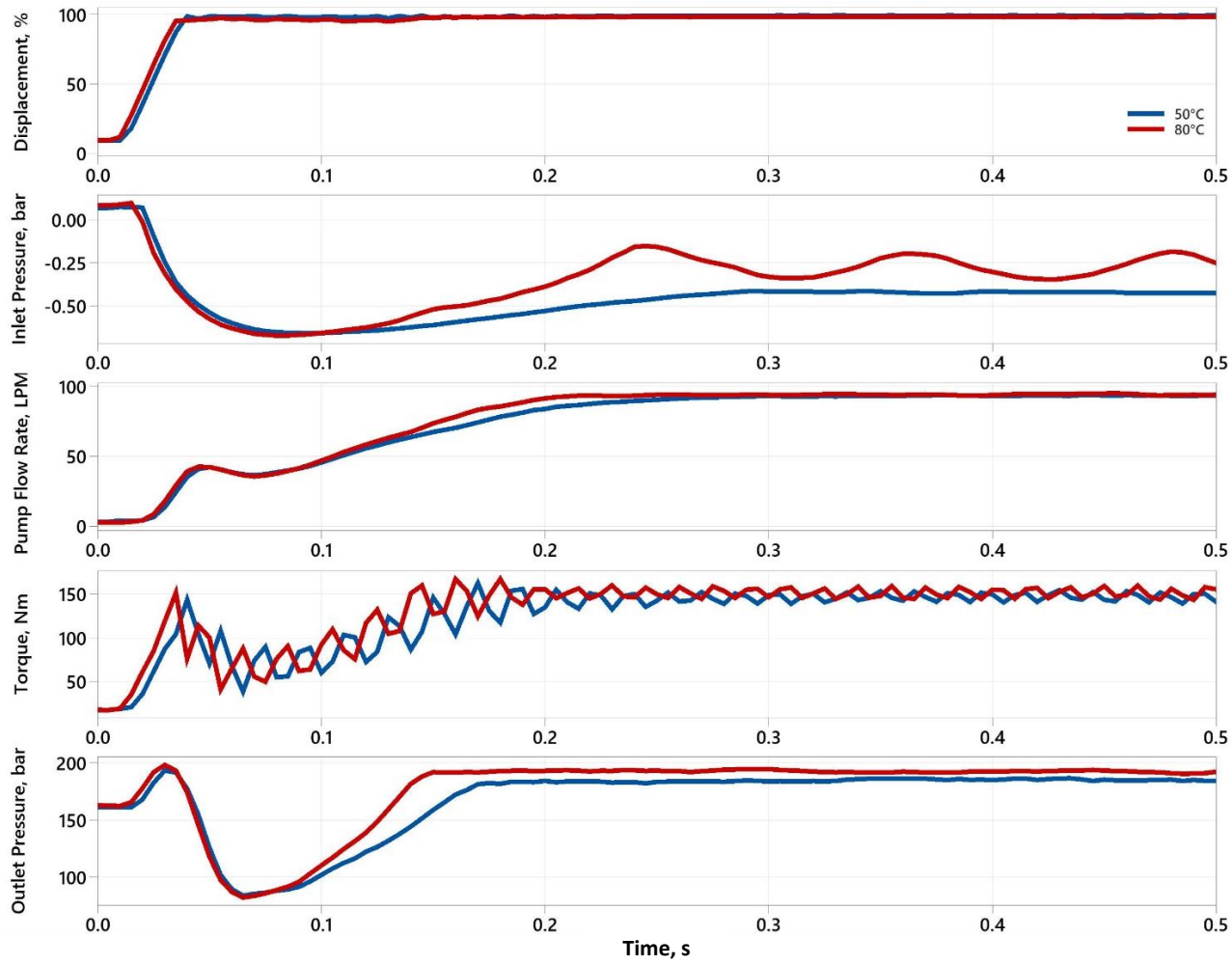

Figure 34 - Response of Pump Inlet Pressure, Outlet Flow, Torque, and Outlet Pressure to Step Increase in Pump Displacement (Fluid 125).

Another interesting observation was that in tests run at 80 °C, a pressure ripple was seen in the inlet line. While the cause of these pressure ripples in still unknown, the study of this phenomenon brought about valuable information. Following are the results of this study.

The Effect of Viscosity on the Inlet Pressure Ripple

Figure 35 shows a comparison of the inlet pressure response to the displacement step up for the four test fluids at 80 °C. The results led to the observation that the amplitude of the pressure ripple decreased as the viscosity increased. The fluid with the lowest viscosity among the four test fluids (Fluid 46), exhibited the highest amplitude pressure ripple amplitude, while the fluid with the highest viscosity (Fluid 125) exhibited the lowest pressure ripple amplitude.

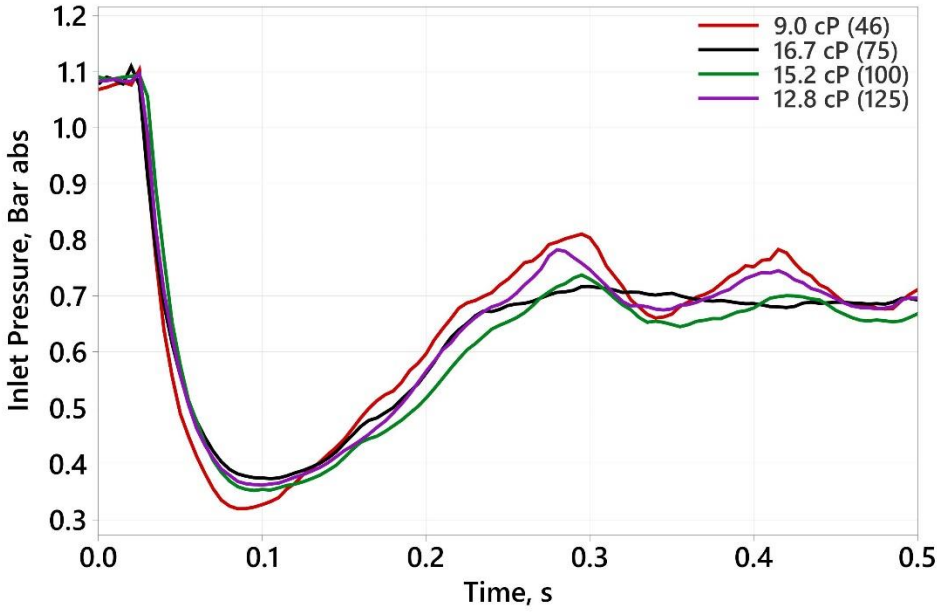

Figure 35 - Comparison of Inlet Pressure Response of the Four Fluids to Displacement Step Up at 80 °C.

The Effect of Shear Thinning on the Inlet Pressure Ripple

The relationship between viscosity and the inlet pressure ripple amplitude was tested using Fluid 125. The selection of Fluid 125 was based upon the fact that it exhibited the highest percentage viscosity loss among the four test fluids (see Table 2). The fluid was sheared down through several break-in procedures. Step tests were performed prior to the initial break-in procedure, as well as after every flowing break-in. Figure 36 shows the results of this study. The result confirmed the hypothesis about the relationship between viscosity and the pressure ripple amplitude. After the 0.25s mark, where the inlet pressure step in reached a steady state, it can be observed that the inlet pressure settles at a higher value with decreasing viscosity. While the first indication of the pressure ripple formation was observed when the fluid was at 13.5cP, the highest amplitude of the pressure ripple was seen at 12.8cP. Further testing did not result in an increase in the pressure ripple amplitude, as at this point the fluid had reached shear stability, solidifying the theory about the relationship between viscosity and ripple amplitude.

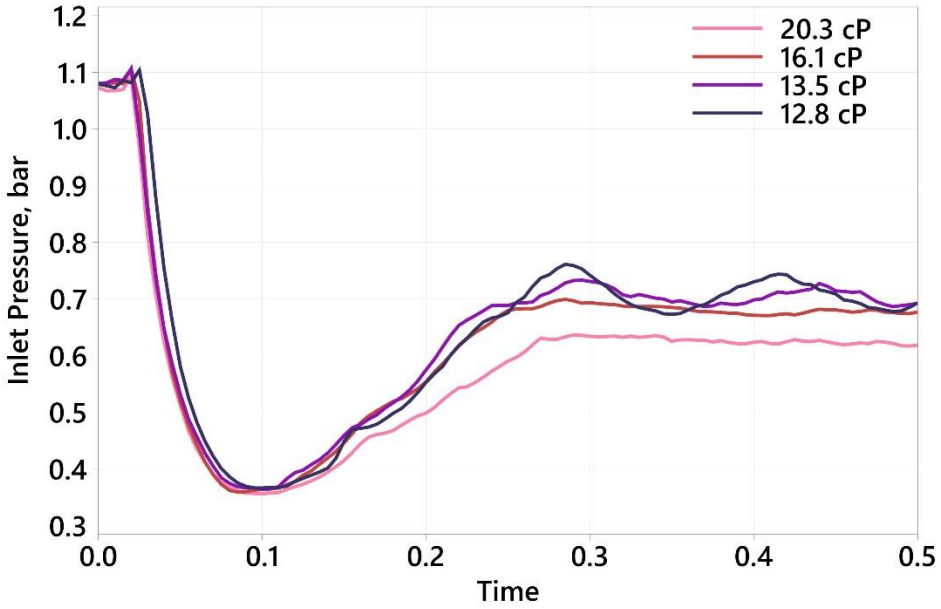

Figure 36 - The Effect Viscosity Drop Through Shear Thinning on Response of the Inlet Pressure at 80 °C (Fluid 125).

Appendix E includes interval plots that show the viscosity and density of the test fluids measured during testing.

A Possible Effect of Fluid Formulations on the Inlet Pressure Ripple

An interesting observation made during the pressure ripple study involves a fluid that was excluded from this report for the sake of comparison. The fluid identified as 46A is a non-formulated test fluid. This fluid has a similar viscosity to Fluid 46. Table 5 shows the physical properties of Fluids 46A and 46.

Table 5 - A Comparison of the Physical Properties of Fluid 46A and Fluid 46.

Fluid ID	46A	46
Base Oil Group	IV	II
Polymer	None	f-OCP
Viscosity Index	138	101
Kin Vis 40°C, cSt (D445)	46.7	45.4
Sheared Vis 40°C, cSt (D5621)	46.6	44.2
Kin Vis 100°C, cSt (D445)	7.86	6.75
Sheared Vis 100°C, cSt (D5621)	7.84	6.57
Vis Loss, %	0.28	2.64
Density, g/ml 15°C	0.8327	0.8669

Figure 37 shows a comparison of the inlet pressure ripple observed in the two fluids at 80°C. Since the fluids are of similar viscosities, according to the hypothesis, they should exhibit similar pressure ripple amplitudes. However, the results show that the inlet pressure ripple seemed to be suppressed and smoothed when compared to 46A, which exhibited much higher spikes in the pressure ripple. This difference could be due to the polymer additives in Fluid 46.

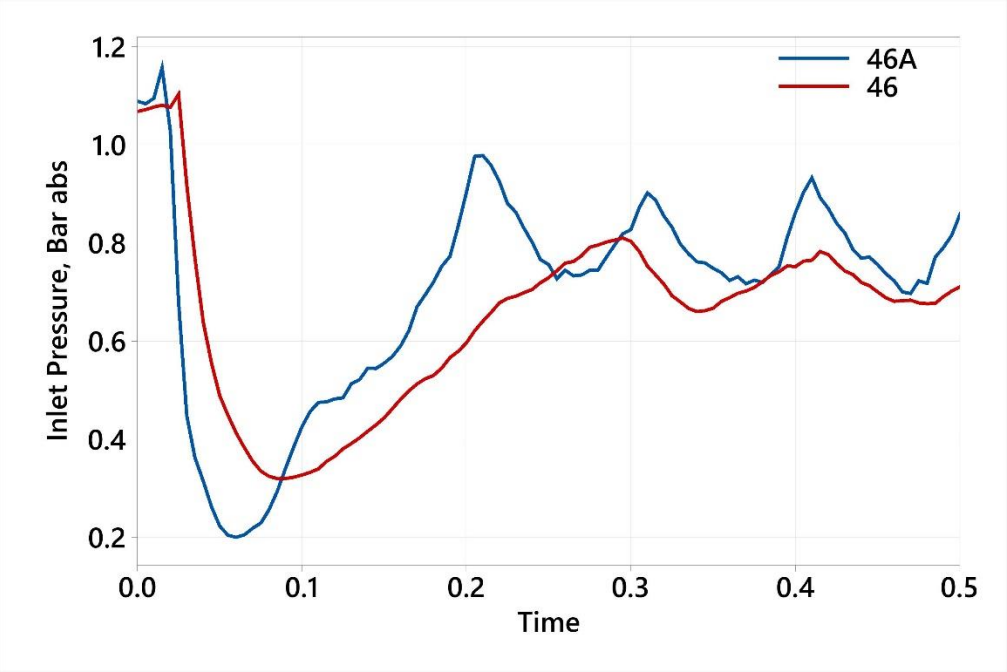

Figure 37 - Comparison of Inlet Pressure Response to Displacement Step Up in Formulated and Non-Formulated Test Fluids at 80 °C.

Inlet Model

A MATLAB Simulink model of the inlet was developed to simulate the effects of fluid properties on the line dynamics. This model used the results from the step tests and the modeling methodologies described in the Methods and Methodology section of this report. To capture the nonlinear nature of the hydraulic capacitance, the pressure dependance of the bulk modulus was incorporated in the inlet model, while a variable Reynolds number was incorporated to calculate the friction factor in order to record the nonlinear nature of resistance. This allowed the model to capture the effects of low oil stiffness in the low-pressure valleys of the simulation.

Table 6 shows the parameters used for the simulation of the displacement step down test. The results of the simulation are shown in Figure 38. The results obtained through the model showed good correlation with the experimental data.

Table 6 - Parameters for Simulating Inlet Pressure Response to Displacement Step Down.

Parameters	Value
Viscosity, cP	40, 30, 20, 10
Density, Kg/m^3	820
Air, ratio	0.003
Bulk Modulus, GPa	1.38
Volume, m^3	300
Area, m^2	2.41
Temperature, °C	80

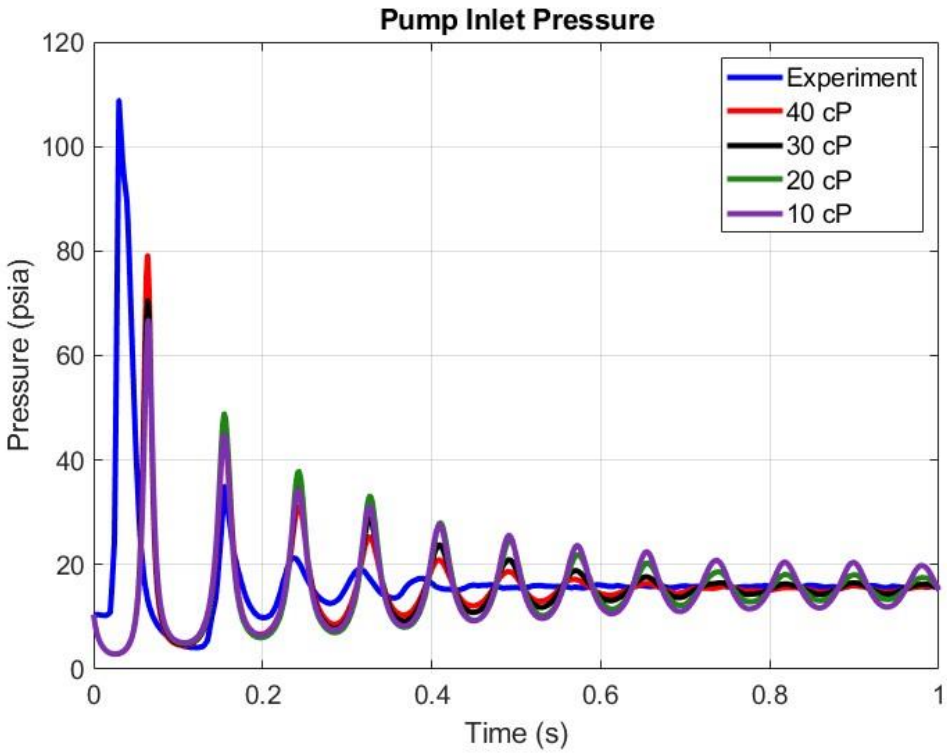

Figure 38 - Displacement Step Down Simulation Results of the Inlet Pressure Response at different Viscosities.

Table 7 shows the parameters used for the simulation of the displacement step up test. The results of the simulation are shown in Figure 39. The results obtained through the model did not match the experimental data completely. The model was, however, able to simulate the relationship between viscosity and inlet pressure, with the exception of ripple formation near the 13cP mark (see Figure 36).

Fluid density and bulk modulus can exhibit a hysteretic response to the changes in pressure, depending on whether the fluid is under compression or decompression [32]. This is due to the difference in the thermodynamic effect in accordance with air solubility. The graphic in Appendix

F illustrates a possible explanation of this phenomenon. This phenomenon could be a reason why different parameters had to be used for simulating step up and down tests.

Table 7 - Parameters for Simulating Inlet Pressure Response to Displacement Step Up.

Parameters	Value
Viscosity, cP	40, 30, 20, 10
Density, Kg/m^3	850, 800, 750, 700
Air, ratio	0.003
Bulk Modulus, GPa	1.38
Volume, m^3	300
Area, m^2	1.55
Temperature, °C	80

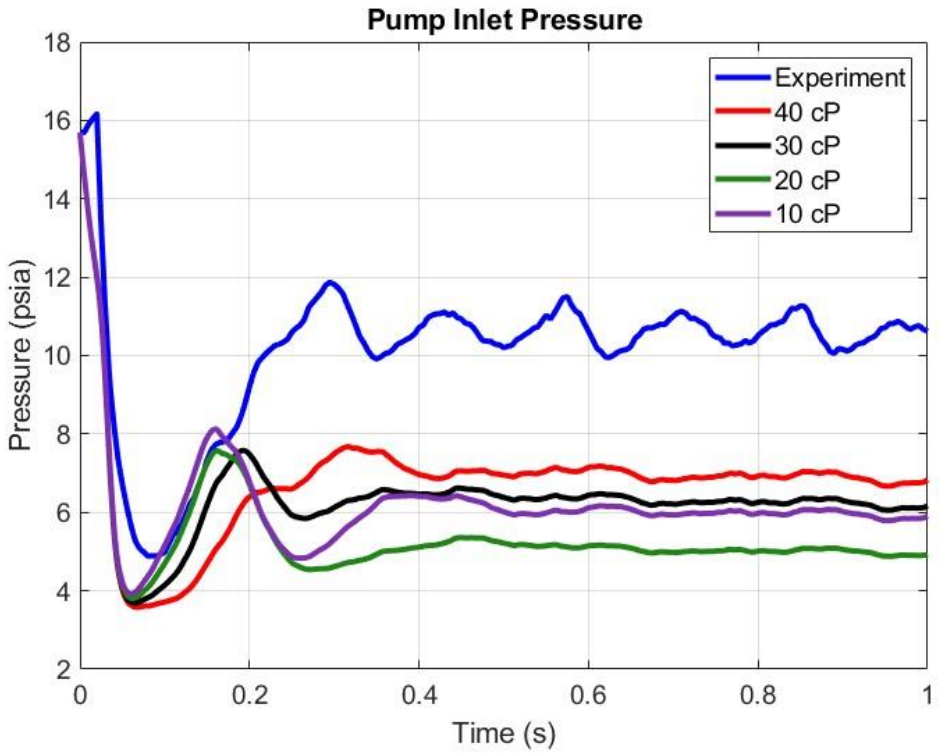

Figure 39 - Displacement Step Up Simulation Results of the Inlet Pressure Response at different Viscosities.

The Parameter Estimator application in the MATLAB Simscape software was used to find the optimum values of the parameters used for the simulations. The Parameter Estimator used pattern recognition and iterations to provide values of the parameters that will result in the best possible match. However, the estimations obtained through the Parameter Estimator did not show much improvement with respect to the simulation results seen in Figures 38 and 39. This led to the conclusion that the inlet model needs further improvements to provide results that are more coherent with the experimental data.

Conclusion and Recommendations

The trenching cycle of a backhoe loader was reproduced in dynamometer testing under dynamic and steady-state conditions. The volumetric efficiency of the pump was approximately 2% higher under steady-state conditions. Inlet line dynamics was identified as the likely cause of this difference. A dynamic model was developed to investigate the effects of fluid properties on the transient behavior. Data from inline viscosity and density sensors were used in a sensitivity analysis. Both the model and experiments using step tests showed that inlet pressure produced a significant transient response that affected volumetric efficiency. Inlet line pressure ripple was found to increase as the fluid viscosity decreased. This effect was also seen as polymer additives sheared.

For future work, the optimization of the inlet model is required to match the experimental data. A model created in the Simscape workspace is suggested to give better results than a Simulink model. Moreover, investigations on the non-ideal form of the pressure-volume behavior should be conducted to understand the effects of air solubility.

References

[1] Milwaukee School of Engineering , "MSOE Fluid Power Institute," [Online]. Available: https://www.msoe.edu/academics/how-we-teach/labs-and-research/engineering/fluid-power-institute/.

[2] ME Mechanical, "Dynamometer: Introduction and Types," 7 January 2021. [Online]. Available: https://mechanicalengineering.blog/dynamometer-introduction-types/.

[3] E. Strmcnik and F. Majdic, "Comparison of Leakage Level in Water and Oil Hydraulics," *Advances In Mechanical Engineering,* vol. 9, no. 11, 2017.

[4] P. Panwar, M. Len, N. Gajghate, P. Michael and A. Martini, "Fluid Effects on Mechanical Efficiency of Hydraulic Pumps: Dynamometer Measurements and Molecular Simulations," in *Fluid Power Systems Technology*, Longboat Key, Florida, USA, 2019.

[5] P. Michael, M. Cheekolu, P. Panwar, M. Devlin, R. Davidson, D. Johnson and A. Martini, "Temporary and Permanent Viscosity Loss Correlated to Hydraulic System Performance," *Tribology Transactions,* vol. 61, no. 5, pp. 901-910, 2018.

[6] E. C. Fitch, Tribolics, Inc., "Machinery Lubrication," Noria, 2022. https://www.noria.com/training/certifications/machinery-lubrication-i/

[7] P. Casoli, M. Pastori, F. Scolari and M. Rundo, "Active Pressure Ripple Control in Axial Piston Pumps through High-Frequency Swash Plate Oscillations — A Theoretical Analysis," *Energies*, vol. 12, no. 7: 1377, 2019.

[8] M. Mary, "Efficiency Flows from polymer VM," 17 09 2019. [Online]. Available: https://www.lubesngreases.com/magazine/efficiency-flows-from-polymer-vm/.

[9] F. Nilsson, "Joint Human-Machine Exploration of Industrial Time Series Using Matrix Profile," Halmstad University, 2021.
https://www.diva-portal.org/smash/record.jsf?pid=diva2%3A1566371&dswid=-7896

[10] U.S. Department of Energy, United States Environmental Protection Agengy, "Detailed Test Information,"
[Online]. Available: https://www.fueleconomy.gov/feg/fe_test_schedules.shtml.

[11] K. King, "Are highway Miles Worse Than City Miles for Your Car's Condition?," Toyota of North Charlotte, 20 July 2018.
[Online]. Available: https://www.toyotaofnorthcharlotte.com/blog/are-highway-miles-worse-than-city-miles-for-your-cars-condition/.

[12] Photogragh Provided by Danfoss.

[13] ISO/FDIS 4409:2019(E), "Hydraulic fluid power — Positive-displacement pumps, motors and integral transmissions — Methods of testing and presenting basic steady state performance," *International Standard,* 2019.

[14] L. Garcia, J. Bin Shahid and P. Michael, *Polymer-Enhanced Fluid Effects on the Dynamic Response of Hydraulic Pumps,* Milwaukee: Fluid Power Institute. [CCEFP Presentation]

[15] P. Panwar, P. Michael, M. Devlin and A. Martini, "Critical Shear Rate of Polymer-Enhanced Hydraulic Fluids," Multidisciplinary Digital Publishing Institute, Milwaukee, 2020.

[16] P. Panwar, "Modeling of Axial Piston Pump Input Torque and Output Flow Rate using MATLAB Simulink," Milwaukee School of Engineering, Milwaukee, 2018. [MSE Capstone Project]

[17] International Organization of Standardization, Petroleum products — Transparent and opaque liquids — Determination of kinematic viscosity and calculation of dynamic viscosity, Switzerland: ISO, 2020.

[18] International Organization of Standardization, Hydraulic fluid power — Positive displacement pumps and motors — Determination of derived capacity, ISO, 2008.

[19] J. L. Johnson, A Brief History of Mathematical Modeling in Hydraulics, WHITEPAPER. [Online]. Available: https://www.fluidpowerworld.com/a-brief-history-of-math-modeling-in-hydraulics/

[20] G. Toet, "Die Bestimmung des theoretischen Hubvolumens von hydrostatischen Verdrangerpumpen und Motoren aus volumetrischen Messungen, Olhydraulik und Pneumatik O+P," vol. 14 (1070) , no. 5, pp. 185-190, 1970.

[21] G. Toet, Johnson, Montague, Garcia-Bravo and Torres, "“The Determination of the Theoretical Stroke Volume of Hydrostatic Positive Displacement Pumps and Motors from Volumetric Measurements," *Energy Efficiency and Controllability of Fluid Power Systems*, 2018.

[22] "Couette Flow," [Online]. Available: https://en.wikipedia.org/wiki/Couette_flow.

[23] P. Michael and J. Garcia-Bravo, "The Determination of Hydraulic Motor Displacement," in *The 17th Scandinavian International Conference on Fluid Power, SICFP*, Linköping, Sweden, 2021.

[24] Electrical4U, "What is a First Order Control System," 24 January 2021. [Online]. Available: https://www.electrical4u.com/first-order-control-system/#:~:text=A%20first%2Dorder%20system%20is,function%20with%20respect%20to%20time..

[25] P. Panwar and P. Michael, "Empirical Modelling of Hydraulic Pumps and Motors based upon the Latin Hypercube Sampling Method," *International Journal of Hydromechatronics*, vol. 1, no. 3, 2018.

[26] P. Michael, K. Stelson, D. Williams and H. Malik, "Dynamometer Testing of Hydraulic Fluids in an Axial Piston Pump Under Simulated Backhoe Loader Trenching Condition," in *ASME/BATH*, Bath, United Kingdom, [Awaiting Publication].

[27] D. A. Hullender, N. N. Snyder and J. C. Gans, "Application of an Analytical Model for Simulating Hydraulic Systems Containing Internal Lines with Turbulent Flow," in *Proceedings of the ASME/Bath Symposium on Fluid Power and Motion ControlSarasota, FL*, 16-19 Oct. 2017.

[28] B. Friedland, *Control System Design: An Introduction to State-Space Methods*, Garden City, New York: Dover, 2005.

[29] L. Moody, "Friction Factors for Pipe Flow," *Transactions of the ASME*, vol. 66, no. 8, pp. 971-684, 1944.

[30] H. E. Merritt, *Hydraulic Control Systems*, Wiley, New York, 1967.

[31] H. Gholizadeh, R. Burton and G. Shoenau, "Fluid Bulk Modulus: A Literature Survey," *International Journal of Fluid Power,* vol. 12, no. 3, pp. 5-15, 2011.

[32] Zhou, J., Vacca, A. and Manhartsgruber, B., "A Novel Approach for the Prediction of Dynamic Features of Air Release in Hydraulic Oils," *Journal of Fluid Engineering,* vol. 135, no. 9, 2013.

Appendix A – ISO 8426 and Toet Method – Calculating the Derived Displacement of the Dynamometer Pump

ISO 8426

Table A1 - Data Collected for ISO 8426 Method at 1800 RPM and 50 °C.

Line #	Inlet Temperature [C]	Low Pressure [bar] See Note 2	High Pressure [bar] See Note 2	Delta Pressure [bar]	Shaft Speed [rpm]	Displacement [%] See Note 1	High Pressure Flow [Lpm]	Inlet Viscosity [cSt or cP] See Note 2 & 3	Inlet Density [kg/m^3] See Note 2 & 3
1	51.0895972	-0.314792241	69.40709313	69.7218854	1800.009	99.84595311	80.11953536	34.6484375	822.0742552
2	51.0930225	-0.315906292	69.37507472	69.690981	1799.999	99.83921056	80.14824793	34.6484375	822.1018396
3	51.1769475	-0.313885963	69.39100289	69.7048889	1800.001	99.84786507	80.13458927	34.6484375	822.0797335
4	51.2598474	-0.31516283	69.34519085	69.6603537	1799.993	99.83383136	80.12470696	34.6484375	822.0340463
5	51.3066745	-0.312792781	83.14550255	83.4582953	1800.004	99.87349137	79.48402597	34.5	821.9340717
6	51.3359499	-0.314255906	83.16582264	83.4800785	1799.999	99.86834469	79.47147466	34.5	821.9766105
7	51.375897	-0.314195449	83.14657973	83.4607752	1799.997	99.86765708	79.4993458	34.796875	821.9557795
8	51.3936305	-0.315510825	83.1576512	83.473162	1800.01	99.86233009	79.46576729	34.796875	821.967793
9	51.1994097	-0.313677038	96.97896025	97.2926373	1799.987	99.89245229	78.83862403	34.796875	821.9807452
10	51.2265805	-0.312267261	96.98055986	97.2928271	1800.01	99.89290214	78.85212567	34.796875	822.0317529
11	51.3084045	-0.312660827	96.98672622	97.299387	1799.992	99.88374265	78.82406717	34.9765625	821.9183223
12	51.4023485	-0.313481584	96.95366881	97.2671504	1800.023	99.87515256	78.87544874	34.9765625	821.9232193
13	51.4812318	-0.308945918	110.7777034	111.086649	1800	99.89567422	78.28632212	34.9453125	821.8399378
14	51.530402	-0.309726088	110.829683	111.139409	1799.99	99.89117797	78.31124971	34.9453125	821.8343629
15	51.5901928	-0.309268544	110.7975531	111.106822	1800.008	99.88746182	78.28930024	34.9453125	821.7574709
16	51.6228996	-0.311271963	110.7835296	111.094802	1800	99.86862516	78.30707331	34.9453125	821.8229357
17	51.3597657	-0.310300431	124.6016926	124.911993	1800.024	99.87565805	77.75120297	34.9453125	821.9126874
18	51.3664099	-0.310915227	124.5916539	124.902569	1799.998	99.86143275	77.75249016	34.9453125	821.8788676
19	51.4265283	-0.308843771	124.57962	124.888464	1800.033	99.87444526	77.76615545	34.8515625	821.8800879
20	51.5300723	-0.309767263	124.6124423	124.92221	1799.966	99.86261043	77.77695265	35.09375	821.8221927
21	51.7650898	-0.307085418	138.4172645	138.72435	1799.976	99.83123952	77.15599825	35	821.6519495
22	51.8122811	-0.306744241	138.3993637	138.706108	1799.993	99.82878181	77.18536462	35	821.6481613
23	51.8396954	-0.306839382	138.3108574	138.617697	1800.003	99.8249447	77.16718195	34.7578125	821.608046
24	51.8342602	-0.308718942	138.3689188	138.677638	1800.005	99.80945275	77.2097012	35	821.6136009
25	51.4993419	-0.309650542	152.188591	152.498242	1799.985	99.74635039	76.6464971	35	821.857256
26	51.4713578	-0.306616454	152.1721233	152.47874	1800.012	99.75482322	76.64529756	35	821.8774514
27	51.4874721	-0.308823456	152.1855587	152.494382	1799.964	99.74890777	76.66124509	34.4453125	821.883678
28	51.5262666	-0.306135802	152.236909	152.543045	1800.025	99.76432222	76.67288171	34.4453125	821.8335077
29	51.5586773	-0.306092057	165.9812089	166.287301	1800	99.68289738	76.12283861	34.4453125	821.8291837
30	51.560433	-0.303082234	166.024526	166.327608	1800.002	99.69699363	76.10102476	34.4453125	821.7789671
31	51.6082923	-0.30566328	165.9877895	166.293453	1800.001	99.68195137	76.12369129	34.4375	821.7479069
32	51.6488259	-0.302509931	166.0257229	166.328233	1799.999	99.69259724	76.08845938	34.4375	821.7309632
33	51.6116226	-0.301221088	179.8279852	180.129206	1799.999	99.58920666	75.48215996	34.59375	821.7550724
34	51.6209447	-0.302543826	179.7927758	180.09532	1800	99.58153744	75.44746857	34.59375	821.7556116
35	51.6832813	-0.303599539	179.7346408	180.03824	1799.981	99.56886751	75.50982552	34.59375	821.7899379
36	51.7660345	-0.300519528	179.8585822	180.159102	1800.01	99.58114381	75.47599191	34.59375	821.7303404
37	51.974534	-0.300953111	193.5204787	193.821432	1800.018	99.48838779	74.90774819	34.53125	821.5055862
38	52.0252673	-0.297503753	193.6658933	193.963397	1799.978	99.50351172	74.89746913	34.53125	821.4977871
39	52.0933978	-0.297780031	193.5327626	193.830543	1800.036	99.50449336	74.87160834	34.53125	821.4938996
40	52.1487803	-0.299728454	193.6413706	193.941099	1799.984	99.49138398	74.90403293	34.53125	821.4545159
41	52.2819505	-0.296675482	207.3810857	207.677761	1800.008	99.4155007	74.35336837	34.6484375	821.3892845
42	52.3294292	-0.294860855	207.4208787	207.71574	1799.995	99.42355026	74.33529088	34.59375	821.3222657
43	52.3867542	-0.294563156	207.3952796	207.689843	1800.023	99.42346555	74.29628914	34.59375	821.2734233
44	52.420999	-0.296803052	207.4116353	207.708438	1799.979	99.3946783	74.31650003	34.59375	821.2145552

Table A2 - Data Collected for ISO 8426 Method at 1800 RPM and 80 °C.

Line #	Inlet Temperature [C]	Low Pressure [bar] See Note 2	High Pressure [bar] See Note 2	Delta Pressure [bar]	Shaft Speed [rpm]	Displacement [%] See Note 1	High Pressure Flow [Lpm]	Inlet Viscosity [cSt or cP] See Note 2 & 3	Inlet Density [kg/m^3] See Note 2 & 3
1	80.415726	-0.212041871	69.35212995	69.5641718	1800.001	98.30436142	80.2283265	14.984375	804.125868
2	80.3824903	-0.209182448	69.37422743	69.5834099	1799.999	98.32661547	80.23422242	14.984375	804.0598005
3	80.354514	-0.210399257	69.3903402	69.6007395	1800.004	98.33161762	80.21637443	14.984375	804.0779122
4	80.3408558	-0.212303512	69.3253187	69.5376222	1800.002	98.33389002	80.23496989	14.984375	804.1135561
5	80.2912695	-0.209200191	83.16524412	83.3744443	1800.007	98.41467427	79.53106753	14.984375	804.0014783
6	80.307276	-0.209215598	83.18452244	83.393738	1800.007	98.4191559	79.51188387	14.8984375	804.1565028
7	80.3052428	-0.208769937	83.20615922	83.4149292	1800.004	98.42317908	79.52653577	14.8984375	804.0916878
8	80.295428	-0.209609982	83.17593918	83.3855492	1800.005	98.41737114	79.51746619	14.8984375	804.0885942
9	80.2824919	-0.210179888	96.96376623	97.1739461	1800.005	98.45226963	78.88409285	14.8984375	804.1209796
10	80.2849067	-0.207701223	96.99828623	97.2059875	1800.009	98.46821117	78.8698359	14.7734375	804.1040241
11	80.2875533	-0.207262057	96.98073332	97.1879954	1799.975	98.46676872	78.85926844	14.7734375	804.0673021
12	80.2852897	-0.210068794	96.93794575	97.1480145	1800.02	98.44907313	78.87401133	14.7734375	804.1262331
13	80.2837006	-0.209343116	110.7946761	111.004019	1799.975	98.47992451	78.26979131	14.8828125	804.188906
14	80.3135344	-0.207103356	110.7959763	111.00308	1800.023	98.48689447	78.27144811	14.8828125	804.1687735
15	80.3507396	-0.209449267	110.7254096	110.934859	1800.002	98.4721413	78.28102617	15.0078125	804.1706694
16	80.3576684	-0.206436368	110.796346	111.002782	1799.982	98.48058055	78.27057077	15.0078125	804.0635971
17	80.3423418	-0.208759678	124.5492217	124.757981	1799.981	98.48892878	77.68136742	15.0078125	804.0580333
18	80.373084	-0.206448943	124.6425002	124.848949	1799.992	98.49317002	77.67558746	15.0078125	804.0693057
19	80.3948124	-0.205447413	124.5551869	124.760634	1799.996	98.48848928	77.65990611	15.0078125	804.0371265
20	80.3935131	-0.208449413	124.5724252	124.780875	1800.016	98.46911425	77.67846397	15.0546875	804.1112056
21	80.4040575	-0.206699871	138.3410594	138.547759	1800.005	98.4817522	77.06633667	15.0546875	804.0523923
22	80.4137695	-0.204762835	138.3917201	138.596483	1799.97	98.48490725	77.06302266	15.0859375	804.1206507
23	80.4360983	-0.207118119	138.4201685	138.627287	1799.992	98.46928188	77.05278251	15.0859375	804.0380107
24	80.4434861	-0.204553054	138.3297031	138.534256	1800.04	98.47559808	77.06085799	15.0859375	804.0560915
25	80.4661762	-0.203129683	152.2831751	152.486305	1799.963	98.48083712	76.47030512	15.0859375	804.0712086
26	80.4813701	-0.204356132	152.1869942	152.39135	1800.017	98.46034516	76.47927509	15.0859375	804.0944893
27	80.5358707	-0.20261677	152.1573285	152.359945	1800.033	98.4653783	76.46413628	15.09375	804.0988086
28	80.5686091	-0.204870585	152.2337509	152.438622	1799.984	98.44320135	76.45881062	15.09375	803.9878704
29	80.5670011	-0.200976544	166.0469582	166.247935	1800.001	98.4544686	75.84872371	15.1328125	803.9882553
30	80.6006924	-0.203137252	166.055328	166.258465	1800.006	98.43537337	75.85389651	15.1328125	804.0224679
31	80.6365045	-0.204104961	166.0226154	166.22672	1800.007	98.41832973	75.84963918	15.1328125	803.9185175
32	80.6464072	-0.202940723	165.9003024	166.103243	1800.021	98.42137486	75.87803786	15.1328125	803.8757829
33	80.6684419	-0.202082692	179.7191586	179.921241	1800.001	98.41497176	75.28474818	15.1328125	803.9254469
34	80.6680897	-0.202785418	179.7126352	179.915421	1800.017	98.39524743	75.28629452	15.046875	803.9288839
35	80.6962103	-0.201479899	179.7416819	179.943162	1799.985	98.39730591	75.28488514	15.046875	803.8541453
36	80.7362066	-0.200352975	179.8633407	180.063694	1800.003	98.39949465	75.26201703	15.0078125	803.8654082
37	80.8005232	-0.199564217	193.6121434	193.811708	1800.023	98.38826549	74.73320491	15.0078125	803.7943195
38	80.8236866	-0.199235461	193.5987895	193.798025	1799.987	98.37839354	74.70668852	15.0078125	803.6818005
39	80.8508943	-0.198961684	193.6125954	193.811557	1800.004	98.37076247	74.72619372	15.0078125	803.73578
40	80.8731335	-0.199267572	193.4932735	193.692541	1799.995	98.3600026	74.73373353	15.0078125	803.7438632
41	80.8812122	-0.199890102	207.3327966	207.532687	1799.991	98.3481223	74.19429517	14.96875	803.7529598
42	80.9214974	-0.200001871	207.4063359	207.606338	1800.027	98.33503317	74.16815254	14.96875	803.7644049
43	80.9752483	-0.198892398	207.3527969	207.551689	1800.018	98.33535432	74.19631033	14.96875	803.7458082
44	81.0000155	-0.197607166	207.3990651	207.596672	1799.982	98.33828812	74.17760578	14.96875	803.7263871

Table A3 - Data Collected for ISO 8426 Method at 2400 RPM and 50 °C.

Line #	Inlet Temperature [C]	Low Pressure [bar] See Note 2	High Pressure [bar] See Note 2	Delta Pressure [bar]	Shaft Speed [rpm]	Displacement [%] See Note 1	High Pressure Flow [Lpm]	Inlet Viscosity [cSt or cP] See Note 2 & 3	Inlet Density [kg/m^3] See Note 2 & 3
1	50.9807878	-0.4408806	69.34144009	69.7823207	2398.457	99.41140105	94.59249471	28.984375	822.0636465
2	51.2012746	-0.438230341	69.33676355	69.7749939	2398.463	99.42102966	94.68635808	28.984375	821.9602337
3	51.4096735	-0.439499197	69.35272687	69.7922261	2398.452	99.40676396	94.71312443	35.296875	821.8510948
4	51.5442109	-0.437503724	69.35700296	69.7945067	2398.498	99.4216405	94.75515019	35.296875	821.7158682
5	51.4684445	-0.439588397	83.14517672	83.5847651	2398.272	99.37679075	94.23582334	35.296875	821.7013953
6	51.4731265	-0.4373707	83.17601918	83.6133899	2398.186	99.38080158	94.19790332	35.296875	821.7285115
7	51.4807485	-0.436546249	83.17792059	83.6144668	2398.28	99.38013354	94.20945482	35.296875	821.7127914
8	51.4460717	-0.439491639	83.17991891	83.6194106	2398.486	99.36548544	94.2041486	32.5078125	821.744252
9	51.1743784	-0.437291707	96.99164267	97.4289344	2397.932	99.33413264	93.54836187	32.5078125	821.9631744
10	51.2211858	-0.439598566	96.91175401	97.3513526	2397.842	99.32136425	93.61322971	32.5078125	821.9116211
11	51.3163696	-0.436977563	97.04264839	97.479626	2397.983	99.33315304	93.66775395	32.5078125	821.8980023
12	51.392179	-0.439379218	96.95594507	97.3953243	2397.827	99.31670289	93.70452699	32.5078125	821.8213092
13	51.4281126	-0.436599926	110.7348855	111.171485	2397.903	99.22645269	93.20589411	33.21875	821.7582047
14	51.4588576	-0.435091467	110.8455861	111.280678	2398.02	99.23289617	93.22913283	34.453125	821.7526768
15	51.5017367	-0.436660909	110.7739489	111.21061	2397.855	99.22467449	93.22742389	34.453125	821.7509825
16	51.5178998	-0.438335792	110.7652882	111.203624	2397.809	99.21428581	93.2939113	34.453125	821.6876661
17	51.3871428	-0.43743989	124.5079178	124.945358	2397.454	99.12986358	92.77340031	34.453125	821.7861004
18	51.4187883	-0.436451386	124.5160236	124.952475	2397.704	99.12894308	92.71454493	34.453125	821.8189358
19	51.4881988	-0.437232566	124.6113444	125.048577	2397.74	99.13002233	92.82568227	34.9921875	821.7954897
20	51.5524466	-0.434071679	124.6532881	125.08736	2397.67	99.14467114	92.78871575	34.6953125	821.7112371
21	51.4805072	-0.435238011	138.3815627	138.816801	2397.247	99.05454892	92.31723467	34.6953125	821.7258925
22	51.5034925	-0.432302845	138.4073845	138.839687	2397.141	99.08092988	92.31525773	34.6953125	821.7647218
23	51.5434114	-0.435053044	138.4413002	138.876353	2397.379	99.06903704	92.29312872	34.6953125	821.7139844
24	51.5696864	-0.432277561	138.4727808	138.905058	2397.051	99.06959082	92.28888595	34.6953125	821.6995399
25	51.4973093	-0.433552569	152.1996087	152.633161	2397.677	98.98335865	91.73313746	34.6953125	821.6712285
26	51.5287527	-0.434516162	152.1330901	152.567606	2397.715	98.9761654	91.79626508	34.4921875	821.7173929
27	51.6153108	-0.433145203	152.1912439	152.624389	2397.623	98.97795116	91.84084773	34.4921875	821.6642397
28	51.6783801	-0.432781835	152.2517616	152.684543	2397.34	98.98120322	91.87358118	34.4921875	821.6051858
29	51.6483089	-0.431705311	165.9829868	166.414692	2397.183	98.911757	91.3933316	34.25	821.6302929
30	51.6844716	-0.429054256	166.017872	166.446926	2397.411	98.92648897	91.37763869	34.25	821.604185
31	51.7445093	-0.430575021	165.9754949	166.40607	2397.173	98.91082642	91.38214058	34.25	821.5875787
32	51.7961336	-0.428886488	166.0700939	166.49898	2397.244	98.91467943	91.39927232	34.25	821.5500821
33	51.7915704	-0.428955263	179.7788487	180.207804	2396.263	98.89342104	90.89349053	34.6640625	821.5087575
34	51.8375112	-0.430074357	179.8032036	180.233278	2396.615	98.8904416	90.93188924	34.9375	821.4409044
35	51.9023699	-0.427803797	179.8533446	180.281148	2397.032	98.91038522	90.93219388	34.9375	821.508896
36	51.966598	-0.427518191	179.7620511	180.189569	2397.017	98.91161749	90.96318686	34.9375	821.5017978
37	52.0619342	-0.427637753	193.5392567	193.966894	2397.135	98.88413659	90.5088	34.9375	821.395371
38	52.1114288	-0.424021457	193.7305361	194.154558	2396.271	98.90645188	90.55179681	34.9375	821.3884661
39	52.1912064	-0.42652942	193.6305829	194.057112	2396.893	98.89005252	90.56971603	34.25	821.2884742
40	52.2496258	-0.426896471	193.6838102	194.110707	2396.836	98.88976382	90.58285016	34.25	821.3049534
41	52.3495526	-0.424735697	207.4334187	207.858154	2397.485	98.83501614	90.074943	34.25	821.206157
42	52.4210032	-0.425415749	207.3966889	207.822105	2397.054	98.82457529	90.12272819	34.0078125	821.2153089
43	52.5223731	-0.421636369	207.4090672	207.830704	2397.027	98.85178085	90.1463783	34.0078125	821.0728531
44	52.6072113	-0.42220745	207.4366745	207.858882	2396.871	98.83718176	90.2435057	34.0078125	821.0836677

Table A4 - Data Collected for ISO 8426 Method at 2400 RPM and 80 °C.

Line #	Inlet Temperature [C]	Low Pressure [bar] See Note 2	High Pressure [bar] See Note 2	Delta Pressure [bar]	Shaft Speed [rpm]	Displacement [%] See Note 1	High Pressure Flow [Lpm]	Inlet Viscosity [cSt or cP] See Note 2 & 3	Inlet Density [kg/m^3] See Note 2 & 3
1	80.5259587	-0.352405537	69.34626485	69.6986704	2398.399	98.24586954	103.0990215		803.8347259
2	80.3464182	-0.355101154	69.35586645	69.7109676	2398.197	98.23774227	103.0600259		803.9203225
3	80.2432707	-0.356606713	69.33738748	69.6939942	2398.548	98.24143398	103.0367105		803.968466
4	80.1884288	-0.353617822	69.3763971	69.7300149	2398.562	98.25894148	103.0566868		804.017623
5	80.2799458	-0.352623323	83.16625231	83.5188756	2398.351	98.28295464	102.2650649		804.043426
6	80.2565439	-0.354544822	83.18205426	83.5365991	2398.355	98.27647631	102.2496446		803.9713685
7	80.2498498	-0.354933755	83.17505801	83.5299918	2398.292	98.27483229	102.2454041		803.9852835
8	80.2607504	-0.352189641	83.21605847	83.5682481	2398.335	98.28840891	102.2626917		804.0461963
9	80.2963611	-0.350053571	97.02491152	97.3749651	2398.461	98.31438348	101.1469445		804.0085158
10	80.3467349	-0.349758747	97.02734671	97.3771055	2398.442	98.31344363	101.1359113		804.0354499
11	80.3781849	-0.351195017	96.94897815	97.3001732	2398.241	98.29864293	101.1245333		804.0446518
12	80.3573284	-0.349673058	97.00744906	97.3571221	2398.321	98.3067714	101.1148107		804.0327508
13	80.3225049	-0.348704168	110.7877463	111.13645	2398.356	98.32439881	100.0966399		804.089815
14	80.3591224	-0.348403777	110.7448028	111.093207	2398.268	98.31616477	100.0863478		803.9856327
15	80.4160343	-0.348315827	110.7255556	111.073871	2398.293	98.30911271	100.0927046		803.9735167
16	80.4187622	-0.345639806	110.8019814	111.147621	2398.258	98.31736769	100.0992454		804.0192682
17	80.3561057	-0.343419809	124.6093465	124.952766	2397.805	98.33504224	99.18498757		804.0038497
18	80.3874835	-0.343190536	124.6819146	125.025105	2397.75	98.32663136	99.18759844		803.9943087
19	80.4509243	-0.343462237	124.5895052	124.932967	2397.769	98.32565555	99.17798435		804.0093147
20	80.4619113	-0.344450222	124.5749989	124.919449	2397.888	98.31256722	99.19825815		803.9716979
21	80.4423603	-0.341277696	138.3995799	138.740858	2397.597	98.3220998	98.41903399		803.942992
22	80.4874785	-0.341124882	138.3793568	138.720482	2397.209	98.31613034	98.41299887		803.8989816
23	80.5279545	-0.343355336	138.3579069	138.701262	2397.837	98.29979829	98.46275762		803.9506843
24	80.5182878	-0.34036368	138.3956246	138.735988	2397.583	98.30595538	98.42293149		803.9738339
25	80.5050238	-0.340676605	152.1728609	152.513537	2397.952	98.29759801	97.76337355		803.9480147
26	80.5437133	-0.341768611	152.0458083	152.387577	2397.853	98.28207293	97.72190121		803.9197282
27	80.610813	-0.339712896	152.0865951	152.426308	2397.774	98.28600256	97.74752778		803.9662404
28	80.6354202	-0.339126216	152.1726358	152.511762	2397.866	98.28322329	97.71095482		803.9090446
29	80.5795168	-0.339141739	165.8913227	166.230464	2397.393	98.27126305	97.1105343		803.8445017
30	80.6305227	-0.340121098	165.9053027	166.245424	2397.198	98.25467186	97.08235845		803.8448191
31	80.7055976	-0.33697716	165.9855409	166.322518	2397.785	98.26262393	97.135692		803.7935145
32	80.740299	-0.338894305	166.0381006	166.376995	2397.099	98.24411936	97.12236473		803.8207551
33	80.629628	-0.337302045	179.8877397	180.225042	2396.628	98.22281468	96.50409206		803.8714761
34	80.708759	-0.338710461	179.8028858	180.141596	2397.174	98.20376918	96.49640386		803.8253324
35	80.7651345	-0.336403402	179.8390695	180.175473	2397.023	98.21216391	96.51162603		803.77188
36	80.7959134	-0.335159612	179.7529226	180.088082	2397.35	98.20755334	96.4979795		803.7762979
37	80.7832563	-0.333949461	193.578571	193.91252	2396.396	98.19627093	96.00000455		803.739902
38	80.8056916	-0.334631506	193.571003	193.905634	2397.51	98.18120879	96.02167277		803.7625478
39	80.837409	-0.336914987	193.6244103	193.961325	2396.958	98.16221163	95.97714228		803.7952283
40	80.8346056	-0.333922835	193.6883365	194.022259	2397.179	98.1756711	95.9835346		803.7740587
41	80.8570081	-0.334417886	207.340961	207.675379	2396.455	98.16520922	95.51197694		803.703578
42	80.9180923	-0.333209084	207.3887706	207.72198	2396.98	98.16416251	95.51204493		803.7268395
43	81.0109452	-0.335281024	207.4702354	207.805516	2397.108	98.14413413	95.55341831		803.7094114
44	81.0165406	-0.335720935	207.3484102	207.684131	2397.207	98.1303844	95.53565448		803.6459839

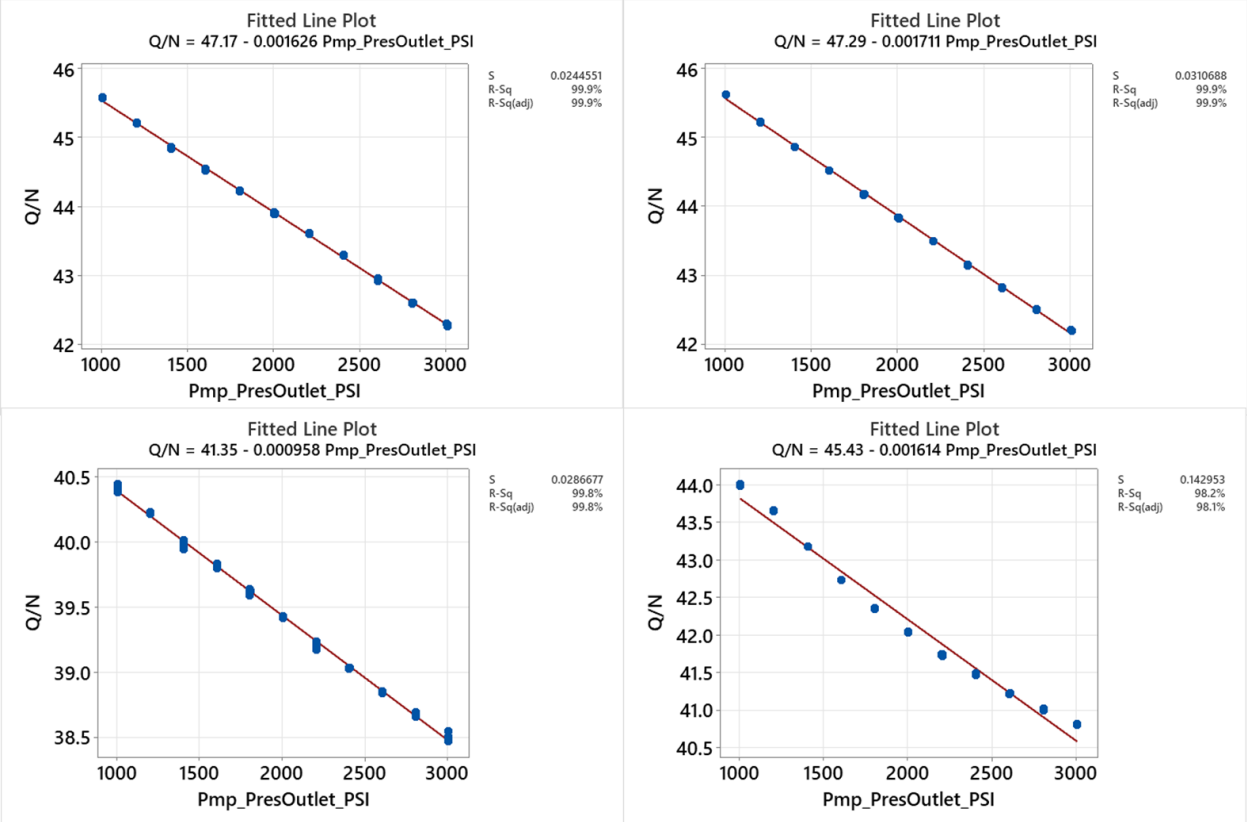

Figure A1 - Pump Flow / Rotational Frequency versus Outlet Pressure at Different ISO 8426 Dynamometer Settings.

Table A5 - Data Collected for the Toet Method at 50 °C.

Line #	Inlet Temperature [C]	Low Pressure [bar]	High Pressure [bar]	Delta Pressure [bar]	Shaft Speed [rpm]	Displacement [%]	High Pressure Flow [Lpm]	Inlet Viscosity [cSt or cP]	Inlet Density [kg/m^3]
1	51.13409154	-0.461026131	41.75804704	42.219073	2398.61	99.46927978	96.49835212	34.95507813	822.2398596
2	51.67917059	-0.45795735	83.19934076	83.657298	2398.29	99.32053114	94.81162202	35.3046875	821.8786079
3	51.74693613	-0.458173041	124.5929528	125.05113	2397.61	99.14713266	93.41000439	35.11523438	821.8556175
4	51.96883263	-0.454375059	165.9621627	166.41654	2397.42	98.92050075	92.0160914	34.44140625	821.688837
5	52.50052625	-0.44812696	207.4400315	207.88816	2397.16	98.7319155	90.72996598	34.1015625	821.3541798
6	49.57422373	-0.341251441	41.75914452	42.100396	2398.42	75.59416694	80.54633493	33.97265625	822.9590722
7	51.80859017	-0.319891351	83.16350981	83.483401	2398.51	75.09653965	77.96705064	33.640625	821.814316
8	52.16069855	-0.30785775	124.5690146	124.87687	2398	74.72413744	75.5910604	33.58203125	821.5824299
9	52.34772926	-0.29572156	165.9714364	166.26716	2397.95	74.34785029	73.16241331	36.35546875	821.4912342
10	52.64141828	-0.285875501	207.424648	207.71052	2397.99	74.18043398	70.95938714	33.71875	821.3198982
11	51.10412398	-0.143857991	41.74036079	41.884219	2398.5	50.71154724	53.42556482	33.61523438	822.237442
12	52.55642405	-0.129479076	83.17399707	83.303476	2398.57	50.12076139	50.62940378	34.41210938	821.3433172
13	52.66621074	-0.121552041	124.5609126	124.68246	2398.32	49.75800592	48.19835935	33.66992188	821.3052239
14	53.14490736	-0.112596637	165.9924536	166.10505	2398.12	49.48821749	46.05394019	33.3203125	821.0464812
15	53.84470334	-0.105957902	207.3703038	207.47626	2398.26	49.31015346	44.23493054	32.91796875	820.5516881
16	53.5451738	0.001450358	41.73736733	41.735917	2398.64	25.70523364	26.12995245	31.9453125	820.806324
17	53.11895488	0.007520683	83.15471075	83.14719	2398.6	25.15086955	23.57989954	32.75	820.8471721
18	52.90843251	0.012057707	124.5569872	124.54493	2398.49	24.79177685	21.22382913	32.74023438	820.9017163
19	53.27695707	0.015732037	165.9691694	165.95344	2398.35	24.56659766	19.19614548	32.02929688	820.6629227
20	53.67821328	0.019007262	207.3317028	207.3127	2398.46	24.31040429	17.22911515	31.390625	820.445609
21	52.02456972	-0.399601025	41.74886591	42.148467	1999.99	99.29087545	90.20951041	31.1171875	821.4232929
22	51.56154349	-0.399617796	83.19392541	83.593543	2000.07	99.56843076	87.78174203	35.10546875	821.8770256
23	51.58994104	-0.395449175	124.5697557	124.9652	2000	99.63610141	86.21948831	34.34375	821.8353037
24	51.83807758	-0.384848614	165.9957536	166.3806	2000	99.45344227	84.11499653	34.23242188	821.7087786
25	52.12800892	-0.373070839	207.4079368	207.78101	2000	99.15052494	82.03978707	34.93945313	821.5383769
26	50.12138781	-0.236728668	41.746814	41.983543	1999.99	75.7195465	67.57740355	36.52929688	822.7872019
27	51.69437155	-0.219252717	83.15658838	83.375841	2000	75.16308389	64.75815367	33.90625	821.9565609
28	51.92669041	-0.211409275	124.5833255	124.79473	2000	74.82345223	62.69663358	34.234375	821.7484086
29	52.28452917	-0.202991153	166.0017196	166.20471	2000	74.56677186	60.75430707	33.86523438	821.5718381
30	52.4981993	-0.196103105	207.3818018	207.5779	2000	74.39092978	58.93638409	33.83007813	821.4579877
31	51.88469333	-0.082378365	41.74167947	41.824058	2000	50.72331844	44.18173691	33.34765625	821.8109974
32	52.35491775	-0.073932885	83.18243941	83.256372	2000	50.18517571	41.69292006	32.6328125	821.5420324
33	52.76197079	-0.067943087	124.5862635	124.65421	2000.01	49.82944249	39.50708722	31.62890625	821.284677
34	53.49649101	-0.055389445	165.9373178	165.99271	2000	49.60782422	37.63956042	31.71679688	820.8494976
35	54.16519954	-0.051748297	207.3857772	207.43753	2000	49.42935448	35.86756106	33.08203125	820.4465357
36	54.10516624	0.024643604	41.74430502	41.719661	2000	25.74445605	21.4655334	33.265625	820.3926751
37	53.10183061	0.029281255	83.16712604	83.137845	2000	25.18672729	19.10405872	32.02734375	821.0680109
38	52.45830651	0.030546148	124.5629026	124.53236	2000	24.8227496	16.8948755	32.40429688	821.5855932
39	53.48215758	0.035298315	165.9588417	165.92354	2000	24.64777776	15.03034977	34.97265625	821.00969
40	53.80138728	0.039311575	207.3940126	207.3547	2000	24.39842609	13.19742929	34.72070313	820.8120015
41	53.71030483	-0.250047634	41.77324428	42.023292	1600	99.36355964	72.52699098	34.296875	820.5424649
42	51.65365408	-0.25636987	83.16626952	83.422639	1600	99.6034241	70.48878719	34.48828125	821.8969588
43	51.66913431	-0.252144196	124.5686107	124.82075	1600	99.72109622	68.85494608	34.8359375	821.8827084
44	51.98361879	-0.247625328	166.0025795	166.2502	1600	99.67229974	67.29432429	34.171875	821.6892278
45	52.17980278	-0.242826619	207.4005024	207.64333	1600	99.54018406	65.72403152	33.76757813	821.5672314
46	51.0779718	-0.138845985	41.75747799	41.896324	1600	75.67662483	53.63927928	33.0703125	822.2071309
47	51.91103242	-0.128220521	83.18228393	83.310504	1600	75.19151895	51.10293495	34.1796875	821.6901943
48	52.01580461	-0.120880807	124.5500613	124.67094	1600	74.84635727	49.20789066	34.09179688	821.6703862
49	52.36069799	-0.117385563	165.9877735	166.10516	1600	74.61915044	47.56997343	33.73046875	821.4701226
50	53.09711742	-0.111596236	207.3857261	207.49732	1600	74.42998906	45.91635848	33.16601563	821.0050594

51	52.57864485	-0.030072358	41.75978763	41.78986	1600	50.72145198	34.91824724	33.47070313	821.4638897
52	52.15524443	-0.025858573	83.17640884	83.202267	1600	50.21204307	32.55640929	34.3515625	821.7258506
53	52.0460087	-0.022734364	124.5830443	124.60578	1600	49.8660747	30.62895222	33.70703125	821.8046108
54	52.2629954	-0.019607061	165.9900353	166.00964	1600	49.64848789	28.91696266	32.67382813	821.6832118
55	52.42945684	-0.013441841	207.3778694	207.39131	1600	49.44528208	27.24660765	32.0859375	821.5927527
56	51.9927505	0.041748407	41.75324821	41.7115	1600	25.75317516	16.77742924	31.50976563	821.6017861
57	51.38066037	0.044306051	83.15847836	83.114172	1600	25.23873995	14.70307728	33.7578125	821.90544
58	52.02734175	0.047464409	124.5861921	124.53873	1600	24.91292751	12.67978554	34.7734375	821.5483304
59	52.34674701	0.052112531	165.9844224	165.93231	1600	24.68941276	10.89046509	35.47070313	821.3301087
60	52.71741628	0.052750019	207.3674776	207.31473	1600	24.44148679	9.12833572	35.21484375	821.1778532
61	51.1119867	-0.136318156	41.77356581	41.909884	1200	99.76434516	54.05627672	34.3046875	822.2118008
62	51.2024714	-0.133415111	83.17796492	83.31138	1200	99.83200792	52.15645862	33.65429688	822.1604361
63	51.67525103	-0.130796674	124.5540806	124.68488	1200	99.8643164	50.57127767	33.66601563	821.8818994
64	52.0489357	-0.126541669	165.9715051	166.09805	1200.01	99.77931907	49.07537493	33.93359375	821.6183881
65	52.63200857	-0.12039858	207.3705741	207.49097	1200	99.5991485	47.58451392	33.9765625	821.2601126
66	51.88370613	-0.056255114	41.75833446	41.81459	1200	75.68710349	39.6806869	33.20117188	821.8104487
67	51.96427606	-0.051618455	83.17875355	83.230372	1200	75.24518496	37.44465319	32.88671875	821.7407841
68	52.09811545	-0.048607517	124.5889643	124.63757	1200	74.96799407	35.77416215	33.25390625	821.6934398
69	52.233429	-0.045493198	165.9724168	166.01791	1200	74.7439168	34.29891375	33.61132813	821.5972942
70	52.61591481	-0.040581513	207.4009313	207.44151	1200	74.51427534	32.76195048	34.14453125	821.3464732
71	52.83425698	0.008575493	41.7522972	41.743722	1200	50.74305286	25.69457218	33.94726563	821.283693
72	52.16258535	0.011456701	83.16721836	83.155762	1200	50.2709121	23.6093245	33.94335938	821.5014439
73	52.12416967	0.013985865	124.5779442	124.56396	1200	49.98175609	21.87193075	34.31835938	821.4293779
74	52.2702539	0.016541452	166.0034122	165.98687	1200	49.73699994	20.29590853	32.94726563	821.3403205
75	52.48929585	0.019803065	207.4055976	207.38579	1200	49.52867789	18.78286655	32.06835938	821.1456961
76	52.66982271	0.055437706	41.75436768	41.69893	1200	25.82088741	12.07902611	30.2421875	821.2647246
77	50.32980118	0.056366315	83.14736941	83.091003	1200	25.33681661	10.32474334	29.1015625	823.023938
78	51.29807626	0.059087463	124.5862624	124.52717	1200	25.06169217	8.528940502	28.5546875	822.09682
79	52.06012479	0.062909467	166.0412241	165.97831	1200	24.83911988	6.858640409	27.6875	821.4945646
80	52.66194672	0.063319768	207.4489389	207.38562	1200	24.59332176	5.213763961	27.18164063	821.210735
81	57.82161352	-0.293006282	41.79642539	42.089432	1800	99.05941706	81.75127581	26.6171875	817.7713488
82	49.97047474	-0.336307214	83.15666685	83.492974	1800	99.48664208	79.65026308	25.82421875	822.9335945
83	51.97619117	-0.320236769	124.5580334	124.87827	1800	99.65530788	77.94151067	25.69726563	821.5486758
84	51.88996922	-0.316503089	166.0200567	166.33656	1800	99.65237303	76.37218442	25.06054688	821.6957315
85	52.16639256	-0.309754684	207.3842565	207.69401	1800	99.49244983	74.62382124	25.4453125	821.5138252
86	50.80179011	-0.183697551	41.74671771	41.930415	1799.99	75.74550986	60.66901768	34.05859375	822.4062549
87	52.00317831	-0.168907063	83.16422739	83.333134	1800	75.22211947	58.08141004	35.734375	821.7247201
88	51.82060722	-0.164220708	124.5714707	124.73569	1800	74.8671732	56.00528727	33.71484375	821.8743932
89	52.15242384	-0.15866216	165.9575504	166.11621	1799.99	74.60483085	54.23936941	33.64257813	821.6558497
90	52.61752226	-0.151893338	207.3573774	207.50927	1800	74.45574754	52.60360465	34.09765625	821.33735
91	52.01173169	-0.053508241	41.74572154	41.79923	1800	50.72773224	39.53940945	34.24609375	821.7096683
92	52.30470526	-0.047561162	83.18149673	83.229058	1800	50.19976241	37.17694329	33.64453125	821.6315862
93	52.50782499	-0.043137965	124.5720729	124.61521	1800	49.83555393	35.05421494	32.80859375	821.4917652
94	52.79387255	-0.039355458	166.0011465	166.0405	1800	49.61923048	33.26023766	33.71679688	821.3511243
95	53.1209836	-0.036235229	207.3718319	207.40807	1800	49.44270347	31.57572919	33.44921875	821.1234556
96	53.32812558	0.034573737	41.7508914	41.716318	1800	25.76273643	19.11244476	33.25	821.0335197
97	52.14499441	0.037661428	83.16125395	83.123593	1800	25.23860736	16.96696143	32.65234375	821.6803901
98	52.02235992	0.040033172	124.573172	124.53314	1800.01	24.89350379	14.87181779	32.59960938	821.5934784
99	51.92898699	0.044569892	165.9825874	165.93802	1800.01	24.67821252	13.02699862	33.453125	821.3975673
100	52.46157727	0.045595686	207.3867418	207.34115	1800	24.43285684	11.22075664	33.8671875	821.1373466

Table A6 - Data Collected for the Toet Method at 80 °C.

Line #	Inlet Temperature [C]	Low Pressure [bar]	High Pressure [bar]	Delta Pressure [bar]	Shaft Speed [rpm]	Displacement [%]	High Pressure Flow [Lpm]	Inlet Viscosity [cSt or cP]	Inlet Density [kg/m^3]
1	81.23801171	-0.373385747	41.73776095	42.111147	2398.66	98.37738964	105.6536585	17.4453125	803.6931958
2	81.09895122	-0.363721284	83.19094805	83.554669	2397.99	98.47493696	102.3483946	17.4453125	803.4998647
3	80.5262687	-0.358148629	124.591913	124.95006	2397.41	98.5409879	99.28256501	17.4453125	803.6331256
4	80.24955694	-0.354522588	166.0490523	166.40357	2397.18	98.54017747	97.17337749	17.4453125	803.7629326
5	80.24603151	-0.349151356	207.4264553	207.77561	2397.14	98.52788686	95.67992063	15.9296875	803.8958646
6	80.43188961	-0.228070146	41.7776159	42.005686	2399.37	75.78122036	81.97982831	15.9296875	803.8340655
7	80.46195984	-0.221272665	83.18050881	83.401781	2397.53	75.02958375	78.4031206	15.9296875	803.8814962
8	79.83356779	-0.211777304	124.5378389	124.74962	2397.7	74.64729158	75.09280061	15.9296875	804.1067736
9	79.75854476	-0.20206754	166.0546709	166.25674	2397.88	74.39333792	72.36199513	15.9296875	804.151383
10	80.05836036	-0.192553502	207.3566748	207.54923	2397.72	74.09128994	69.28982379	15.9296875	804.1241547
11	80.23189819	-0.086144099	41.74466331	41.830807	2398.8	50.7877262	53.78728177	15.9296875	804.0012916
12	80.42457274	-0.07980954	83.14569083	83.2255	2397.49	50.08947631	50.47890706	15.9296875	803.9311859
13	80.42158682	-0.074282346	124.5611551	124.63544	2398.28	49.75629316	47.79766982	14.9140625	803.8756079
14	80.25556154	-0.070075924	166.1135201	166.1836	2397.99	49.5607794	45.65807658	14.9140625	803.8832691
15	80.23794756	-0.066390219	207.5348293	207.60122	2398.32	49.39446724	43.76468811	14.9140625	803.8779654
16	80.39675054	0.014760069	41.75094255	41.736182	2398.28	25.76217252	26.2730769	14.9140625	803.694848
17	80.34864329	0.017219019	83.15789724	83.140678	2398.38	25.0941286	23.29623198	14.9140625	803.6767993
18	80.59078332	0.021693409	124.5160327	124.49434	2398.63	24.80984029	20.81444505	14.9140625	803.5780908
19	80.77148406	0.024918576	165.8709389	165.84602	2398.25	24.55557688	18.4792436	15.140625	803.4307867
20	80.86898627	0.027491662	207.3470928	207.3196	2398.54	24.34762514	16.40962134	15.140625	803.4857617
21	81.50031669	-0.278081277	41.79553909	42.07362	1999.87	98.09496564	90.59642101	15.140625	803.5350485
22	82.30322119	-0.270705177	83.16941794	83.440123	1998.84	98.29350437	88.35822954	15.140625	803.1694668
23	82.28135004	-0.267617347	124.564331	124.83195	1998.91	98.43350232	86.38773582	15.140625	802.9985844
24	81.78018263	-0.268560325	165.9620885	166.23065	1998.93	98.46831524	84.42716568	15.140625	803.0640163
25	81.34858307	-0.262070894	207.3391538	207.60122	1998.95	98.48445095	82.20477304	15.140625	803.3168442
26	81.13742056	-0.153159885	41.78345367	41.936614	2004.56	75.80504375	68.35321046	15.140625	803.4517239
27	81.07104864	-0.148839565	83.1773153	83.326155	1999.16	75.1131292	64.91537209	15.109375	803.5979454
28	80.54247586	-0.145276252	124.5650764	124.71035	1999.2	74.80284903	62.57250881	15.109375	803.8592436
29	80.23001168	-0.138073299	166.0084342	166.14651	1999.2	74.62171377	60.40671837	15.1328125	804.1127209
30	80.33734976	-0.133043878	207.3900242	207.52307	1999.22	74.42637801	58.41293456	15.1328125	804.0251479
31	80.48393285	-0.048093734	41.76314045	41.811234	2003.4	50.77917435	44.54066287	15.1328125	803.963082
32	80.61092483	-0.043379985	83.17561269	83.218993	1999.47	50.11741239	41.48700952	15.1328125	803.7841336
33	80.64680907	-0.039550475	124.5036147	124.54317	1999.45	49.80693494	39.11653601	14.8515625	803.6785084
34	80.61513839	-0.03460799	166.0512693	166.08588	1999.46	49.62588304	37.08303167	14.8515625	803.6436129
35	80.59746722	-0.032039802	207.4163238	207.44836	1999.47	49.4097794	35.04929935	14.8515625	803.7541284
36	80.57088001	0.028450762	41.77058318	41.742132	2002.3	25.79494919	21.60704757	14.8515625	803.730828
37	80.50177468	0.029204093	83.15590817	83.126704	1999.75	25.13746176	18.84538411	14.6171875	803.6229938
38	80.65314825	0.031785232	124.5730385	124.54125	1999.75	24.85590357	16.52238754	14.6171875	803.5533424
39	80.6861673	0.033944803	166.0015578	165.96761	1999.72	24.6430006	14.379559	14.6171875	803.5137243
40	80.76278775	0.036434187	207.3150317	207.2786	1999.75	24.43327548	12.37605201	14.6171875	803.4663455
41	81.42014517	-0.17172291	41.80055819	41.972281	1600	98.13331512	72.47455095	14.875	803.5162684
42	82.23774019	-0.169791754	83.18299648	83.352788	1598.96	98.297036	70.18300051	14.875	803.1400143
43	82.41033834	-0.166191818	124.5620301	124.72822	1599.02	98.44597146	68.27282026	14.875	803.0213017
44	82.08947468	-0.161940329	166.0447775	166.20672	1599.02	98.51716953	66.56625025	14.875	803.0072977
45	81.66312145	-0.162970561	207.4202649	207.58324	1599.05	98.52746762	65.11626578	14.875	803.1705354
46	81.35973834	-0.088236947	41.76125971	41.849497	1604.06	75.78292788	54.18411298	14.875	803.3666703
47	81.21011265	-0.081096569	83.18899435	83.270091	1599.25	75.18561645	51.16492988	15.015625	803.3419307
48	80.92724242	-0.078979126	124.5655176	124.6445	1599.3	74.88727217	49.02971501	15.015625	803.5647375
49	80.60822701	-0.077261251	165.9921319	166.06939	1599.27	74.71109299	47.19368865	14.9609375	803.6812625
50	80.59779739	-0.070848143	207.4987737	207.56962	1599.27	74.51646109	45.28496708	14.9609375	803.7286784

51	80.65664625	-0.010015453	41.804249	41.814264	1603.14	50.80393891	35.11419969	14.9609375	803.660688
52	80.76055451	-0.008762192	83.16827423	83.177036	1599.5	50.17395886	32.49770496	14.9609375	803.5987554
53	80.8590211	-0.00542473	124.5128082	124.51823	1599.52	49.88231024	30.29273007	14.9375	803.48899
54	80.91753572	-0.003625315	165.8662675	165.86989	1599.52	49.68801336	28.4138276	14.9375	803.4219734
55	80.9152422	-0.00111338	207.4352191	207.43633	1599.51	49.52376369	26.64381621	14.7109375	803.4678743
56	80.83694051	0.040534247	41.77024548	41.729711	1602.14	25.84226013	16.85494533	14.7109375	803.5222107
57	80.70331213	0.042370215	83.179878	83.137508	1599.75	25.22827422	14.3991239	14.7109375	803.5367863
58	80.65777903	0.042742996	124.6055254	124.56278	1599.75	24.93235374	12.16737171	14.7109375	803.5634118
59	80.55175452	0.044169255	165.9545369	165.91037	1599.76	24.72712349	10.22019829	14.5625	803.662697
60	80.55424945	0.046329032	207.2693034	207.22297	1599.76	24.54537817	8.458268557	14.5625	803.6831938
61	80.98417215	-0.07978178	41.79188446	41.871666	1199.93	98.14299991	53.92777063	14.7578125	803.7112498
62	81.75066542	-0.078727317	83.16801532	83.246743	1198.99	98.30556418	51.8883074	14.7578125	803.3899352
63	81.9746224	-0.077063683	124.554819	124.63188	1199.02	98.47388666	50.2362061	14.7578125	803.136508
64	82.04440742	-0.073756153	165.9985185	166.07227	1199.07	98.56361989	48.51703895	14.7578125	802.9890486
65	81.9378583	-0.071059017	207.3602686	207.43133	1199.03	98.58993542	47.0077783	14.7578125	802.9348153
66	81.75982453	-0.028162971	41.74133565	41.769499	1204.11	75.73713178	40.02630063	14.7578125	803.1277352
67	81.64016892	-0.024120194	83.20196949	83.22609	1199.25	75.23613659	37.42817864	14.8359375	803.1574567
68	81.46049623	-0.020505019	124.6388635	124.65937	1199.26	74.98967979	35.53423654	14.8359375	803.2078801
69	81.25662885	-0.018718071	166.0465302	166.06525	1199.27	74.8060993	33.80164405	14.8828125	803.3368855
70	81.12538254	-0.016627681	207.318491	207.33512	1199.28	74.61221238	32.12367598	14.8828125	803.4806095
71	81.08912076	0.022273199	41.80860324	41.78633	1203.13	50.80669476	25.79638566	14.8828125	803.4550568
72	81.10738649	0.023851898	83.19117179	83.16732	1199.5	50.24527219	23.3996035	14.8828125	803.38288
73	81.18128481	0.023757423	124.6465966	124.62284	1199.5	49.97605727	21.45972952	14.8828125	803.4474126
74	81.21306902	0.025698854	166.0166532	165.99095	1199.5	49.77504301	19.66715098	14.8828125	803.36605
75	81.2984834	0.027488648	207.414369	207.38688	1199.52	49.6257404	18.02897161	14.8828125	803.3787175
76	81.25967312	0.050804731	41.77151871	41.720714	1202.14	25.88324081	12.01233543	14.8828125	803.2392879
77	81.0961359	0.05272457	83.22018218	83.167458	1199.74	25.29794568	9.839094825	14.8046875	803.2610247
78	80.95366317	0.05434166	124.5358844	124.48154	1199.76	25.02948424	7.855855345	14.8046875	803.4084084
79	80.84999955	0.056008372	165.8524449	165.79644	1199.78	24.8262747	6.004161986	14.59375	803.5906916
80	80.76877193	0.05771715	207.1574764	207.09976	1199.76	24.66172672	4.352380461	14.59375	803.67618
81	81.3718411	-0.219768675	41.77238815	41.992157	1801.12	98.17720659	81.81006684	14.59375	803.7835979
82	82.60231267	-0.21336007	83.17387657	83.387237	1798.94	98.31789208	79.36052821	14.59375	803.1574676
83	82.70354823	-0.213407452	124.4857636	124.69917	1798.86	98.43600354	77.55382009	14.59375	802.8713116
84	82.14762979	-0.210618523	165.9816694	166.19229	1798.84	98.48203233	75.7565266	14.59375	802.8282971
85	81.54004252	-0.207448496	207.3655337	207.57298	1799.14	98.49393525	74.06191281	14.625	803.1171838
86	81.11738086	-0.114105145	41.78183135	41.895936	1804.33	75.80707693	61.31712939	14.625	803.4289571
87	80.9471857	-0.111808761	83.18595398	83.297763	1799.24	75.18138666	58.16822153	14.625	803.5006103
88	80.53324719	-0.104640695	124.6277424	124.73238	1799.25	74.8768324	55.78702577	14.625	803.8115503
89	80.24250005	-0.102836141	165.9574358	166.06027	1799.14	74.67474063	53.8948978	14.625	804.0836428
90	80.33183625	-0.098778429	207.4575228	207.5563	1799.2	74.46928023	51.91753858	14.625	804.1312957
91	80.46264032	-0.02543508	41.77798995	41.803425	1803.3	50.79590267	39.90802824	14.6796875	803.9764784
92	80.61560697	-0.021283716	83.1972296	83.218513	1799.51	50.17646829	37.05612953	14.6796875	803.896347
93	80.72922525	-0.018768572	124.5559473	124.57472	1799.52	49.88128914	34.84673416	14.6328125	803.715276
94	80.66497771	-0.015108359	166.0869177	166.10203	1799.51	49.65767754	32.80518421	14.6328125	803.7134998
95	80.69666332	-0.009985242	207.4185316	207.42852	1799.45	49.48827859	30.88351312	14.6328125	803.6051717
96	80.63387927	0.038219214	41.78438574	41.746167	1802.17	25.83509425	19.24205497	14.6328125	803.6440699
97	80.58533555	0.039024854	83.16045491	83.12143	1799.73	25.1908435	16.6138242	14.6328125	803.6075014
98	80.62877343	0.041333747	124.5400534	124.49872	1799.76	24.91046088	14.39276495	14.6328125	803.6353703
99	80.59085042	0.043074508	165.9099311	165.86686	1799.77	24.69901788	12.3742792	14.6328125	803.6336677
100	80.59421722	0.044622422	207.4145883	207.36997	1799.77	24.50899208	10.46444107	14.6328125	803.6036859

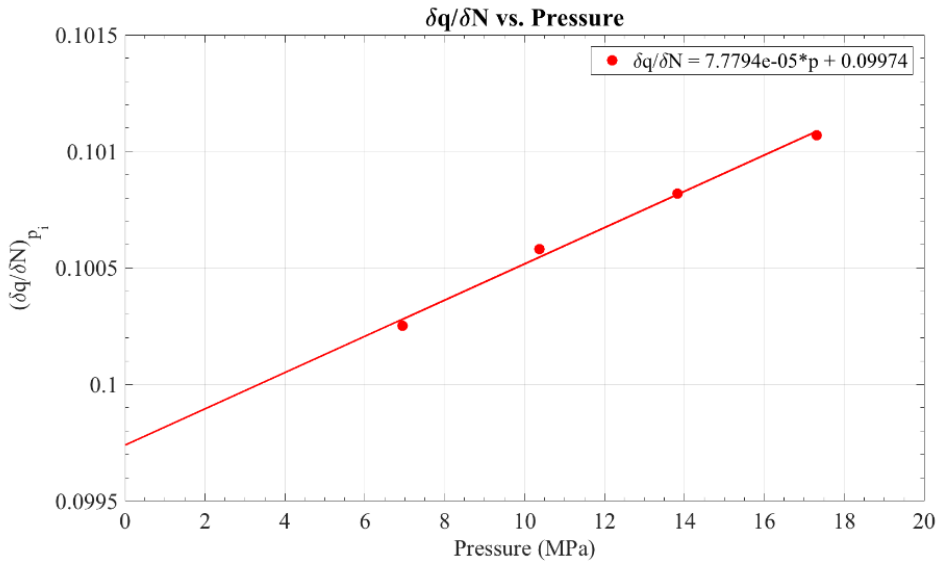

Figure A2 - Rate of Change of Flow / Rate of Change of Rotational Speed versus Outlet Pressure.

Appendix B – Dynamic Duty Cycle Tests

Duty Cycle MATLAB code

```
clear
% folder location where runs to be loaded are kept
data_dir = 'C:\Users\malikm\Documents\MSOE\Research Assistant\Cell 2\Duty Cycle
Tests\Duty_Cycle_21_03_02_122F';
sensor_name_row = 20;    %row in csv where labels for columns are
data_start_row = 24;     %row in csv where data starts
Tspan = 11.98;  %time span on recording, must be divisible by sample rate
sample_rate = 200; %sample rate in Hz
run = 1;     %the desired run number to load into simulink

script_dir = char(pwd);
eval (['cd '' ' data_dir ''''])
files = dir('*.csv');
sample_time = 1 / sample_rate;
time = (0:sample_time:Tspan);
last_data_point = Tspan*sample_rate+1;
sensor_name_row = sensor_name_row -1;
data_start_row = data_start_row - 1;
data_table = readtable(files(1).name,'HeaderLines',sensor_name_row);
column_heading = data_table.Properties.VariableNames;

%creating variable with
for n = 1:1:length(column_heading)
    sensor = char(column_heading(n));
    n_char = int2str(n);
    eval([sensor ' = ' n_char ';']);
end

%creating timeseries for simulink for each run
for i=1:length(files)
    %data_table = readtable(files(i).name,'Range','A23:AK1323');
    data_table = readtable(files(i).name,'HeaderLines',data_start_row);
    for n = 1:1:length(column_heading)
        data_array(:,i,n) = table2array(data_table(1:last_data_point,n));
        sensor = char(column_heading(n));
        i_char = int2str(i);
        eval([sensor         '_timeseries_'         i_char         '         =
timeseries(data_array(:,i,n),time);']);
    end
end

for var = 1:100
    Tau_inv_flow = 15.7;   %tau inverse, first order transfer function for swash
input flow output
    [a,b,c,d] = tf2ss([Tau_inv_flow],[1 Tau_inv_flow]); %need in state space
for initial conditions
    flow_ss = ss(a,b,c,d);
    Tau_inv_press = var+59;    %tau inverse, first order transfer function for
swash input pressure output
    [a,b,c,d] = tf2ss([Tau_inv_press],[1 Tau_inv_press]); %need in state space
for initial conditions
```

```
    press_ss = ss(a,b,c,d);
    K = 1354690000; %bulk modulus in Pa
    viscosity = 26.7; %cP
    compress_gain = 1/0.60; %compressability flow loss gain
    press_driven_gain = 1/900000; %preasure driven flow loss gain
    laminar_gain = 38; %laminar loss torque gain
    turbulent_gain = 1/(1000000); %turbulent loss torque gain
    for i = 1:length(files)
        delta_P_PSI(:,i)      =      data_array(:,i,Pmp_PresOutlet_PSI)      -
data_array(:,i,Pmp_PresInlet_PSI);
        delta_P_Pa(:,i) = delta_P_PSI(:,i) * 6894.76;
        speed_radps(:,i) = 2 * pi * data_array(:,i,Pmp_Speed_RPM) / 60;
        displacement_lprev(:,i) = data_array(:,i,Swash_Angle)/100 * 0.0461;
        press_ss_X0(:,i) = displacement_lprev(1,i)/Tau_inv_press;
        [displacement_lprev_tf_press(:,i),t,x]                              =
lsim(press_ss,displacement_lprev(:,i),time,press_ss_X0(:,i));
        torque_theory_nm(:,i)     =     displacement_lprev_tf_press(:,i)     .*
delta_P_Pa(:,i) * 0.001 / (2*pi);
        torque_loss_1_nm(:,i)     =     (displacement_lprev_tf_press(:,i)     .*
speed_radps(:,i) * viscosity) * laminar_gain;
        torque_loss_2_nm(:,i)     =     ((speed_radps(:,i)     .^     2)     .*
data_array(:,i,Pmp_DensityIn_gcc)     .*     (displacement_lprev_tf_press(:,i)
.^(5/3))) *turbulent_gain;
        torque_model_ftlb(:,i)        =        (torque_theory_nm(:,i)        +
torque_loss_1_nm(:,i) + torque_loss_2_nm(:,i)) * 0.7376;
        torque_error(:,i)       =       data_array(:,i,Pmp_Torque_FTLB)       -
torque_model_ftlb(:,i);
        torque_MSE(i)         =         immse(data_array(:,i,Pmp_Torque_FTLB),
torque_model_ftlb(:,i));
        torque_RMSE(i) = sqrt(torque_MSE(i));
        torque_RMSEP(i)        =        sqrt(mean((torque_error(:,i)        ./
data_array(:,i,Pmp_Torque_FTLB)).^2))*100;

        swash_ss_X0(:,i) = data_array(1,i,Swash_Angle)/Tau_inv_flow;
        [swash_transformed(:,i),t1,x1]                                      =
lsim(flow_ss,data_array(:,i,Swash_Angle),time,swash_ss_X0(:,i));
        displacement_lprev_tf_flow(:,i) = swash_transformed(:,i)/100 * 0.0461;
        flow_theroy_lpm(:,i)      =      displacement_lprev_tf_flow(:,i)      .*
data_array(:,i,Pmp_Speed_RPM);
        flow_loss_compress(:,i) = (speed_radps(:,i) .* delta_P_Pa(:,i) / K) *
compress_gain;
        flow_loss_press_driven(:,i) = (delta_P_Pa(:,i) ./ (speed_radps(:,i) .*
viscosity * 0.001))* press_driven_gain;
        flow_model_GPM(:,i) = (flow_theroy_lpm(:,i) - flow_loss_compress(:,i)
- flow_loss_press_driven(:,i)) * 0.26417287472922;
        flow_error(:,i) = data_array(:,i,Pmp_Flow_GPM) - flow_model_GPM(:,i);
        flow_MSE(i) = immse(data_array(:,i,Pmp_Flow_GPM),flow_model_GPM(:,i));
        flow_RMSE(i) = sqrt(flow_MSE(i));
        flow_RMSEP(i)          =          sqrt(mean((flow_error(:,i)          ./
data_array(:,i,Pmp_Flow_GPM)).^2))*100;
    end
    torque_MSE_ave(var) = mean(torque_MSE);
    torque_RMSE_ave(var) = mean(torque_RMSE);
    torque_RMSEP_ave(var) = mean(torque_RMSEP);
```

```
    torque_STD_ave(var) = mean(std(torque_error));
    flow_MSE_ave(var) = mean(flow_MSE);
    flow_RMSE_ave(var) = mean(flow_RMSE);
    flow_RMSEP_ave(var) = mean(flow_RMSEP);
    flow_STD_ave(var) = mean(std(flow_error));
end
max(flow_RMSEP_ave);
min(flow_RMSEP_ave);
%{
deltaP = (data_array(:,run,1)-data_array(:,run,4));
Inlet_Pressure_timescale = timeseries(data_array(:,run,4),time);
Outlet_Pressure_timescale = timeseries(data_array(:,run,1),time);
Pressure_timescale = timeseries(deltaP,time);
Torque_timescale = timeseries(output_array(:,run,1),time);
Swash_timescale = timeseries(data_array(:,run,2),time);
Flow_timescale = timeseries(output_array(:,run,2),time);
Flow_case_timescale = timeseries(output_array(:,run,3),time);
Speed_timescale = timeseries(data_array(:,run,3),time);
Mass_flow_timescale = timeseries(output_array(:,run,4),time);

Tau_inv = 17;    %tau inverse, first order transfer function for swash input
flow output
[a,b,c,d] = tf2ss([Tau_inv],[1 Tau_inv]);
swash_ss = ss(a,b,c,d);
for runs = 1:length(files)
    swash_ss_X0 = data_array(1,runs,2)/Tau_inv;
    [swash_tf(:,runs),t,x]                                                    =
lsim(swash_ss,data_array(:,runs,2),time,swash_ss_X0);
end

test                        =                       iddata([output_array(:,run,1),
output_array(:,run,2)],[deltaP,data_array(:,run,2),data_array(:,run,3)],0.01)
;
test.inputName = {'pressure';'swash';'speed'};
test.outputName = {'torque';'flow'};

deltaP2 = (input_array(:,2,1)-input_array(:,2,4));
test2                        =                        iddata([output_array(:,2,1),
output_array(:,2,2)],[deltaP2,input_array(:,2,2),input_array(:,2,3)],0.01);
test2.inputName = {'pressure';'swash';'speed'};
test2.outputName = {'torque';'flow'};
nx = 1:10;
mi = impulseest(test,50);
mp = ssest(test,2);
compare(test2,mp)
showConfidence(impulseplot(mi),3);
tfest(test, 2, 1);
ss2tf(mp.A,mp.B,mp.C,mp.D,3);
tf = tf(mp);
%}
eval (['cd '' ' script_dir ''''])
```

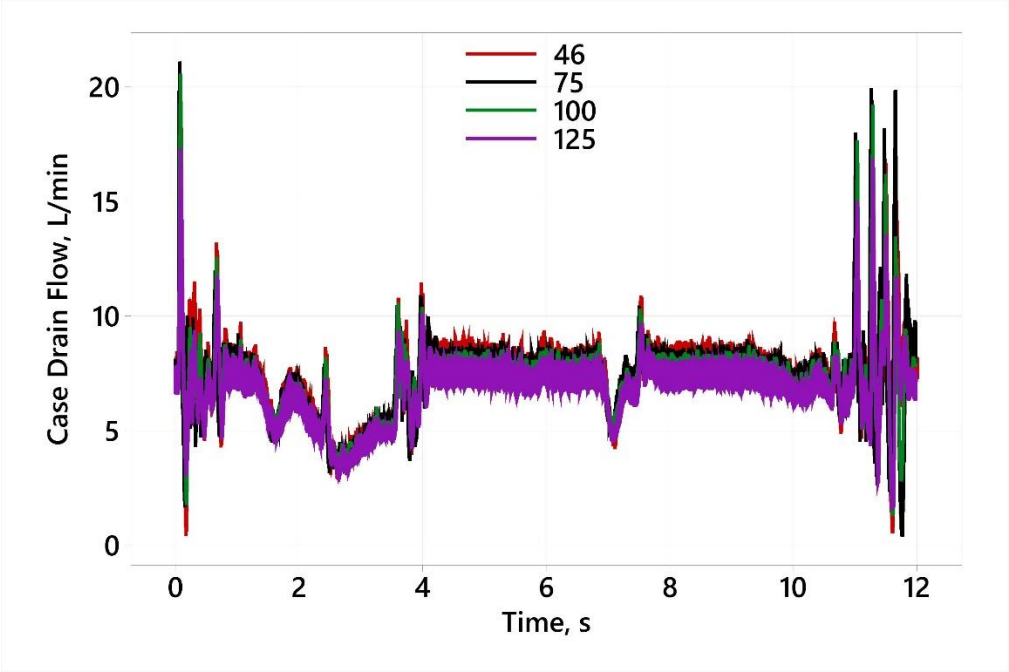

Figure B1 - Dynamic Duty Cycle Case Drain Flow versus Time for All Test Fluids.

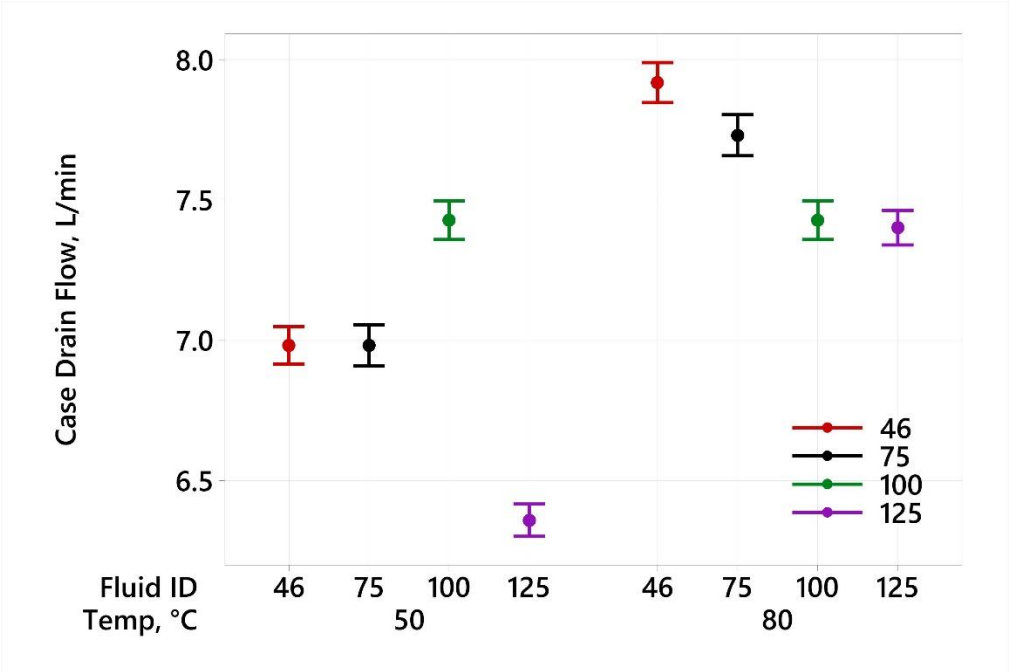

Figure B2 - Interval Plot for Dynamic Case Drain Flow (All Test Fluids).

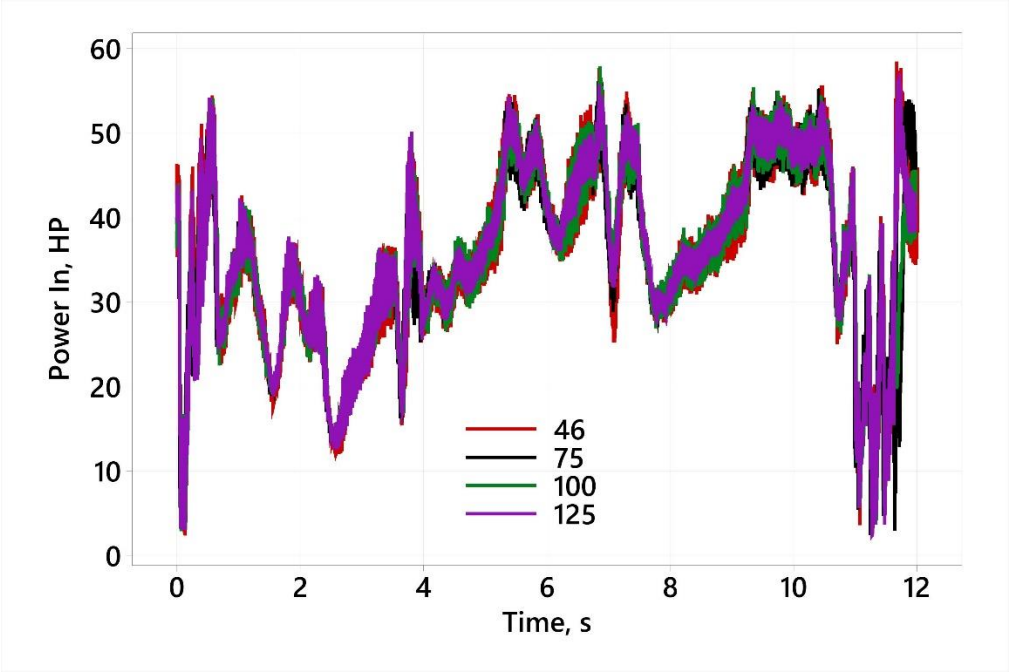

Figure B3 - Dynamic Duty Power In versus Time for All Test Fluids.

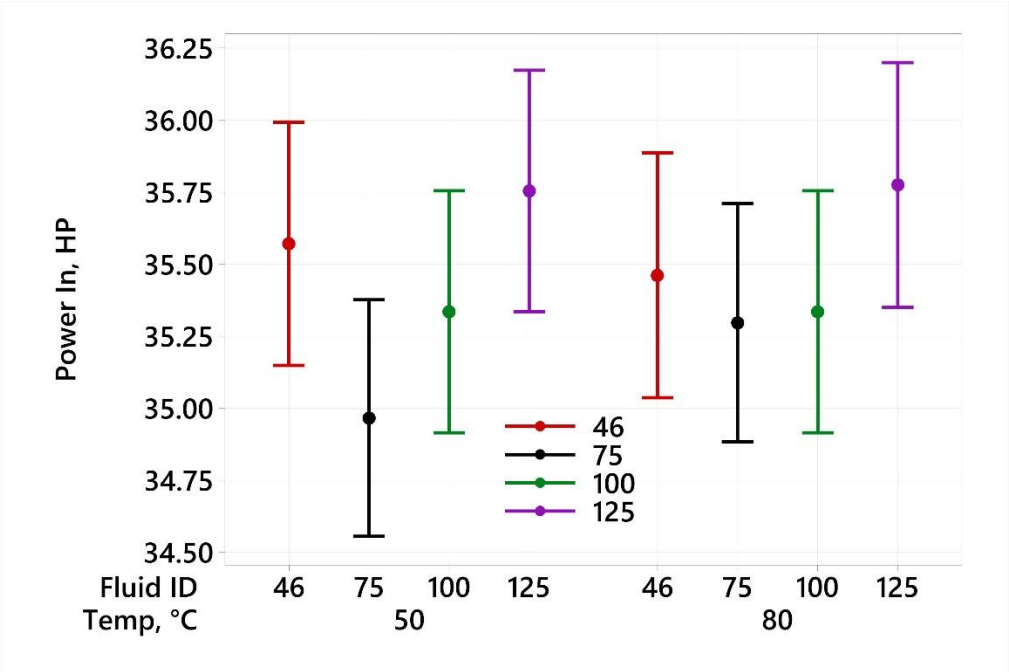

Figure B4 - Interval Plot for Dynamic Power In (All Test Fluids).

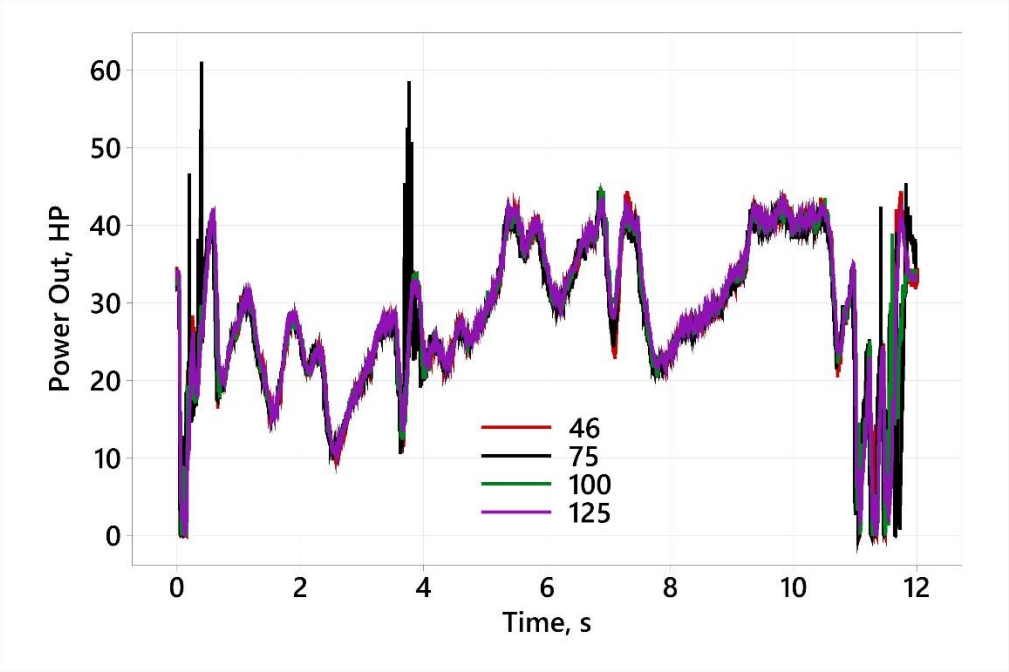

Figure B5 - Dynamic Duty Power Out versus Time for All Test Fluids.

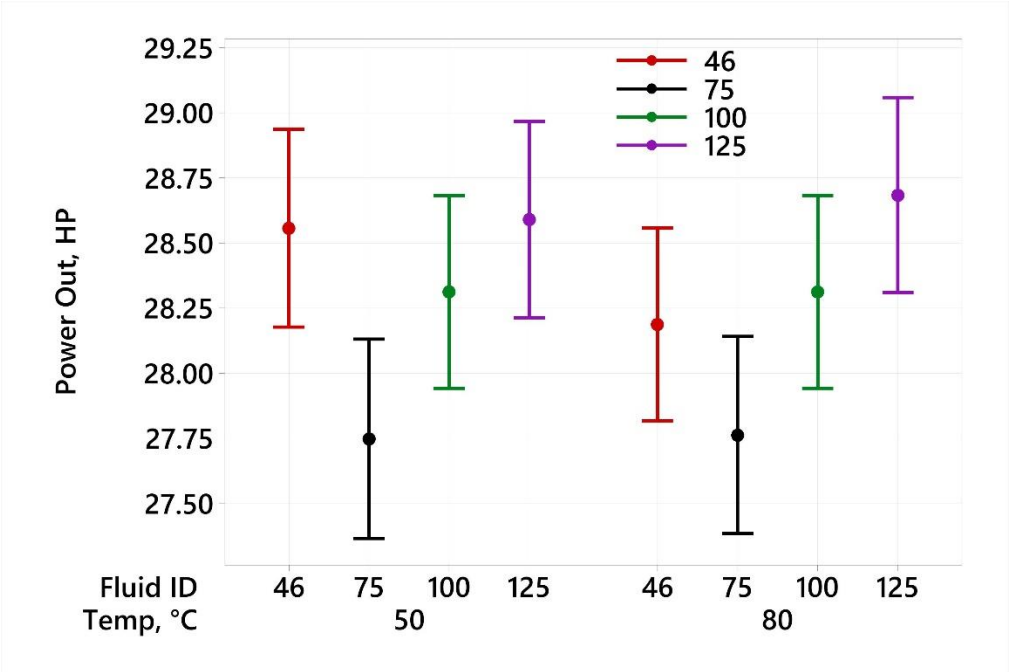

Figure B6 - Interval Plot for Dynamic Power Out (All Test Fluids).

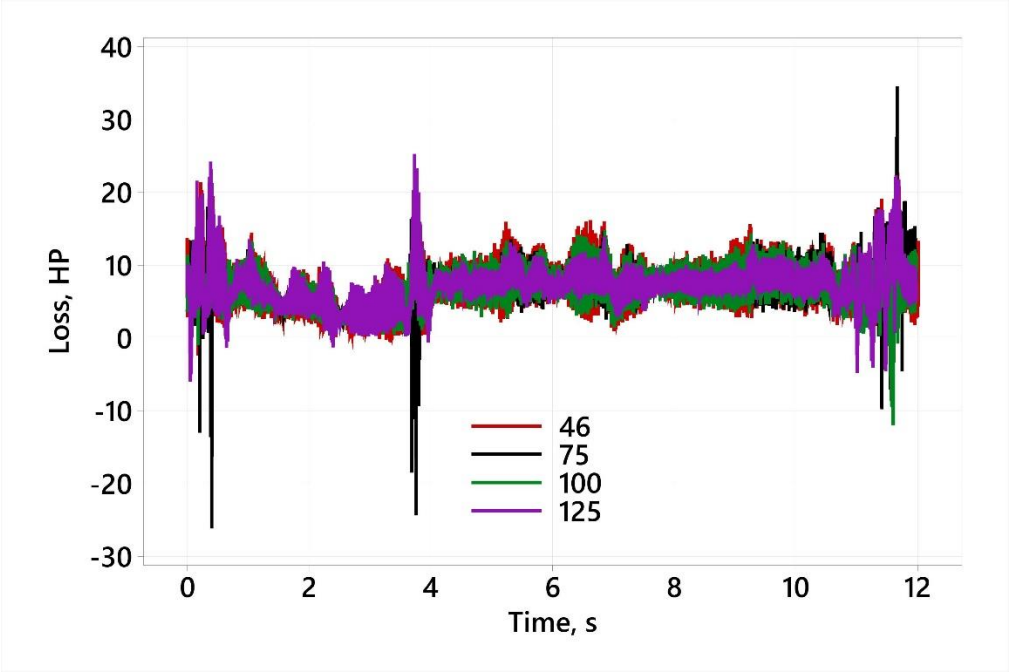

Figure B7 - Dynamic Duty Power Loss versus Time for All Test Fluids.

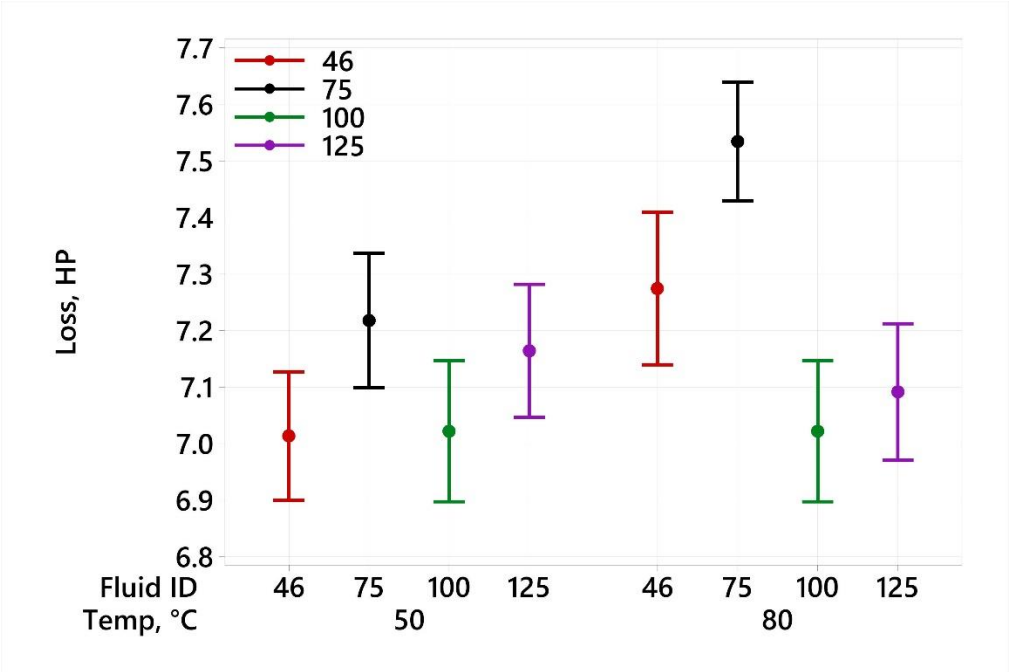

Figure B8 - Interval Plot for Dynamic Power Loss (All Test Fluids).

Appendix C – Removing Outliers from Efficiency Results

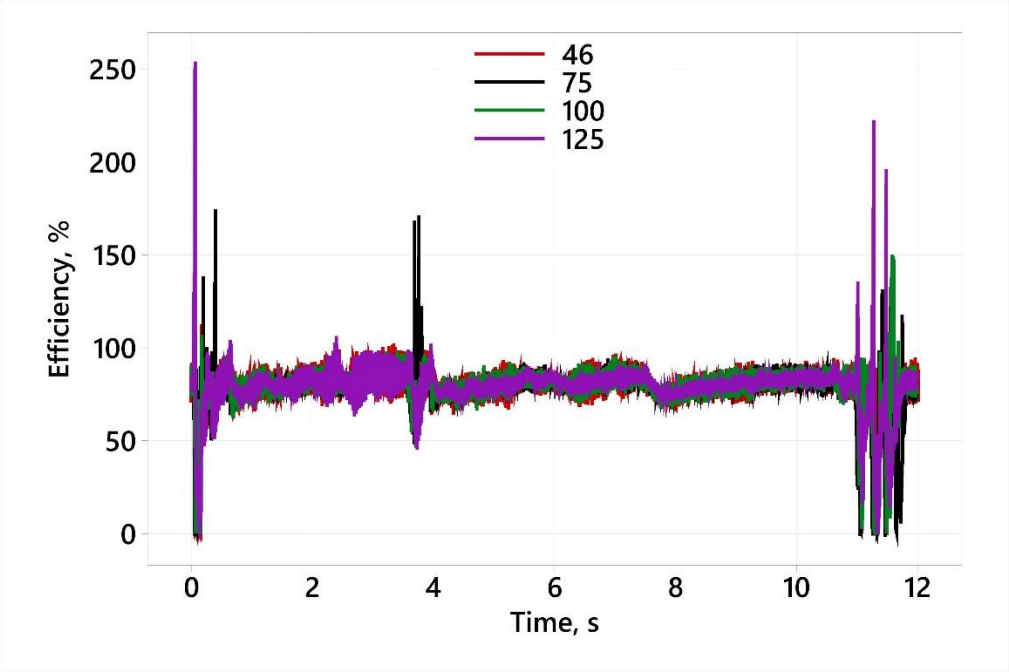

Figure C1 - Dynamic Duty Overall Efficiency versus Time for All Test Fluids.

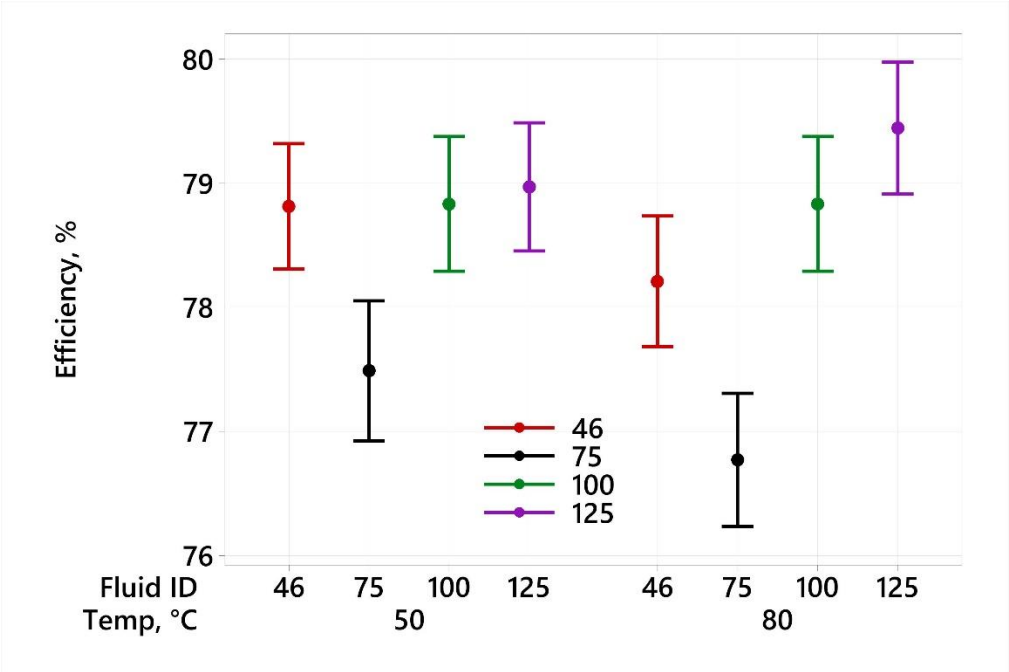

Figure C2 - Interval Plot for Dynamic Overall Efficiency (All Test Fluids).

First Outlier Test (2980 Rows of Data)

Grubbs' Test

Table C1 - Grubbs' Test for Finding Outliers in Efficiency Results (First).

Variable	N	Mean	StDev	Min	Max	G	P
Overall Eff, %	2980	78.938	12.779	-0.670	191.962	8.84	0.000
Vol Eff, %	2980	86.097	16.470	-174.429	556.809	28.58	0.000
HM Eff, %	2980	91.954	13.781	-9.764	386.736	21.39	0.000

Outlier

Table C2 - Outliers for Overall, Volumetric, and Hydromechanical Efficiencies (First).

Variable	Row	Outlier
Overall Eff, %	2320	191.962
Vol Eff, %	2255	556.809
HM Eff, %	2313	386.736

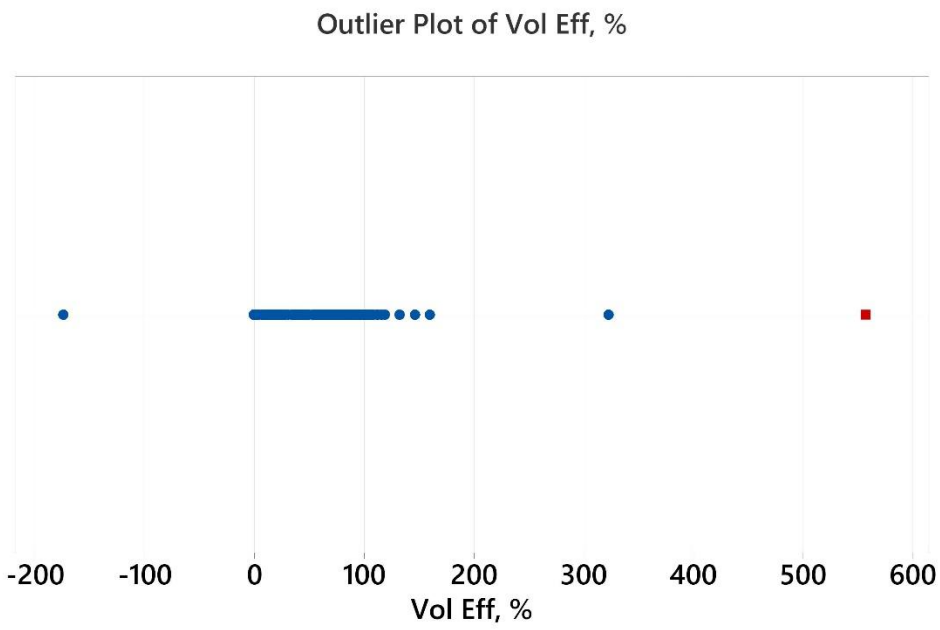

Figure C3 - Outliers in Volumetric Efficiency (First).

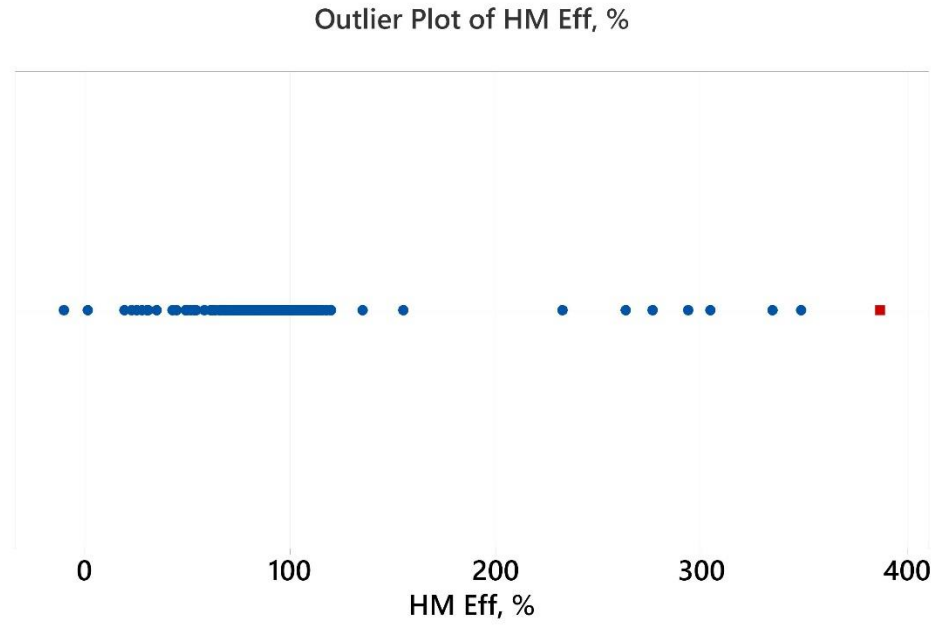

Figure C4 - Outliers in Hydromechanical Efficiency (First).

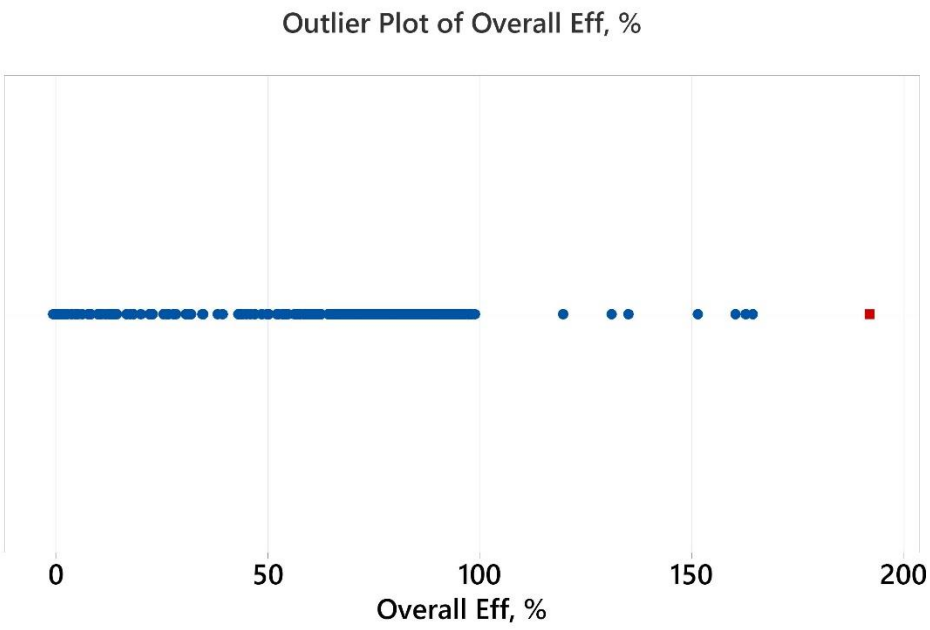

Figure C5 - Outliers in Overall Efficiency (First).

Fourth Outlier Test (2968 Rows of Data)

Grubbs' Test

Table C3 - Grubbs' Test for Finding Outliers in Efficiency Results (Fourth).

Variable	N	Mean	StDev	Min	Max	G	P
Overall Eff, %	2968	78.806	11.990	-0.670	98.857	6.63	0.000
Vol Eff, %	2968	86.062	12.304	-0.696	159.849	7.05	0.000
HM Eff, %	2968	91.448	7.273	23.252	135.314	9.38	0.000

Outlier

Table C4 - Outliers for Overall, Volumetric, and Hydromechanical Efficiencies (Fourth).

Variable	Row	Outlier
Overall Eff, %	29	-0.6703
Vol Eff, %	29	-0.6960
HM Eff, %	2293	23.2524

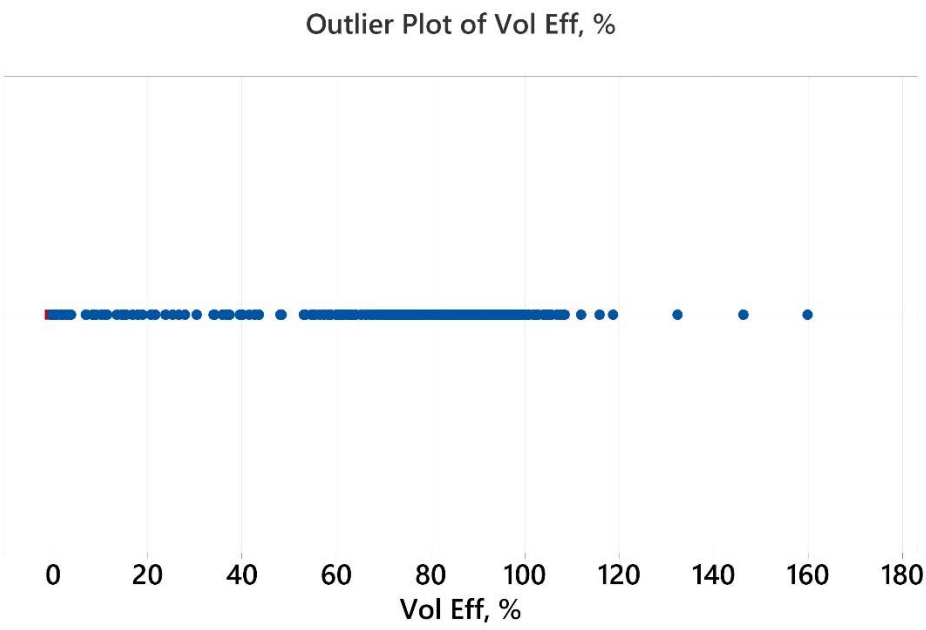

Figure C6 - Outliers in Volumetric Efficiency (Fourth).

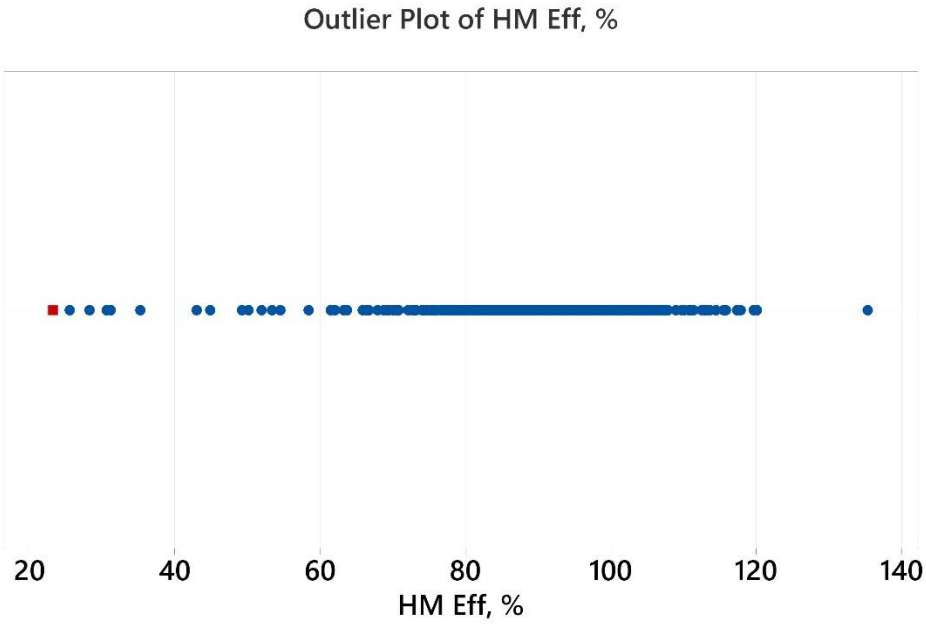

Figure C7 - Outliers in Hydromechanical Efficiency (Fourth).

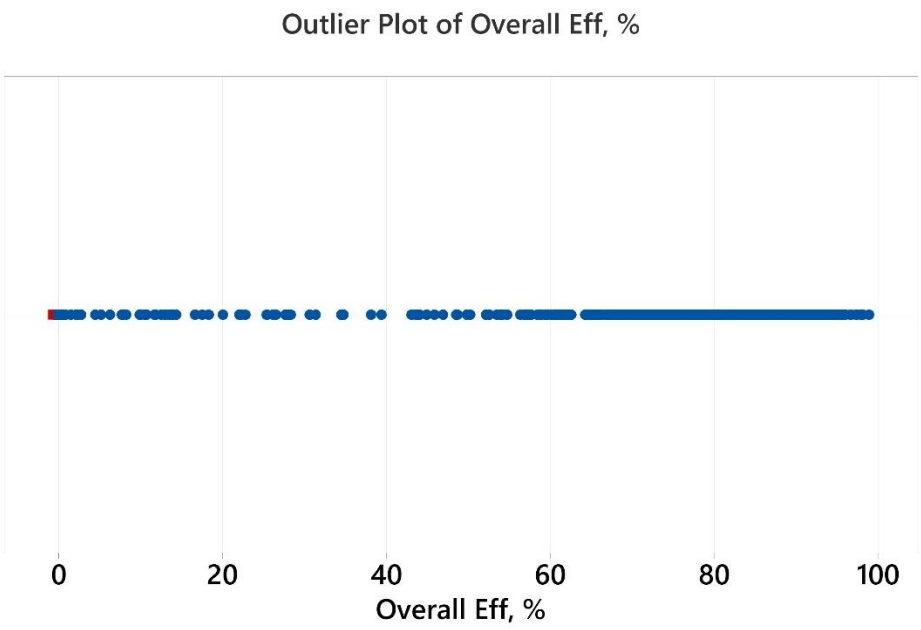

Figure C8 - Outliers in Overall Efficiency (Fourth).

Appendix D – Step Response Tests

Step Response MATLAB code

```
clear
cd           'C:\Users\malikm\Documents\MSOE\Research           Assistant\Cell
2\Testing_20210325\122F\Step Response'
Tspan = 0.98;       %length of file to use in seconds
sample_rate = 200;  %sample rate in Hz

press_up_files = dir('*Pressure_Up/*.csv');
press_down_files = dir('*Pressure_Down/*.csv');
swash_up_files = dir('*Swash_Up/*.csv');
swash_down_files = dir('*Swash_Down/*.csv');
speed_up_files = dir('*Speed_Up/*.csv');
speed_down_files = dir('*Speed_Down/*.csv');
Ts = 1/sample_rate;
time = (0:Ts:Tspan);
last_data_point = Tspan*sample_rate+1;
include_all_tf = 1;

for n = 1:8
    switch n
        case 1
        files = press_up_files;
        cd Pressure_Up
        input_col = 18; %pressure
        output_col = 8; %torque
        case 2
        files = press_down_files;
        cd Pressure_Down
        input_col = 18;
        output_col = 8;
        case 3
        files = swash_up_files;
        cd Swash_Up
        input_col = 24; %swash angle
        output_col = 16; %flow
        case 4
        files = swash_down_files;
        cd Swash_Down
        input_col = 24; %swash angle
        output_col = 16; %flow
        case 5
        files = speed_up_files;
        cd Speed_Up
        input_col = 10; %speed
        output_col = 16; %flow
        case 6
        files = speed_down_files;
        cd Speed_Down
        input_col = 10; %speed
        output_col = 16; %flow
        case 7
        files = swash_up_files;
```

```
        cd Swash_Up
        input_col = 24; %swash angle
        output_col = 8; %torque
        case 8
        files = swash_down_files;
        cd Swash_Down
        input_col = 24; %swash angle
        output_col = 8; %torque
    end

    for i=1:length(files)
        data_table = readtable(files(i).name, 'HeaderLines', 23);
        input_array(:,i,n)                                                    =
table2array(data_table(1:last_data_point,input_col));
        output_array(:,i,n)                                                   =
table2array(data_table(1:last_data_point,output_col));
    end

    cd ..
end

Pressure_timescale = timeseries(input_array(:,1,1),time);
Torque_timescale = timeseries(output_array(:,1,1),time);
Swash_timescale = timeseries(input_array(:,1,4),time);
Flow_timescale = timeseries(output_array(:,1,4),time);
Speed_timescale = timeseries(input_array(:,1,6),time);

for i=1:8
    if length(files) == 5
        input_cell = mat2cell(input_array(:,:,i),last_data_point,[1 1 1 1 1]);
        output_cell  =  mat2cell(output_array(:,:,i),last_data_point,[1  1  1  1
1]);
    end
    if length(files) == 6
        input_cell  =  mat2cell(input_array(:,:,i),last_data_point,[1  1  1  1  1
1]);
        output_cell = mat2cell(output_array(:,:,i),last_data_point,[1 1 1 1 1
1]);
    end
    if length(files) == 30
        input_cell = mat2cell(input_array(:,:,i),last_data_point,[1 1 1 1 1 1
1 1 1 1 1 1 1 1 1 1 1 1 1 1 1 1 1 1 1 1 1 1 1 1 1 1 1 1]);
        output_cell = mat2cell(output_array(:,:,i),last_data_point,[1 1 1 1 1
1 1 1 1 1 1 1 1 1 1 1 1 1 1 1 1 1 1 1 1 1 1 1 1 1 1 1 1]);
    end
    switch i
        case 1
            Pressure_Up = iddata(output_cell,input_cell,Ts);
            Pressure_Up.InputName = {'Pressure'};
            Pressure_Up.OutputName = {'Torque'};
        case 2
            Pressure_Down =  iddata(output_cell, input_cell,Ts);
            Pressure_Down.InputName = {'Pressure'};
            Pressure_Down.OutputName = {'Torque'};
```

```
        case 3
            Swash_Up =  iddata(output_cell, input_cell,Ts);
            Swash_Up.InputName = {'Swash Angle'};
            Swash_Up.OutputName = {'Flow'};
        case 4
            Swash_Down =  iddata(output_cell, input_cell,Ts);
            Swash_Down.InputName = {'Swash Angle'};
            Swash_Down.OutputName = {'Flow'};
        case 5
            Speed_Up =  iddata(output_cell, input_cell,Ts);
            Speed_Up.InputName = {'Pump Speed'};
            Speed_Up.OutputName = {'Flow'};
        case 6
            Speed_Down =  iddata(output_cell, input_cell,Ts);
            Speed_Down.InputName = {'Pump Speed'};
            Speed_Down.OutputName = {'Flow'};
        case 7
            Swash_Torque_Up =  iddata(output_cell, input_cell,Ts);
            Swash_Torque_Up.InputName = {'Swash Angle'};
            Swash_Torque_Up.OutputName = {'Torque'};
        case 8
            Swash_Torque_Down =  iddata(output_cell, input_cell,Ts);
            Swash_Torque_Down.InputName = {'Swash Angle'};
            Swash_Torque_Down.OutputName = {'Torque'};
    end
end

Options = tfestOptions;
Options.InitialCondition = 'backcast';
Options.SearchOptions.MaxIterations = 250;

swash_flow_down_tf = tfest(Swash_Down, 1, 0, Options);
swash_flow_up_tf = tfest(Swash_Up, 1, 0, Options);
pvec1 = getpvec(swash_flow_down_tf);
pvec2 = getpvec(swash_flow_up_tf);
fprintf('Swash --> Flow up = %f down = %f\n', 1/pvec2(2), 1/pvec1(2));

if include_all_tf
    pressure_torque_down_tf = tfest(Pressure_Down, 1, 0, Options);
    pressure_torque_up_tf = tfest(Pressure_Up, 1, 0, Options);
    speed_flow_down_tf = tfest(Speed_Down, 1, 0, Options);
    speed_flow_up_tf = tfest(Speed_Up, 1, 0, Options);
    swash_torque_down_tf = tfest(Swash_Torque_Down, 1, 0, Options);
    swash_torque_up_tf = tfest(Swash_Torque_Up, 1, 0, Options);

    pvec3 = getpvec(pressure_torque_down_tf);
    pvec4 = getpvec(pressure_torque_up_tf);
    pvec5 = getpvec(speed_flow_down_tf);
    pvec6 = getpvec(speed_flow_up_tf);
    pvec7 = getpvec(swash_torque_down_tf);
    pvec8 = getpvec(swash_torque_up_tf);

    fprintf('Pressure --> Torque up = %f down = %f\n', 1/pvec4(2), 1/pvec3(2));
    fprintf('Speed --> Flow up = %f down = %f\n', 1/pvec6(2), 1/pvec5(2));
```

```
    fprintf('Swash --> Torque up = %f down = %f\n', 1/pvec8(2), 1/pvec7(2));
end

%test                          =                          iddata([output_array(:,1,3),
output_array(:,1,4)],[input_array(:,1,3),input_array(:,1,4)],0.01);
%test.inputName = {'swash';'speed'};
%test.outputName = {'flow';'flow1'};
%mi = impulseest(Speed_Up,50);
%mp = ssest(Speed_Up);
%tf = tf(mp);
%showConfidence(impulseplot(mi),3);
cd            'C:\Users\malikm\Documents\MSOE\Research            Assistant\Cell
2\Testing_20210325\122F\Step Response '
```

Pressure Step Results

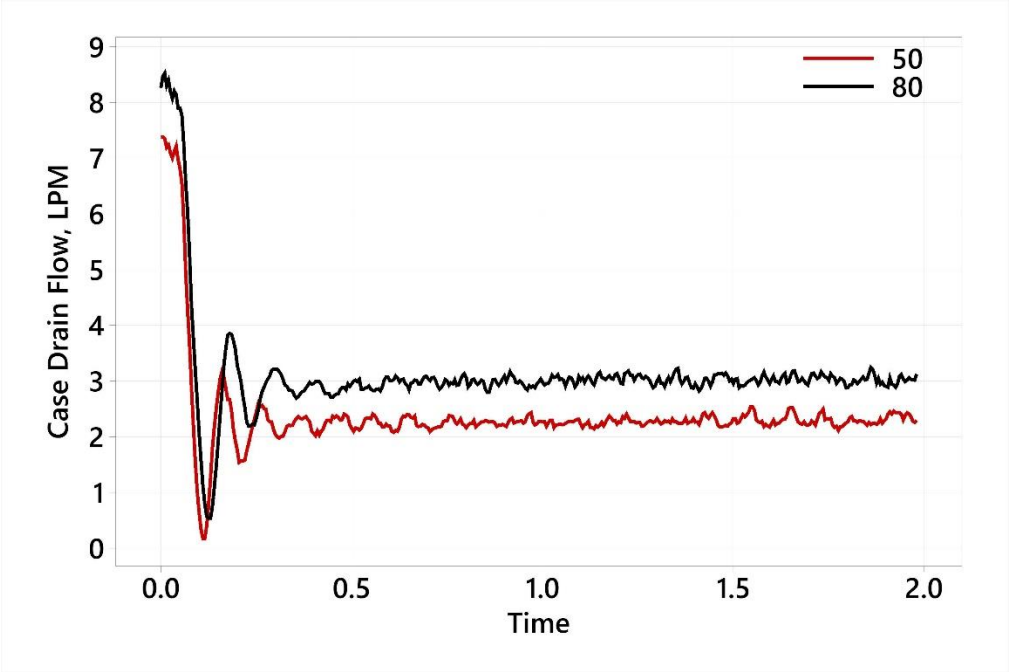

Figure D1 - Pressure Step Down - Case Drain Flow.

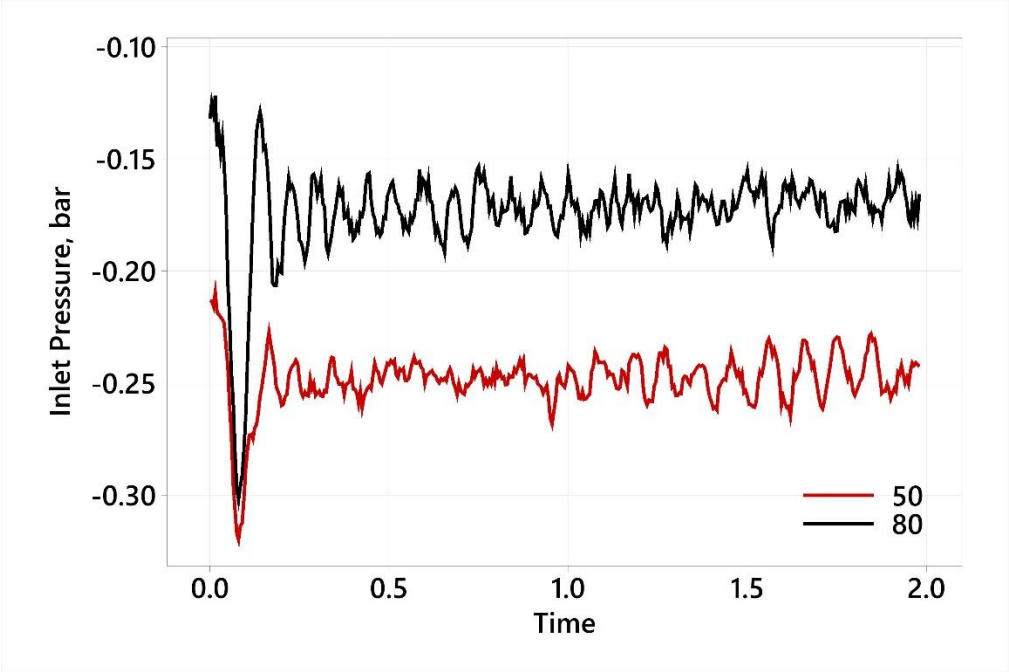

Figure D2 - Pressure Step Down - Inlet Pressure.

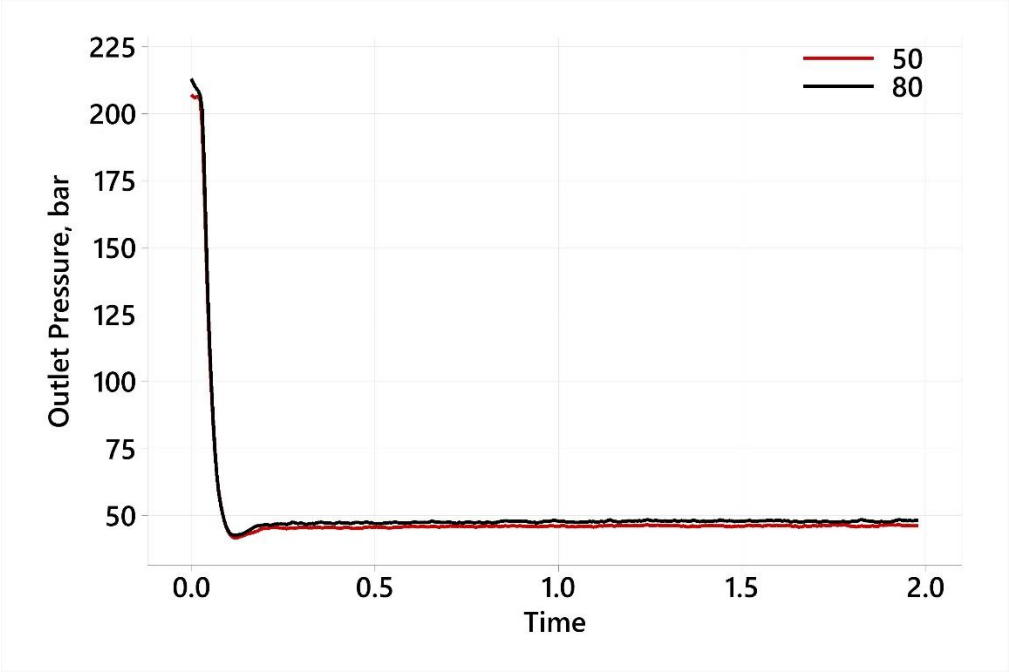

Figure D3 - Pressure Step Down - Outlet Pressure.

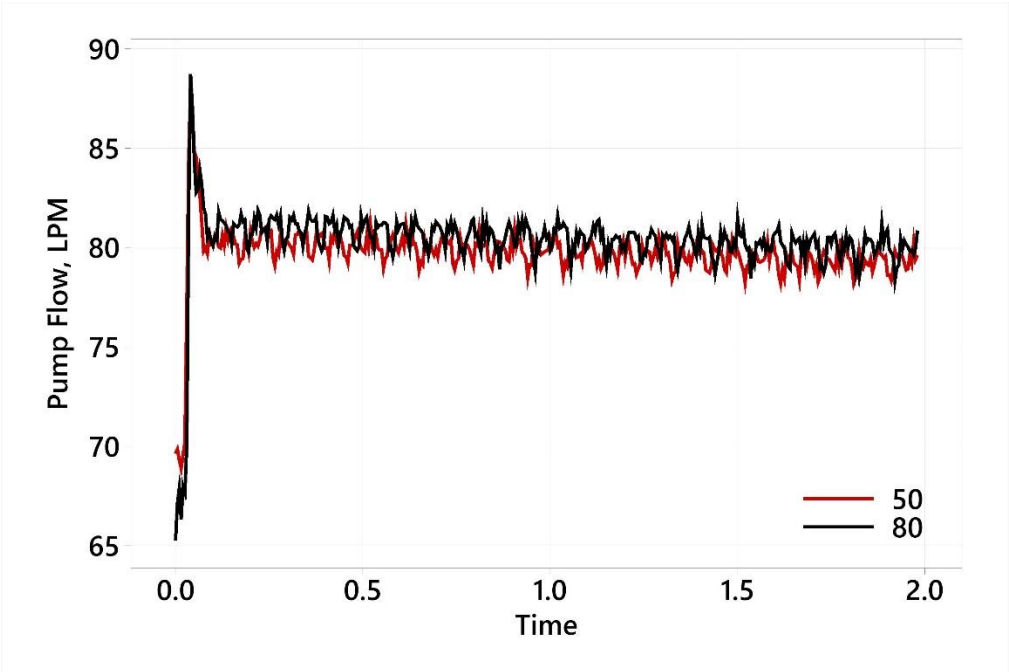

Figure D4 - Pressure Step Down - Pump Flow.

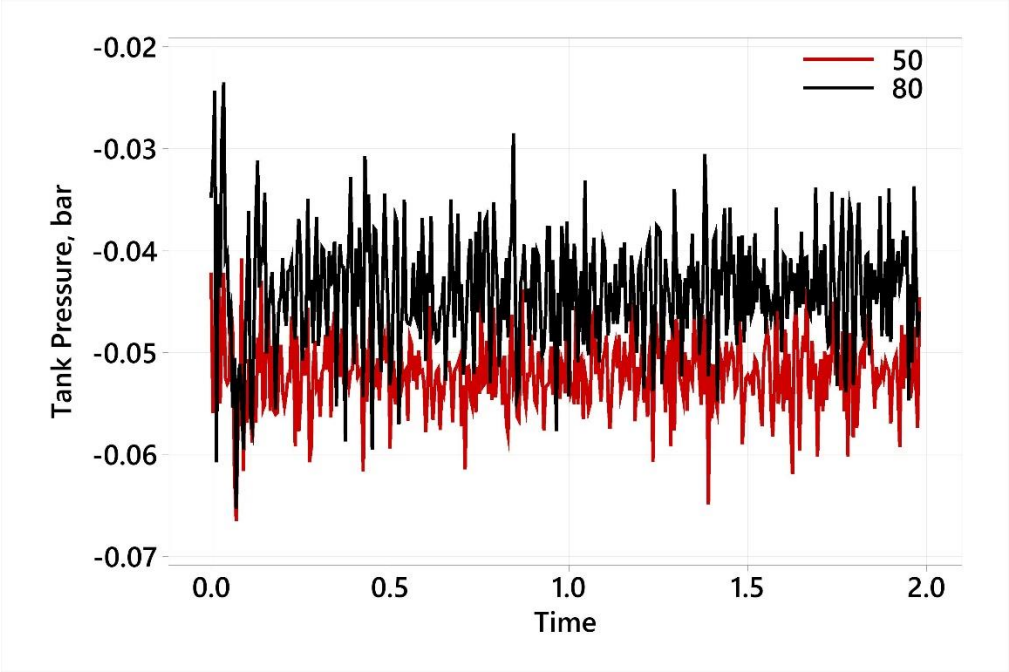

Figure D5 - Pressure Step Down - Tank Pressure.

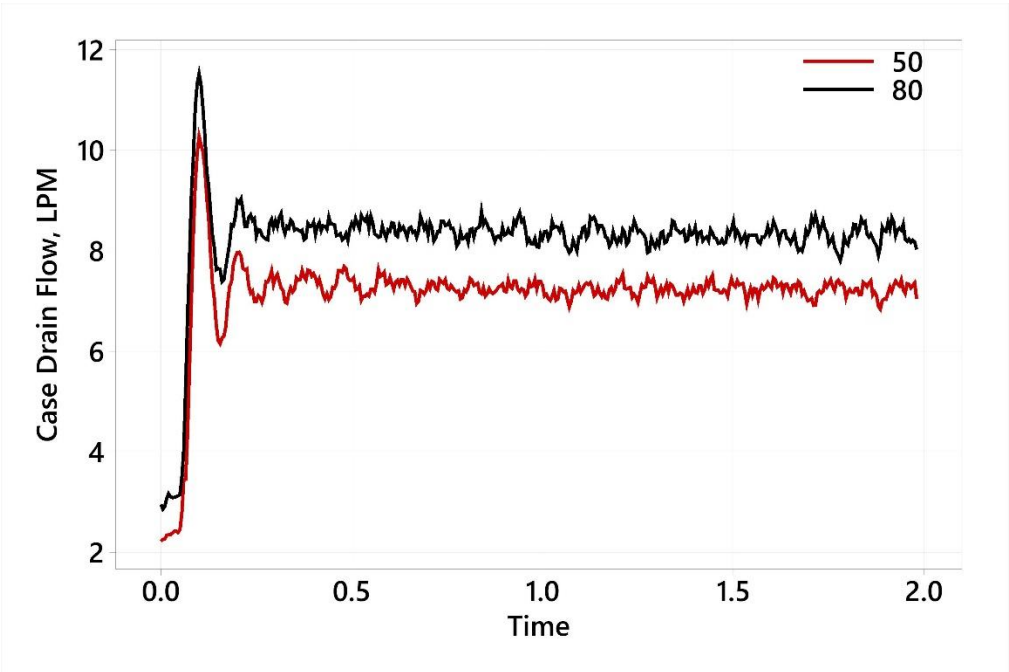

Figure D6 - Pressure Step Up - Case Drain Flow.

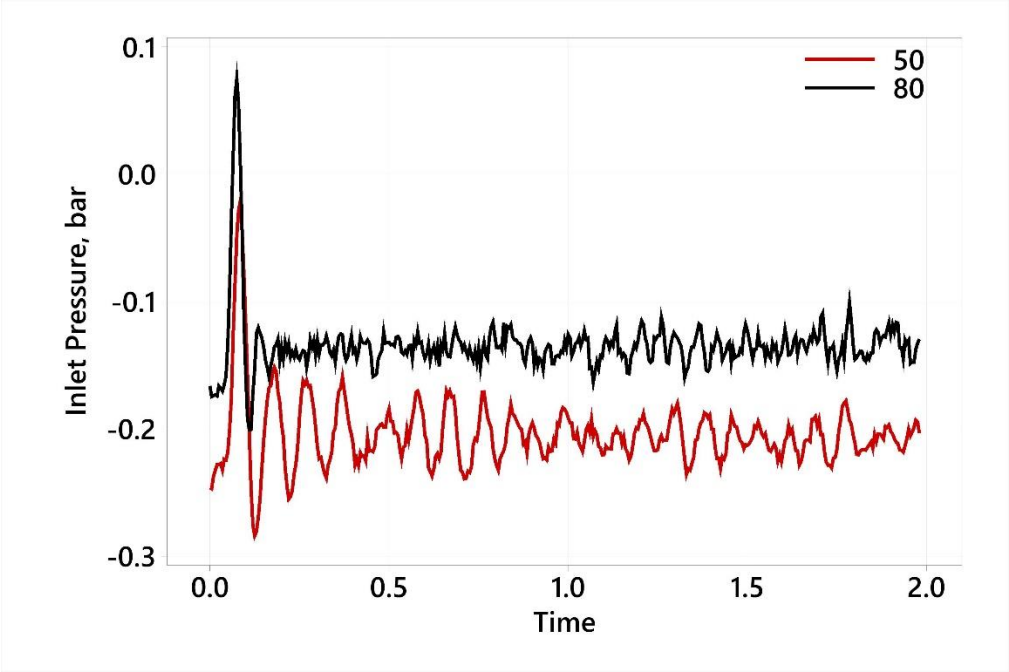

Figure D7 - Pressure Step Up - Inlet Pressure.

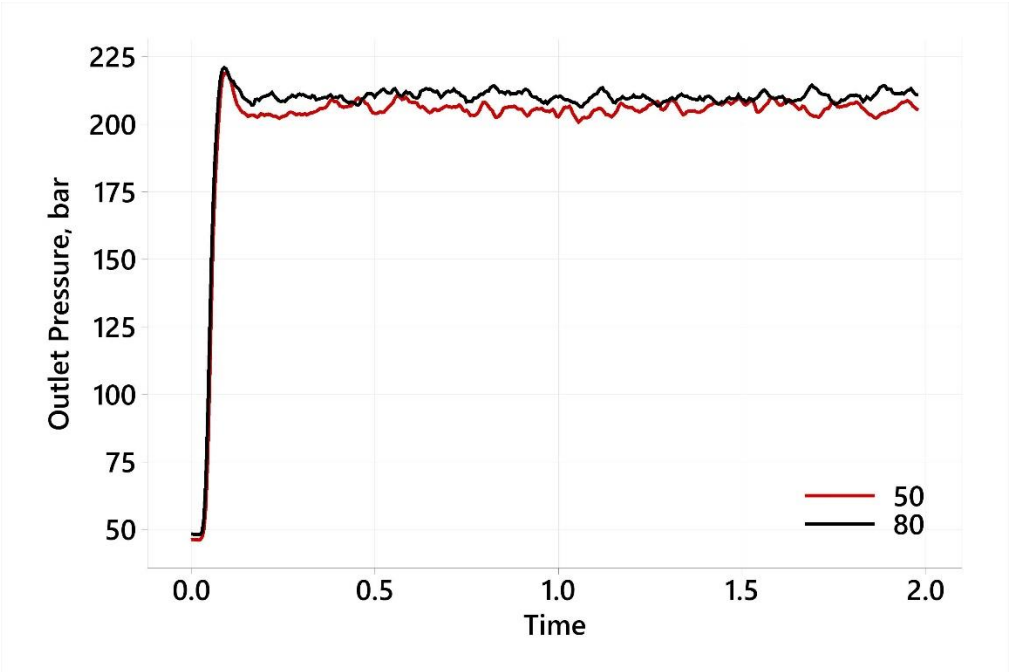

Figure D8 - Pressure Step Up - Outlet Pressure.

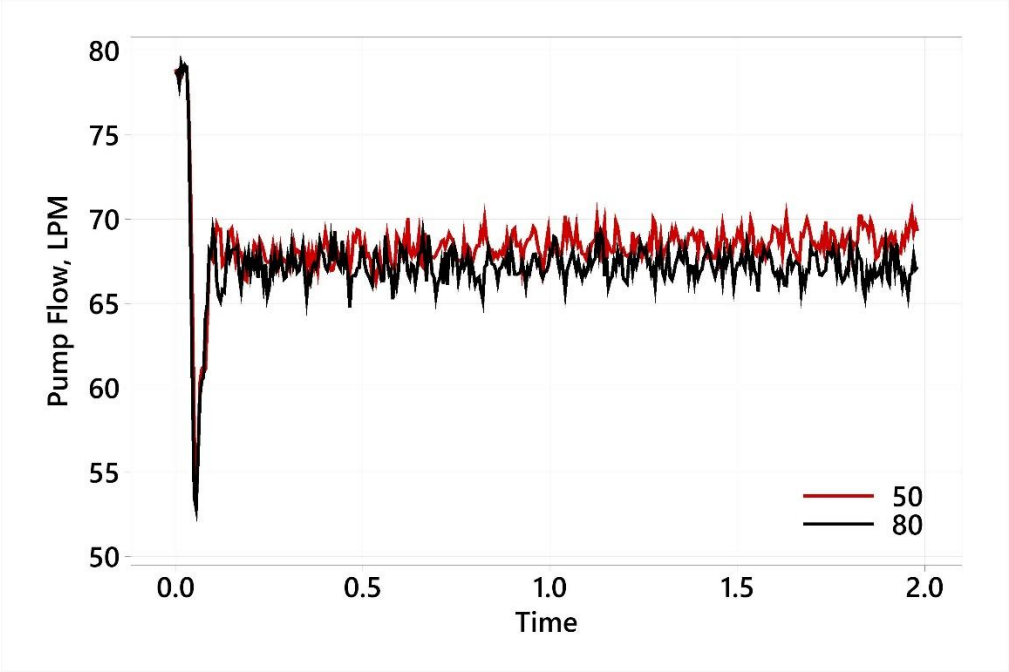

Figure D9 - Pressure Step Up - Pump Flow.

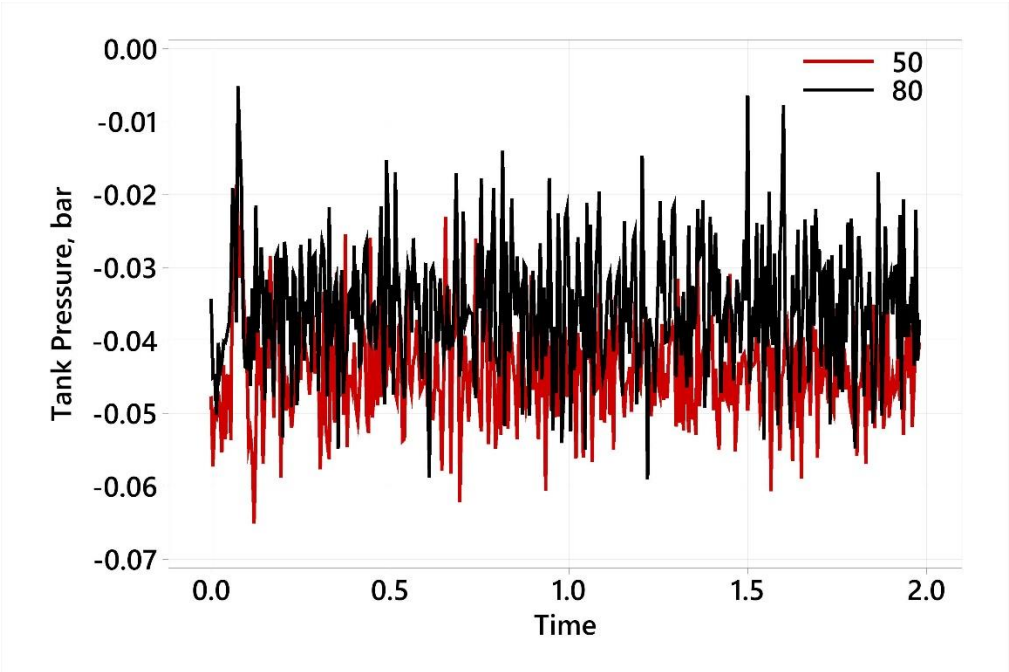

Figure D10 - Pressure Step Up - Tank Pressure.

Speed Steps

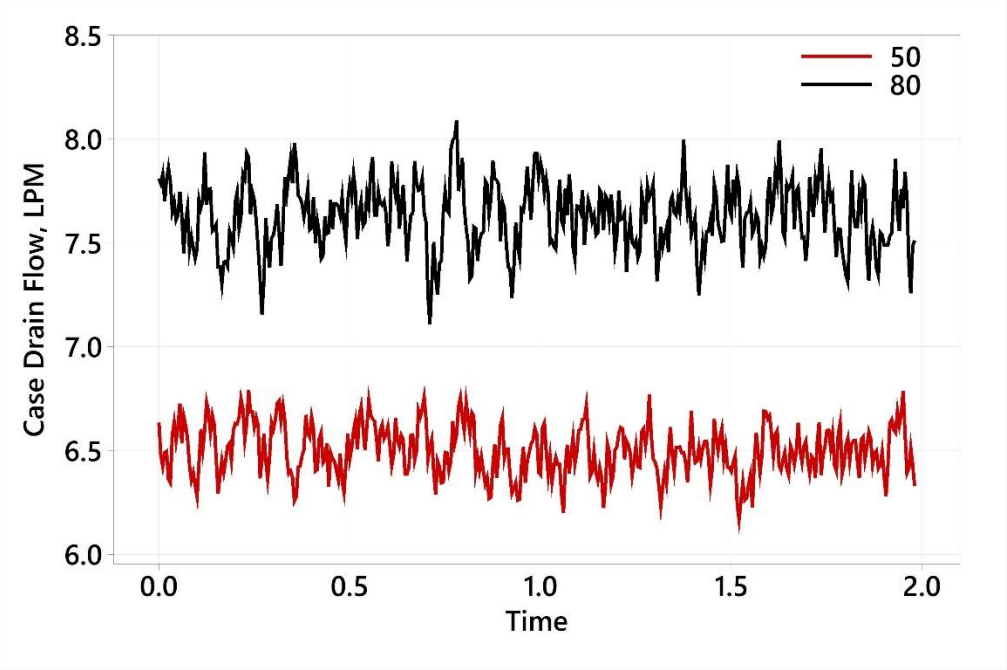

Figure D11 - Speed Step Down - Case Drain Flow.

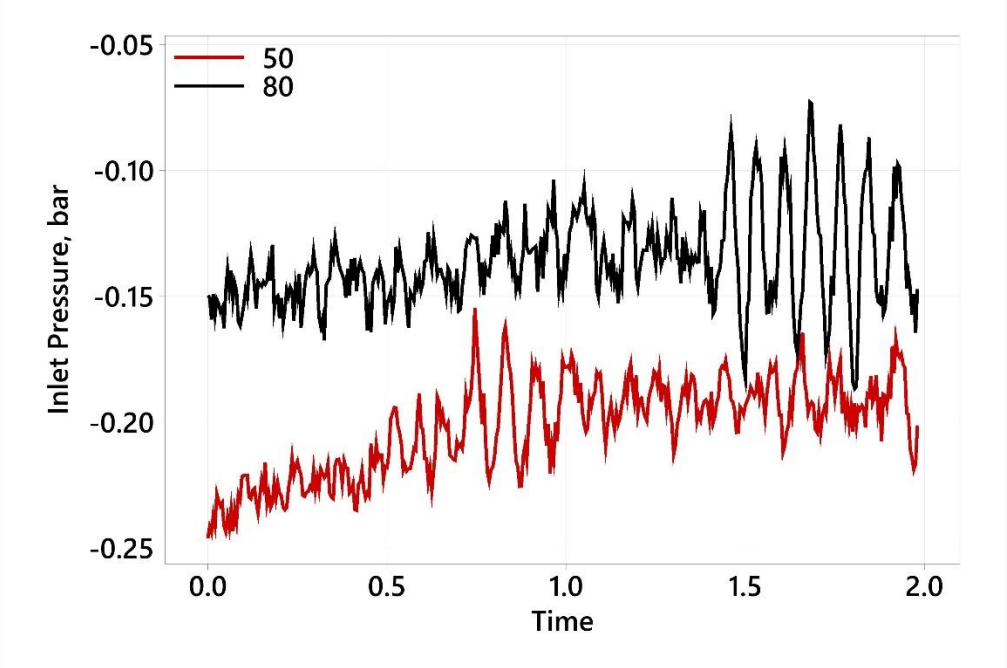

Figure D12 - Speed Step Down - Inlet Pressure.

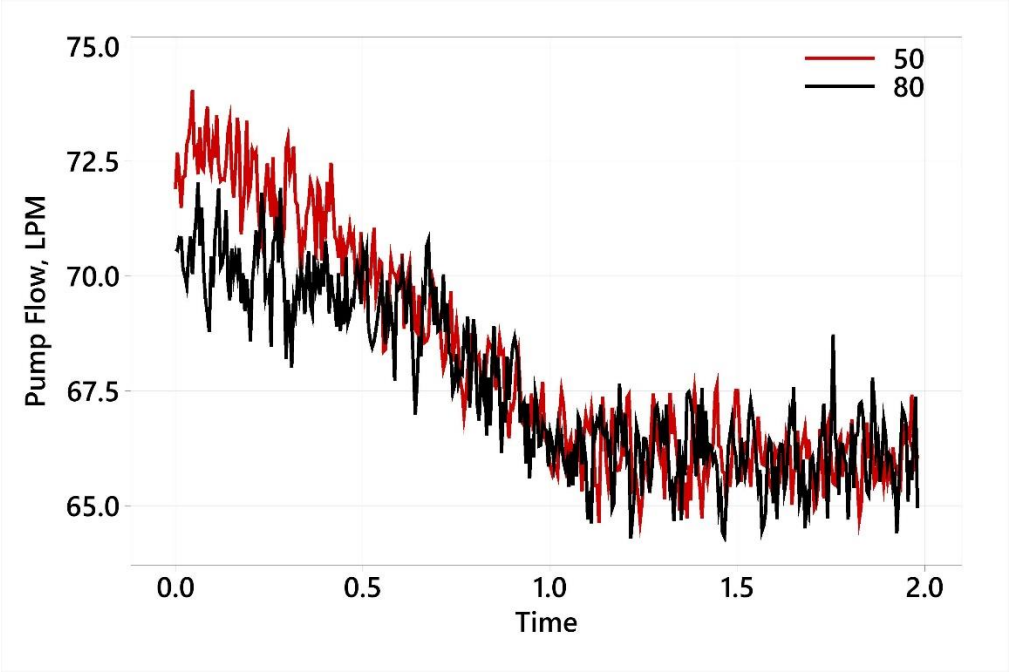

Figure D13 - Speed Step Down - Pump Flow.

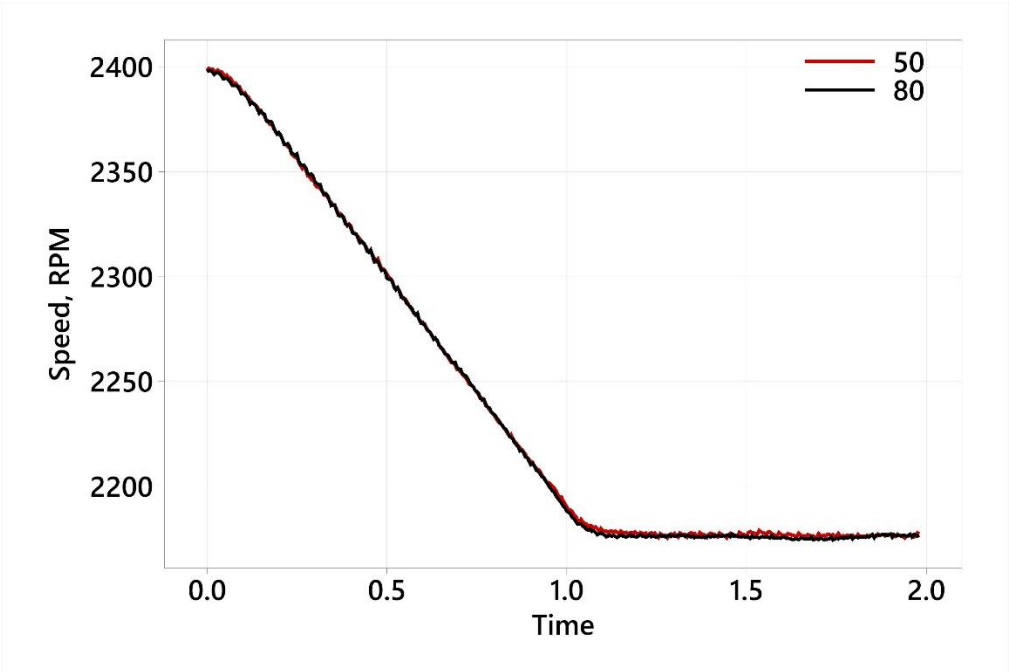

Figure D14 - Speed Step Down – Speed.

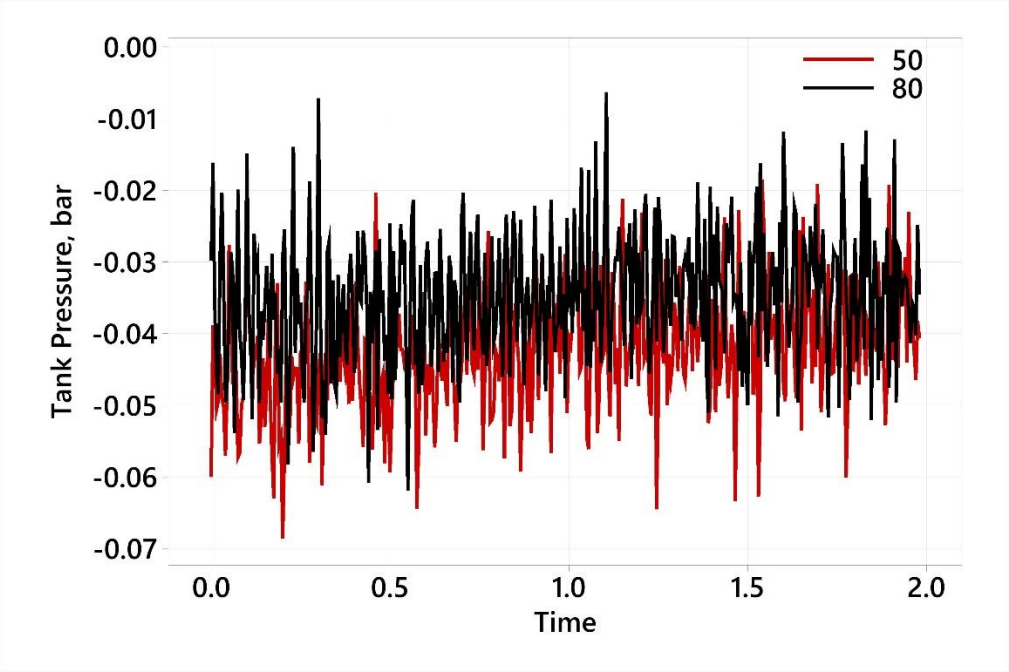

Figure D15 - Speed Step Down - Tank Pressure.

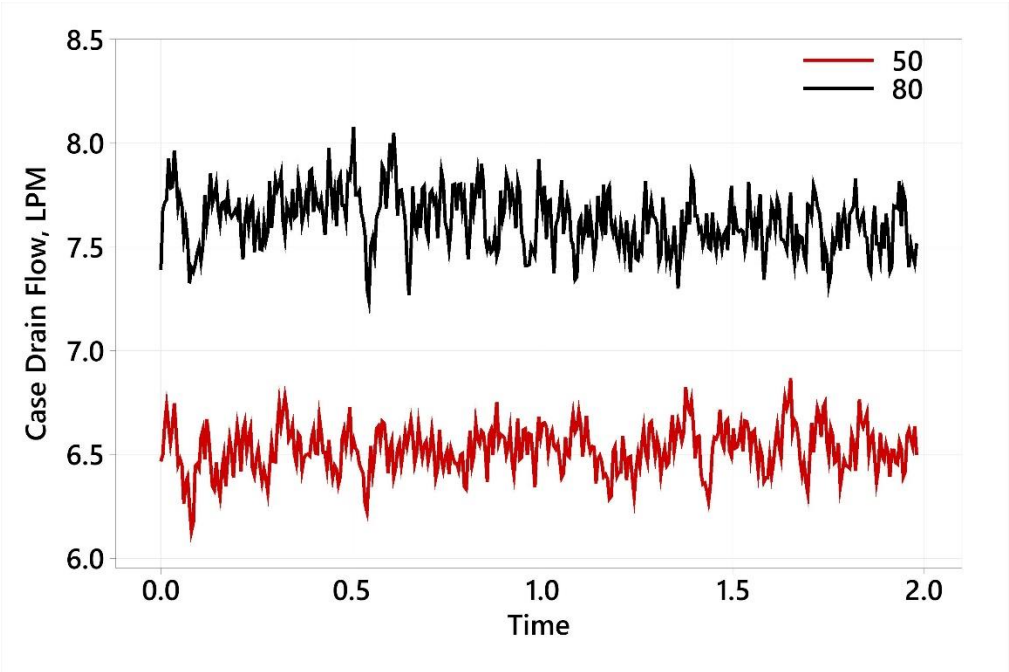

Figure D16 - Speed Step Up - Case Drain Flow.

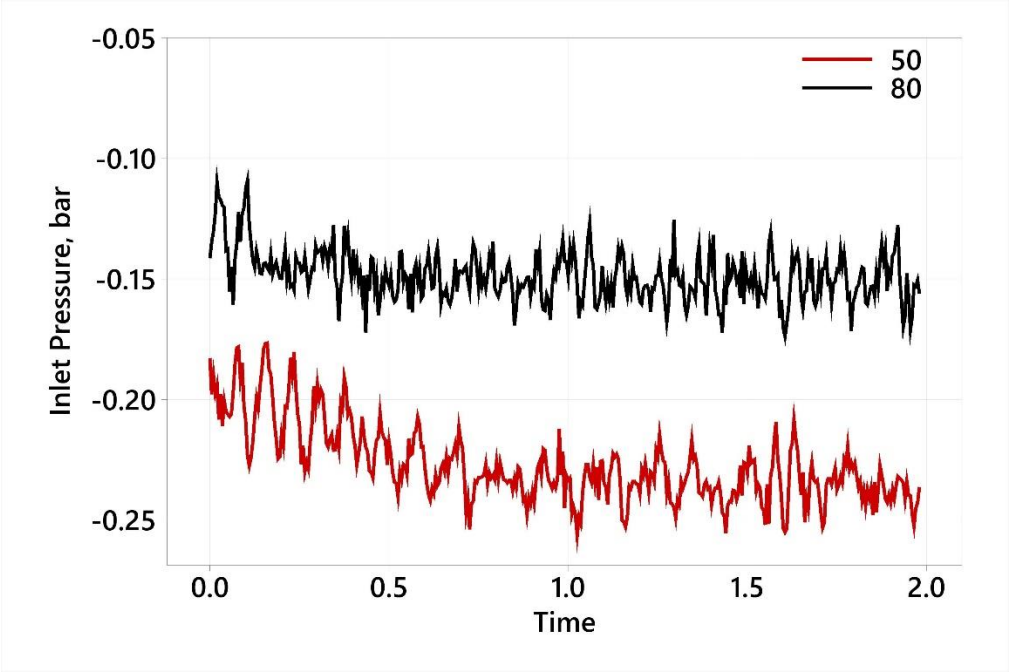

Figure D17 - Speed Step Up - Inlet Pressure.

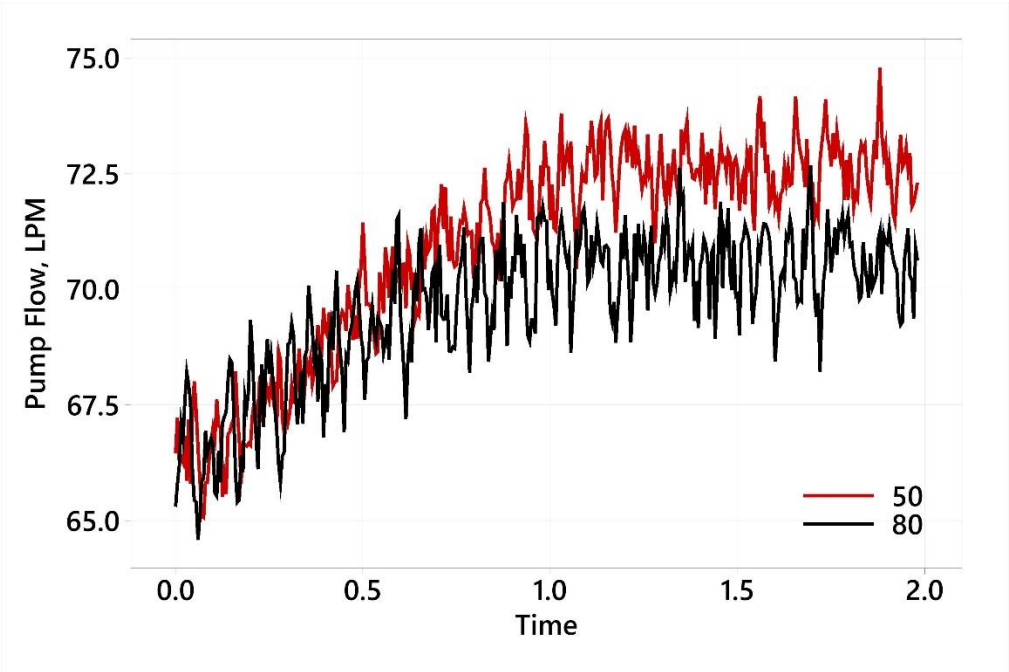

Figure D18 - Speed Step Up - Pump Flow..

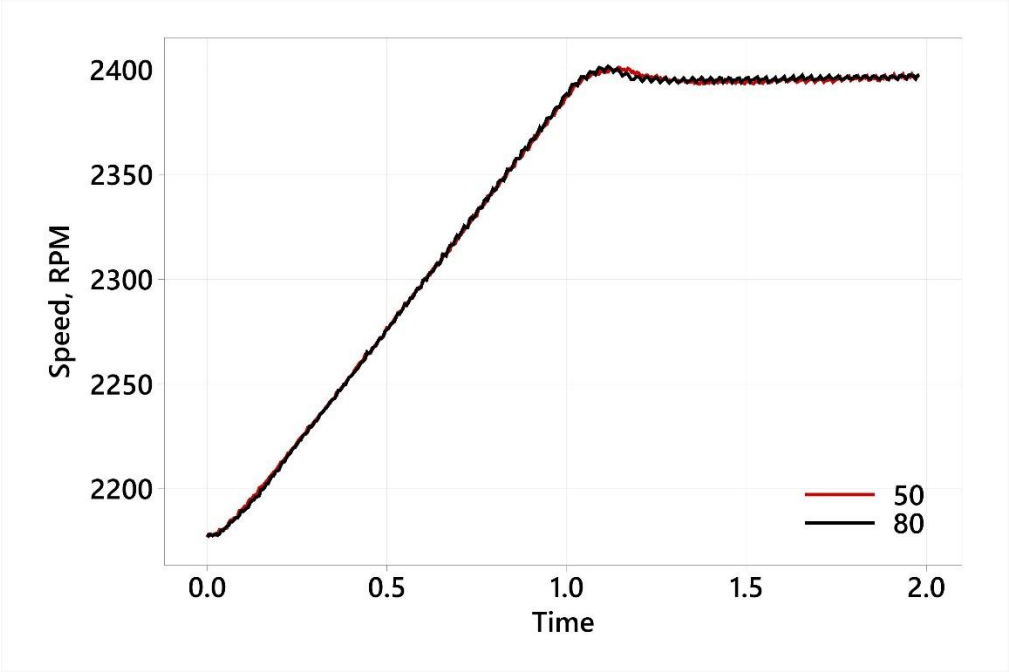

Figure D19 - Speed Step Up – Speed.

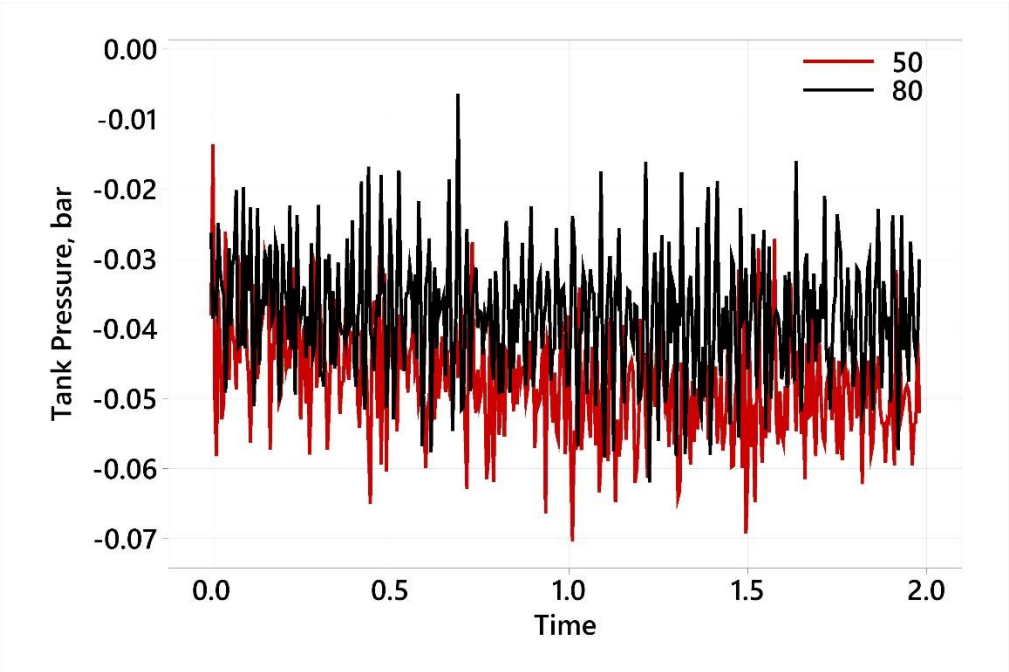

Figure D20 - Speed Step Up - Tank Pressure.

Swash Steps

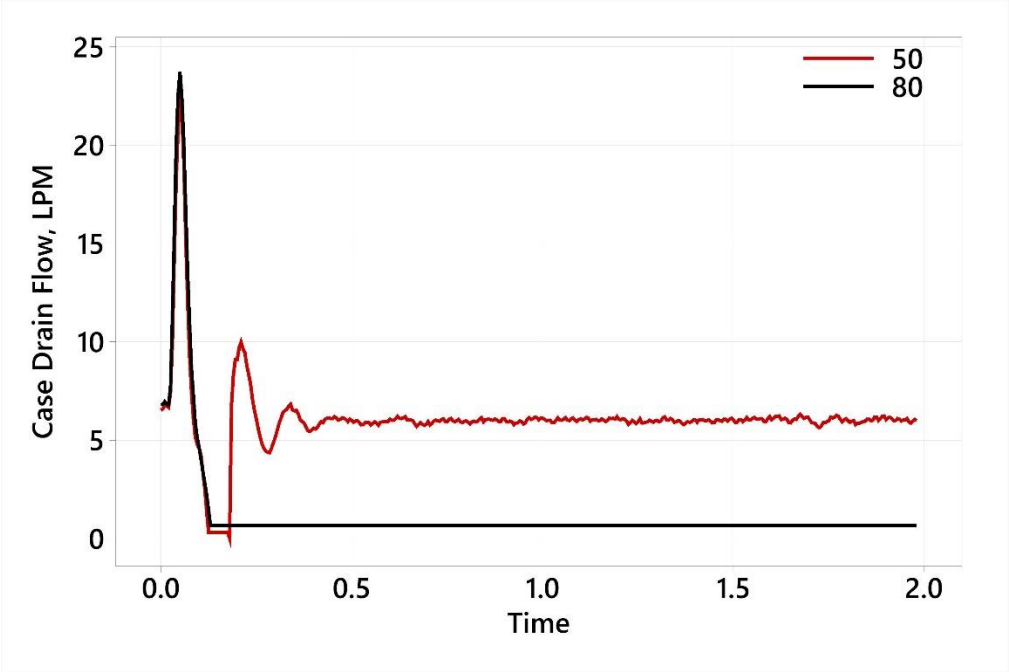

Figure D21 - Swash Step Down - Case Drain Flow.

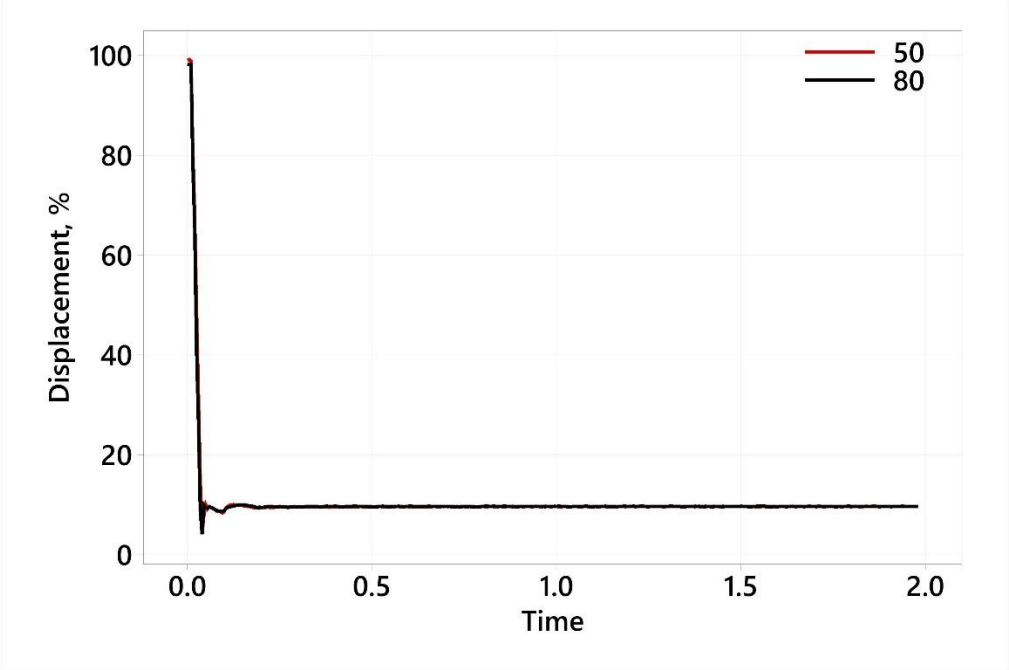

Figure D22 - Swash Step Down – Displacement.

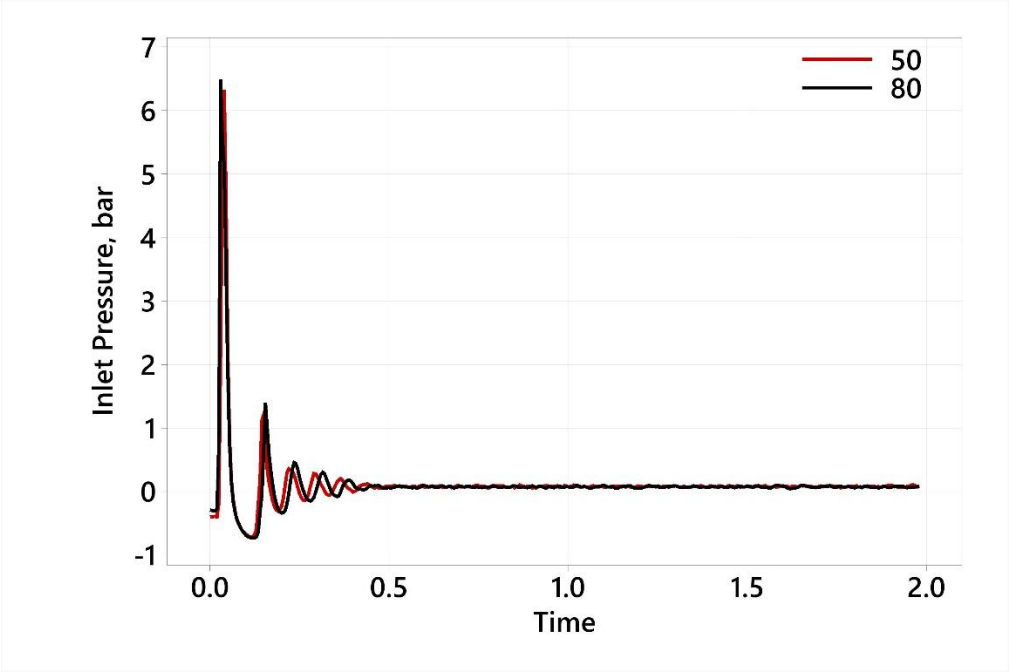

Figure D23 - Swash Step Down - Inlet Pressure.

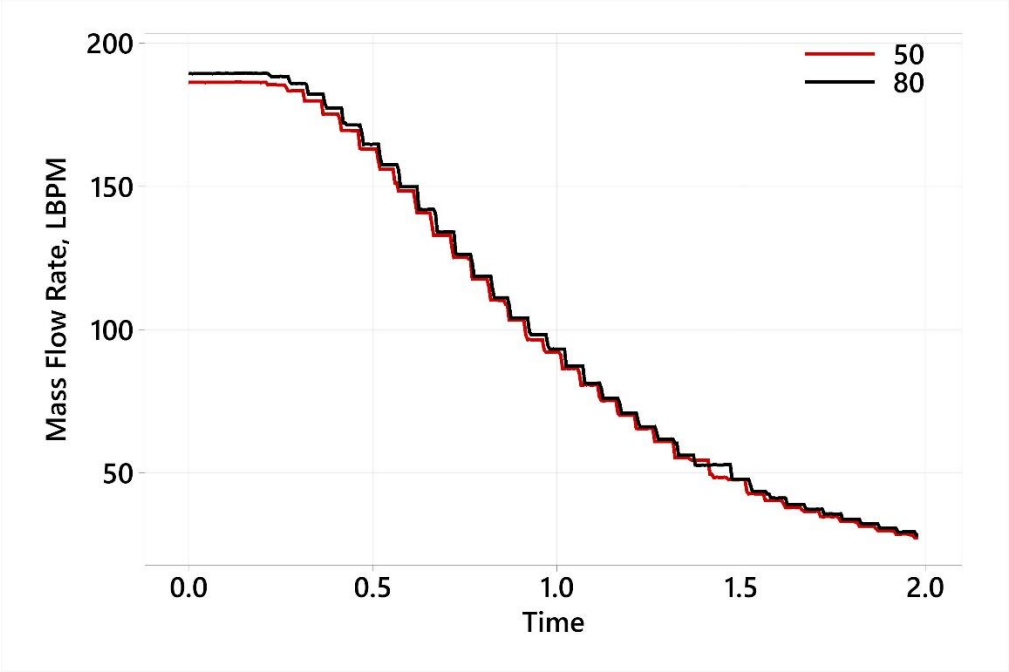

Figure D24 - Swash Step Down - Mass Flow Rate.

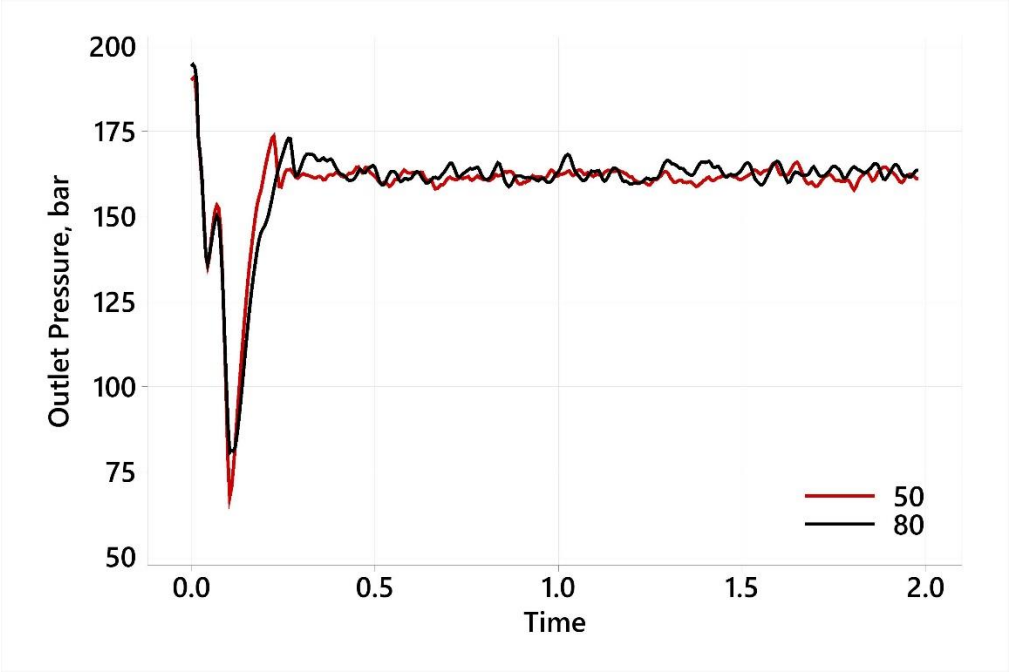

Figure D25 - Swash Step Down - Outlet Pressure.

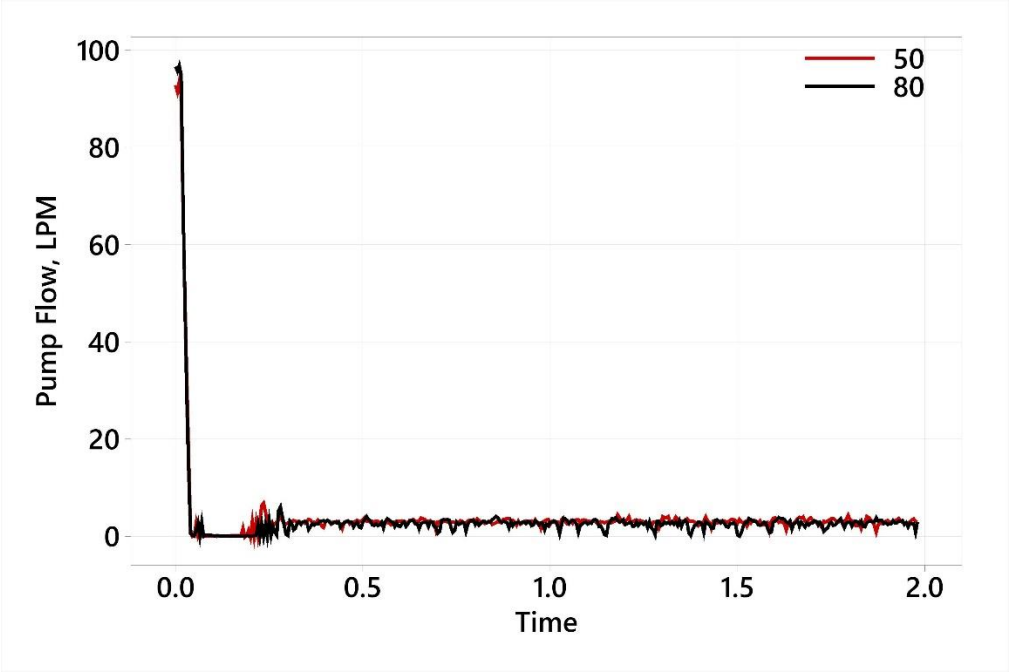

Figure D26 - Swash Step Down - Pump Flow.

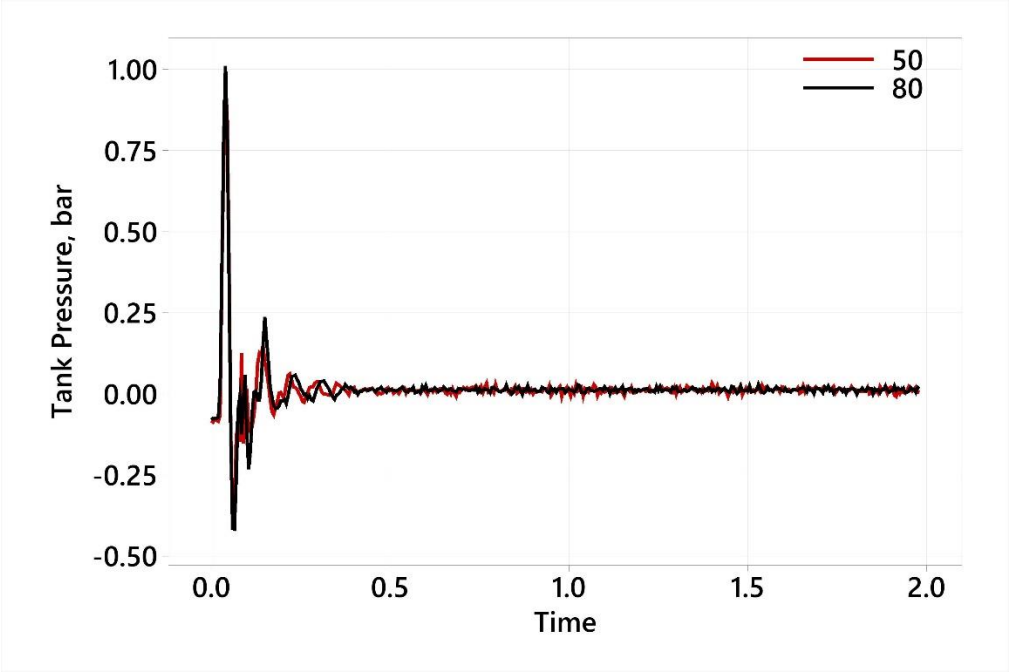

Figure D27 - Swash Step Down - Tank Pressure.

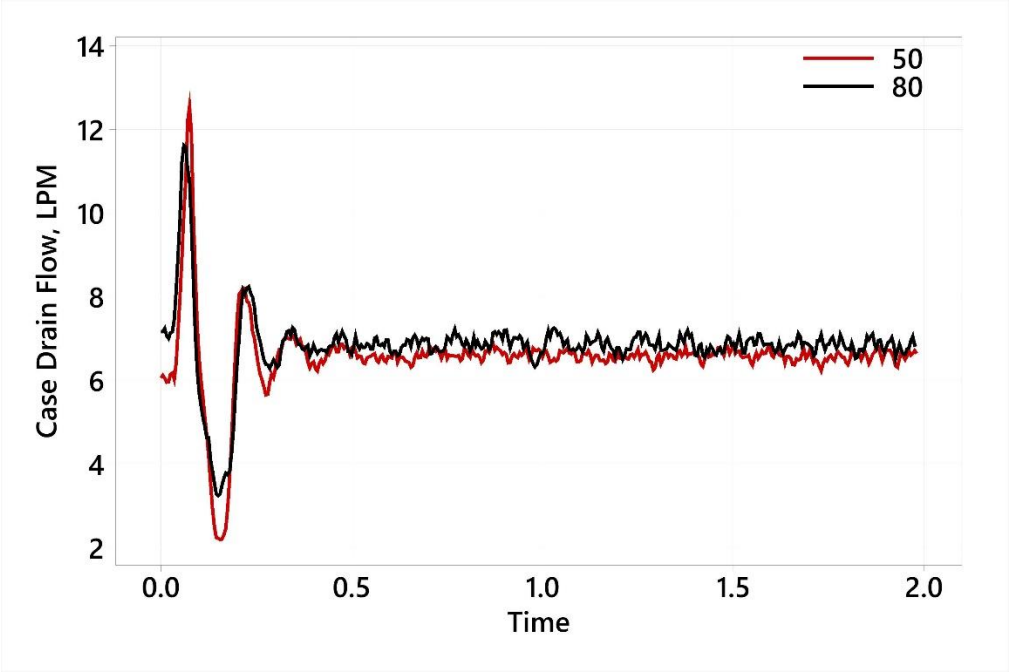

Figure D28 - Swash Step Up - Case Drain Flow.

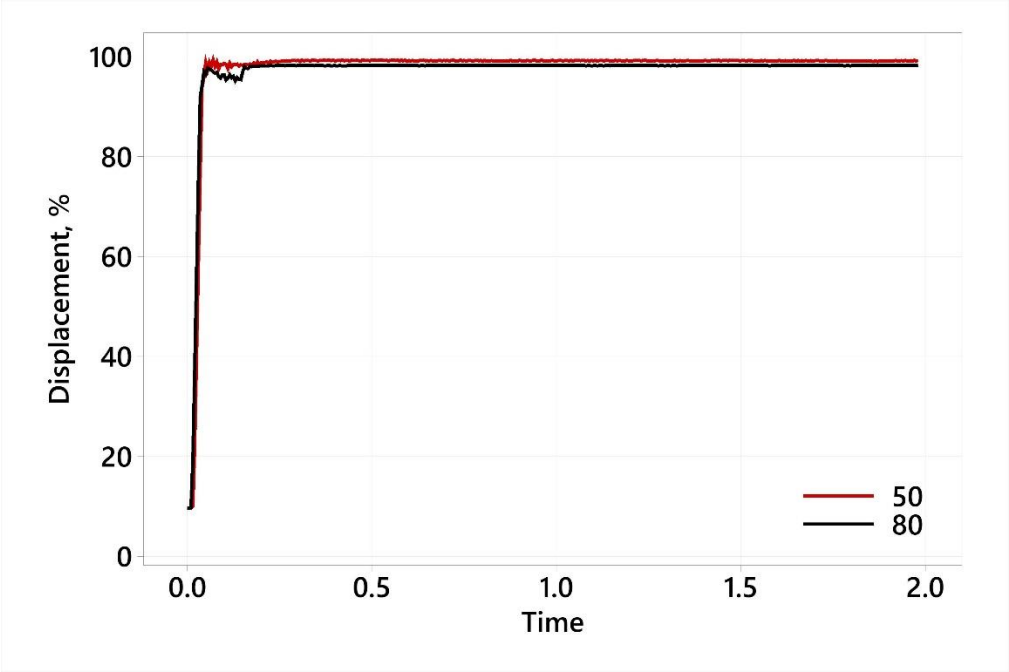

Figure D29 - Swash Step Up – Displacement.

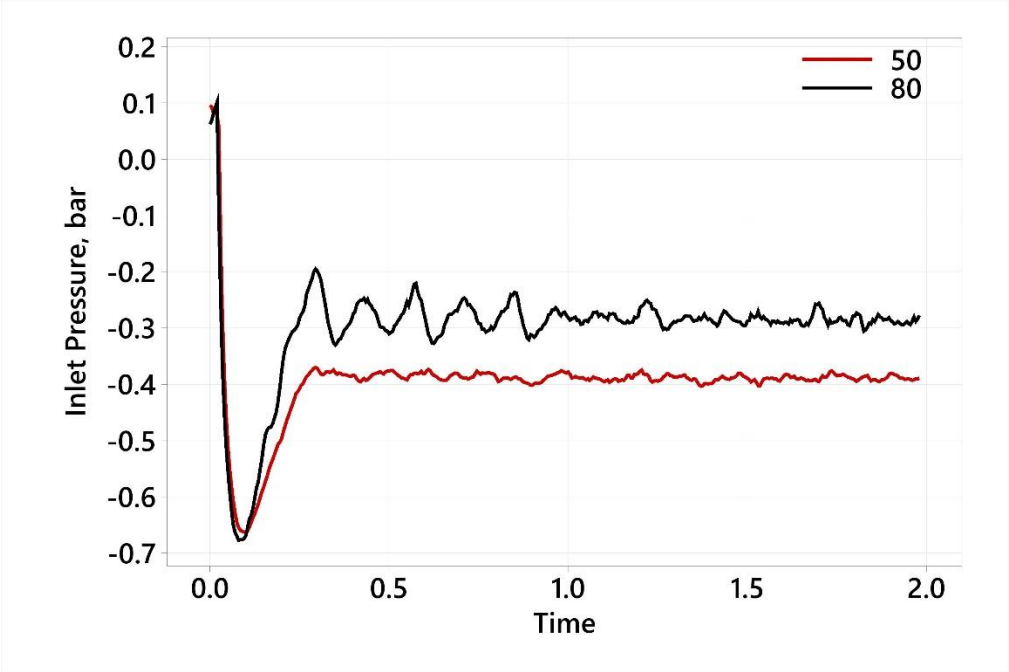

Figure D30 - Swash Step Up - Inlet Pressure.

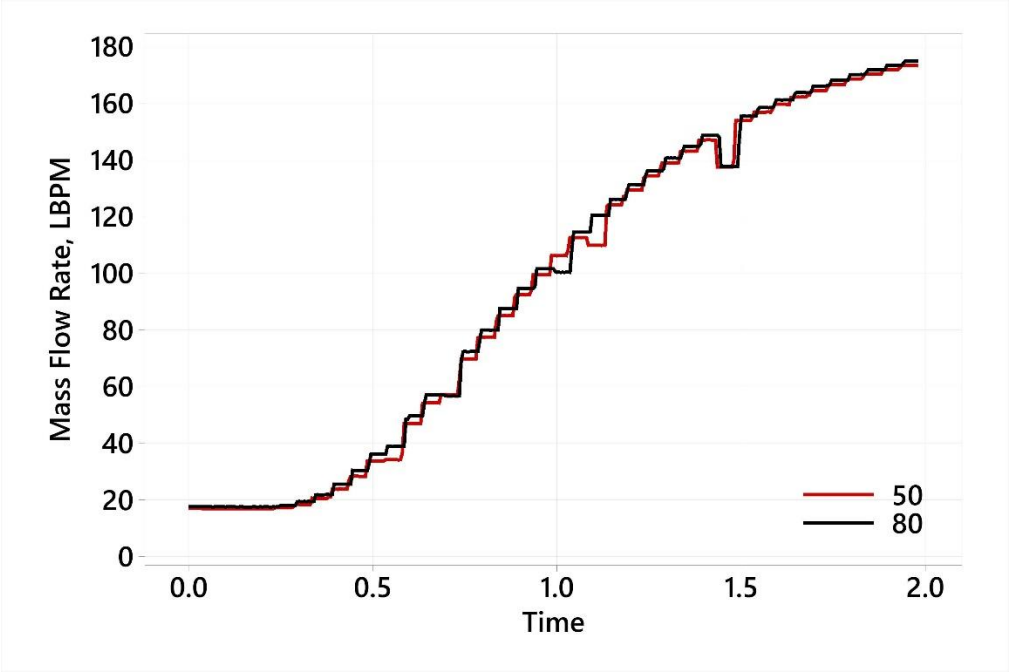

Figure D31 - Swash Step Up - Mass Flow Rate.

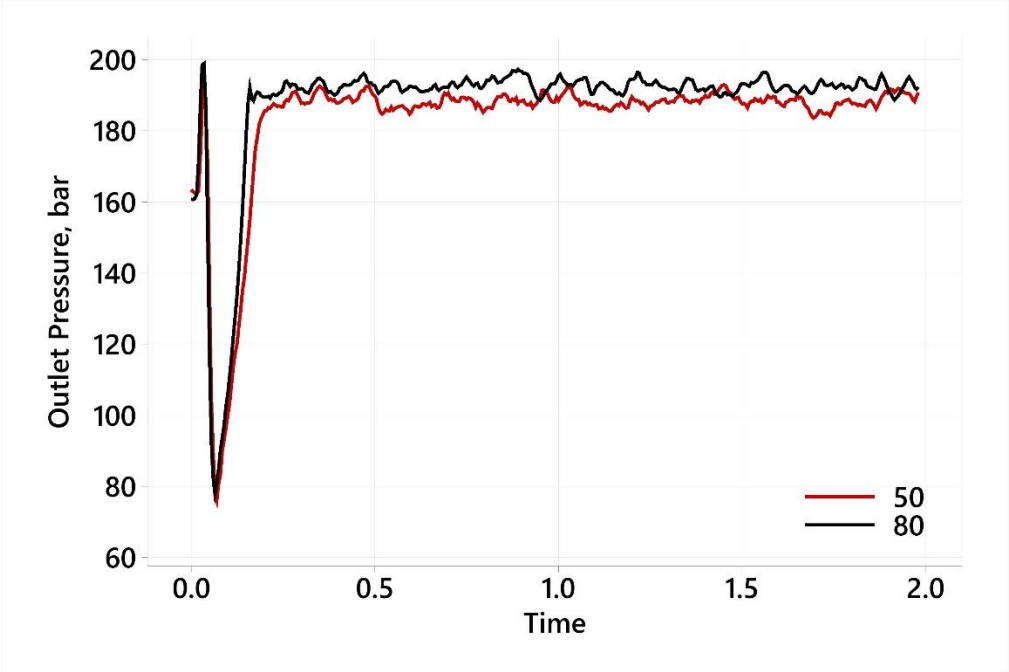

Figure D32 - Swash Step Up - Outlet Pressure.

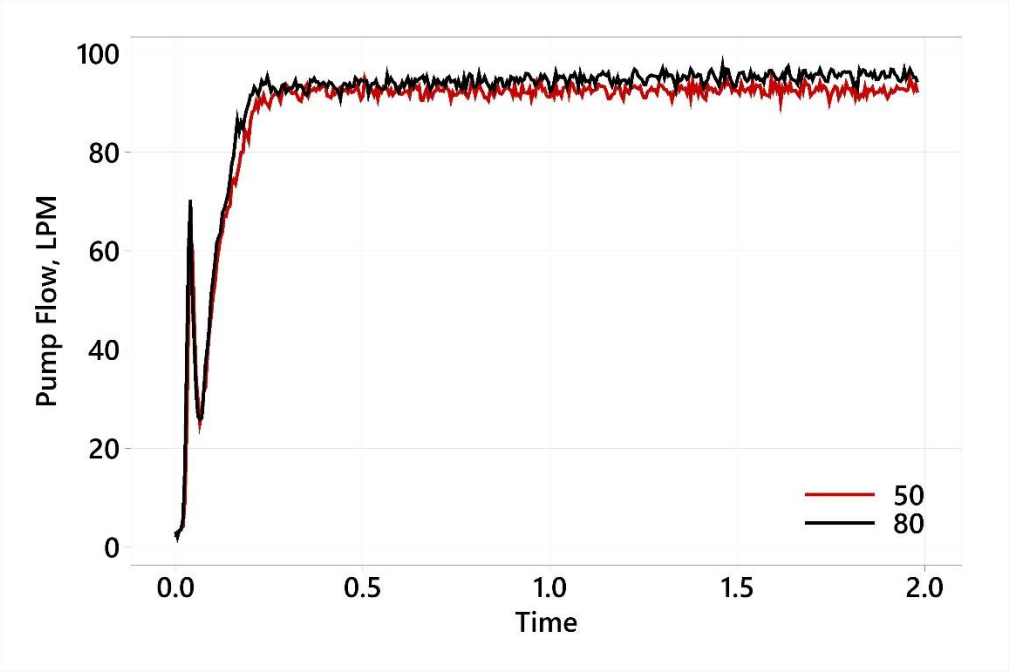

Figure D33 - Swash Step Up - Pump Flow.

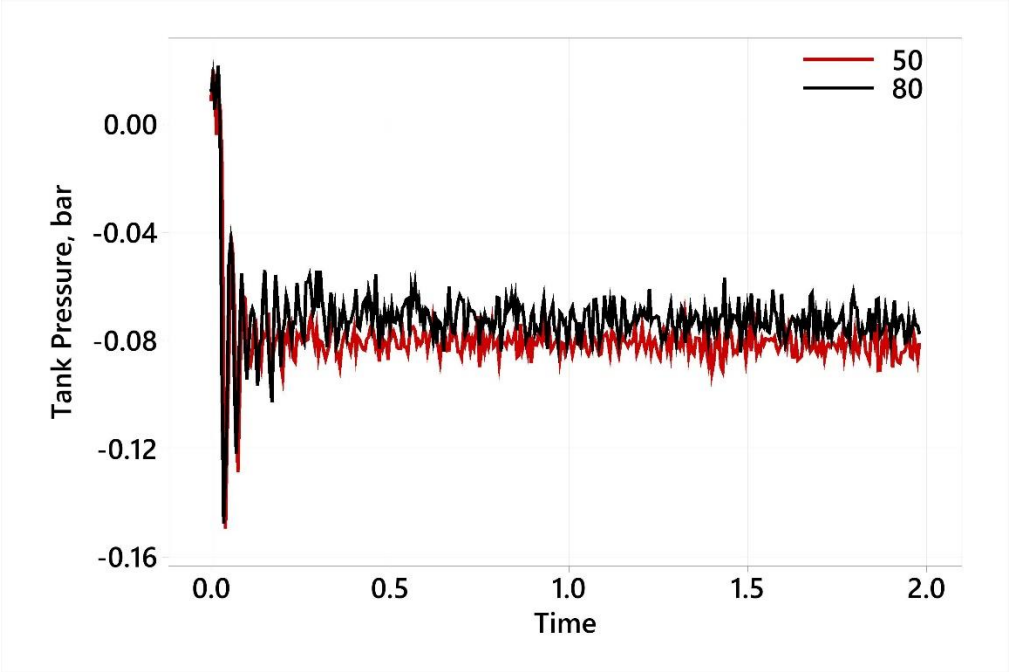

Figure D34 - Swash Step Up - Tank Pressure.

Appendix E – Viscosity and Density Results

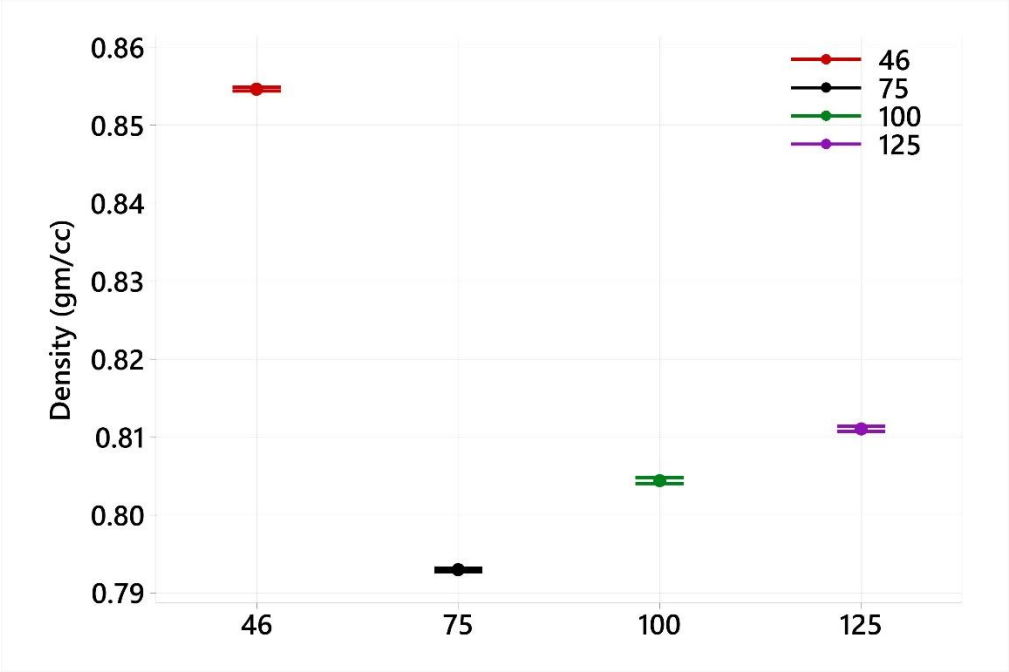

Figure E1 - Comparison of Fluid Density at 50 °C.

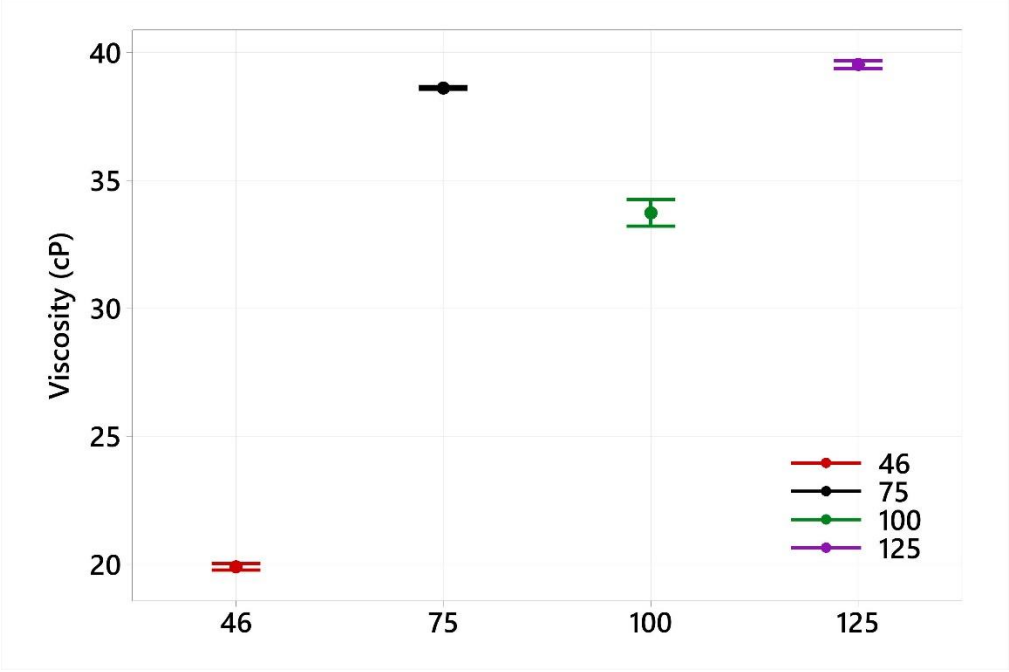

Figure E2 - Comparison of Fluid Viscosity at 50 °C.

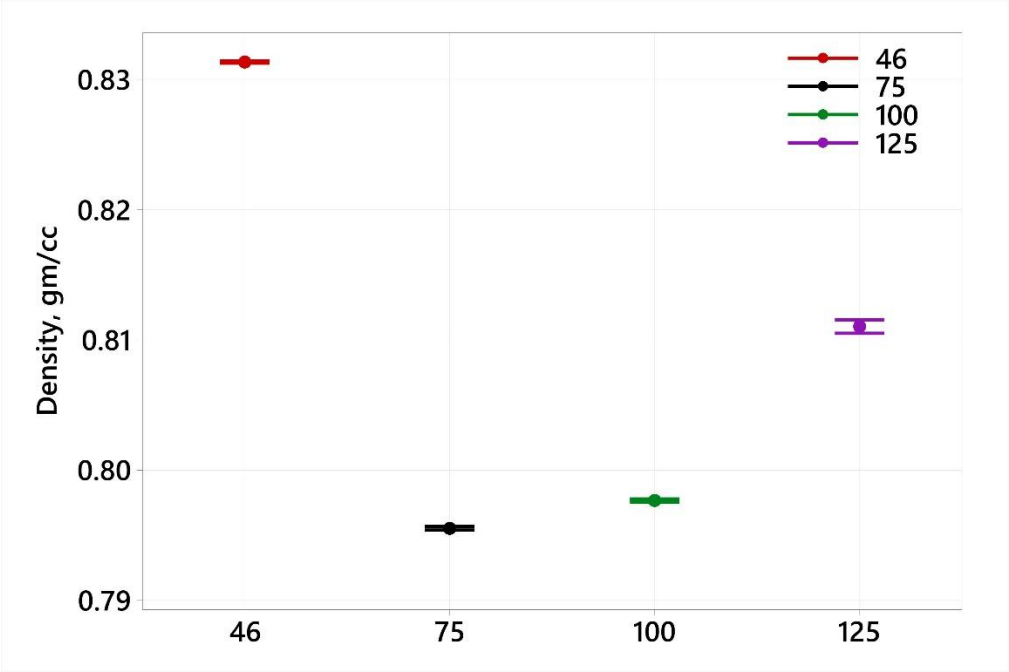

Figure E3 - Comparison of Fluid Density at 80 °C.

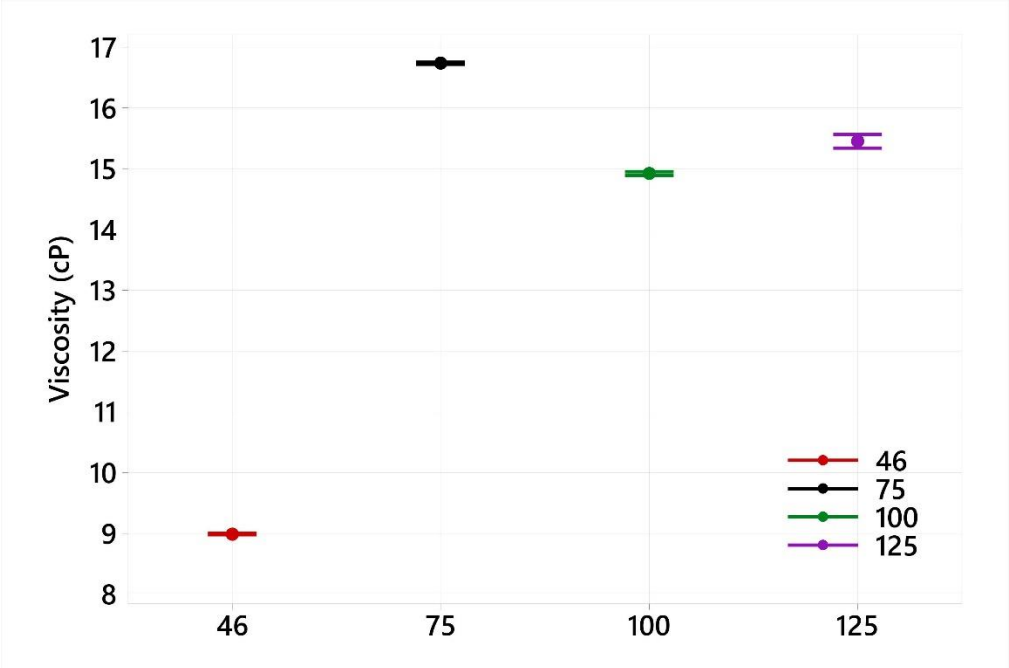

Figure E4 - Comparison of Fluid Viscosity at 80 °C.

Appendix F – Air Solubility

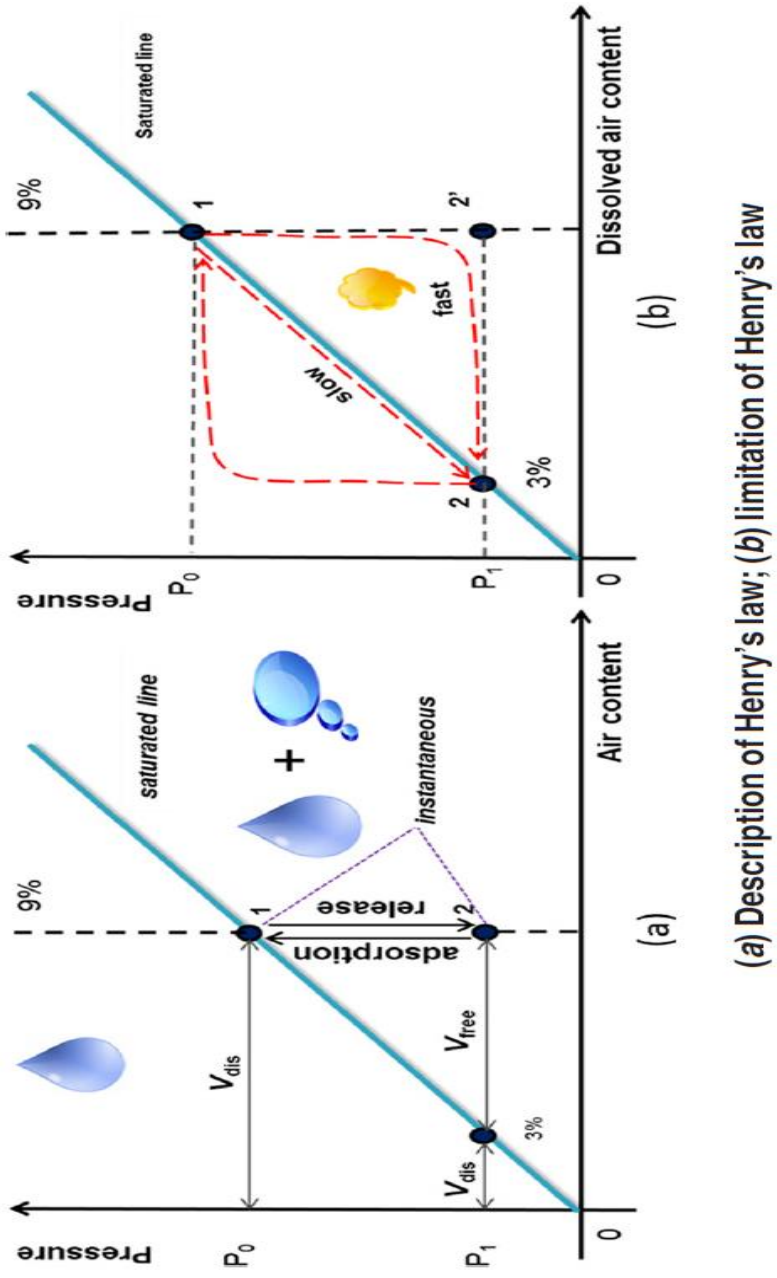

Figure F1 – Air Solubility Explained Through Henry's Law[1].

[1] Zhou, J., Vacca, A. and Manhartsgruber, B., "A Novel Approach for the Prediction of Dynamic Features of Air Release and Absorption in Hydraulic Oils," *Journal of Fluids Engineering*, vol. 135, no. 9, 2013.

Appendix G – Inlet Modeling (Code and Model Work by Dr. Daniel Williams)

Inlet Model Code

```
Qinit=90;%40; %90 for off-stroking
Q0 = Qinit;
Qf = Q0;
Tstart = 0;
Tend = 10;
Tinc = 0.001;
Ptank = 15;
t1 = Tstart+0.1;
t2 = t1 + 0.2;
Flows = [Q0 Q0 Qf Qf]; % These are changed in run4.m
FlowTimes = [Tstart t1 t2 Tend];
if exist('T') == 0
    T = 122
end
FEA = 0.01;%0.005;%0.01 for better damping (lower stiffness)
if T==122
    cP = 32;
    SG = 0.835;
%     p0(7) = 17;
else
    cP = 14;
    SG = 0.820;
%     p0(7) = 17;
end
density = SG*62.4/1728/386.1
viscosity = cP/1000/4.448/39.37^2
% rho = zeros(1,20);
% mu = zeros(1,20);
BaseBulkModulus = 220000; % psi
Air = 0.01; % Volumetric fraction
Cratio = 1.4; % Gas law volume exponent
for ic = 1:20
    rho(ic) = density;
    mu(ic) = viscosity;
    p0(ic) = 16.8;
end
[values,txt,raw] = xlsread('CircuitLossParameters.xlsx');
A7.diameter = values(1);
A7.length = values(2);
A7.roughness = values(3);
A7.angle = values(6);

A9.Kfactor = values(9);
A9.diameter = values(10);

A10.Kfactor = values(14);
A10.diameter = values(15);

A11.Kfactor = values(19);
```

```
A11.diameter = values(20);

A12.Kfactor = values(24);
A12.diameter = values(25);

A12b.diameter = values(29);
A12b.length = values(30);
A12b.roughness = values(31);
A12b.angle = values(34);

A13.Kfactor = values(37);
A13.diameter = values(38);

A13b.diameter = values(42);
A13b.length = values(43);
A13b.roughness = values(44);
A13b.angle = values(47);

A14.Kfactor = values(50);
A14.diameter = values(51);

A15.diameter = values(55);
A15.length = values(56);
A15.roughness = values(57);
A15.angle = values(60);

A17.Kfactor = values(63);
A17.diameter = values(64);

A19.diameter = values(68);
A19.length = values(69);
A19.roughness = values(70);
A19.angle = values(73);

A20.Kfactor = values(76);
A20.diameter = values(77);

% Inertance parameters
volume = 303; % in^3
area = 1.25;  % in^2
```

Test Data Code

```
% clear
init_model_3
switch SimType
    case 3
        filename = '.\Oil HV 46-4\Step_Response_176_3_17_Swash_Up.csv';
    otherwise
        filename = '.\Oil HV 46-4\Step_Response_176_3_18_Swash_Down.csv';
end
[num,txt,raw] = xlsread(filename);
tIC = 0;
timev = tIC + num(2:end,11);
timev = [0:Tinc:tIC timev']';
CQ = 231/60;
Patm = 14.7;
Qdrain = num(2:end,12)*CQ;
QpumpO = num(2:end,16)*CQ;
pumpP = num(2:end,20) + Patm;
tankP = num(2:end,28) + Patm;
QpumpI = QpumpO + Qdrain;
QresIC = 0;
DataTimes = timev;
tankPIC = tankP(1);
PpiIC = pumpP(1);
QpumpIIC = QpumpI(1);
PumpPressureData = [PpiIC*ones(size([0:Tinc:tIC])) ...
    pumpP']';
ReservoirPressureData = [tankPIC*ones(size([0:Tinc:tIC])) ...
    tankP']';
PumpFlowData = [QpumpIIC*ones(size([0:Tinc:tIC])) QpumpI']';
x1 = tIC-1;x2 = tIC+1;
% figure(1)
% plot(DataTimes,PumpFlowData)
% axis([x1 x2 0 150])
% grid
% title('Pump Inlet Flow Data')
% figure(2)
% plot(DataTimes,ReservoirPressureData)
% axis([x1 x2 0 40])
% grid
% title('Reservoir Pressure Data')
% init_model
Ptank = tankP(1);
Qinit = QpumpI(1);
Flows = Qinit*ones(size(Flows));
p0 = tankP(1)*ones(size(p0));
```

Test Run Code

```
ktIC = 5;
close all
for SimType = 2
    % SimType = 2; % 2 for swash down and 3 for swash up

    % Load test data for boundary conditions and comparisons
    testdataV3

    % These parameters were used to tune the model to match the
    % measured steady-state pressure differential.
    A19.diameter = 0.75;
    A19.length = 50;
    A7.length = 20;

    % These parameters can be adjusted to study the sensitivity of
    % of the simulated results.

    volume = 300; % Of inlet circuit (in^3)
    area = 2.41;  % Average of inlet circuit (in^2)
    SG = 0.82;   % Specific gravity of oil
    density = SG*62.4/1728/386.1; % English units
    cP = 40;      % Viscosity (cP)
    viscosity = cP/1000/4.448/39.37^2; % English units
    BaseBulkModulus = 200000; % of fluid and container(s) (psi)
    Air = 0.003; % Volumetric fraction of air at atmospheric pressure
    Cratio = 1.4; % Gas law volume exponent PxV^Cratio = constant

%     Tend = tIC + 1;
%     out = sim('Pump_Inlet_Circuit_V3');
%     istart = 1000*tIC+1;
%     tv = out.simout.Time(istart:end);
%     PIexp = out.simout.Data(istart:end,4);
%     PIsim = out.simout.Data(istart:end,3);
%     figure(SimType)
%     plot(tv,PIexp,'b',tv,PIsim,'r')
%     title('Pump Inlet Pressure')
%     xlabel('Time (s)'), ylabel('Pressure (psia)')
%     grid on
%     legend('Experiment','Simulation')

%     Testing sim results only for viscosity
    Tend = tIC + 1;
    out = sim('Pump_Inlet_Circuit_V3');
    istart = 1000*tIC+1;
    tv = out.simout.Time(istart:end);
    PIexp = out.simout.Data(istart:end,4);
    PIsim = out.simout.Data(istart:end,3);
    figure(SimType)
    plot(tv,PIexp,'b',tv,PIsim,'r')
```

```
    title('Pump Inlet Pressure')
    xlabel('Time (s)'), ylabel('Pressure (psia)')
    grid on
    hold on

%     legend('Experiment','40 cP')
%
%     volume = 300; % Of inlet circuit (in^3)
%     area = 2.41;  % Average of inlet circuit (in^2)
%     SG = 0.5;   % Specific gravity of oil
%     density = SG*62.4/1728/386.1; % English units
%     cP = 30;      % Viscosity (cP)
%     viscosity = cP/1000/4.448/39.37^2; % English units
%     BaseBulkModulus = 220000; % of fluid and container(s) (psi)
%     Air = 0.003; % Volumetric fraction of air at atmospheric pressure
%     Cratio = 1.4; % Gas law volume exponent PxV^Cratio = constant
%     out = sim('Pump_Inlet_Circuit_V3');
%     istart = 1000*tIC+1;
%     tv = out.simout.Time(istart:end);
%     PIexp = out.simout.Data(istart:end,4);
%     PIsim = out.simout.Data(istart:end,3);
%     hold on
%     plot(tv,PIsim,'r')
%
%     volume = 300; % Of inlet circuit (in^3)
%     area = 2.41;  % Average of inlet circuit (in^2)
%     SG = 0.5;   % Specific gravity of oil
%     density = SG*62.4/1728/386.1; % English units
%     cP = 20;      % Viscosity (cP)
%     viscosity = cP/1000/4.448/39.37^2; % English units
%     BaseBulkModulus = 220000; % of fluid and container(s) (psi)
%     Air = 0.003; % Volumetric fraction of air at atmospheric pressure
%     Cratio = 1.4; % Gas law volume exponent PxV^Cratio = constant
%     out = sim('Pump_Inlet_Circuit_V3');
%     istart = 1000*tIC+1;
%     tv = out.simout.Time(istart:end);
%     PIexp = out.simout.Data(istart:end,4);
%     PIsim = out.simout.Data(istart:end,3);
%     hold on
%     plot(tv,PIsim,'k')

% Testing Simulation at different Viscosities

    cP = 30;      % Viscosity (cP)
    viscosity = cP/1000/4.448/39.37^2; % English units
%     SG = 0.80;   % Specific gravity of oil
%     density = SG*62.4/1728/386.1; % English units
    out = sim('Pump_Inlet_Circuit_V3');
    istart = 1000*tIC+1;
    tv = out.simout.Time(istart:end);
%     PIexp = out.simout.Data(istart:end,4);
    PIsim = out.simout.Data(istart:end,3);
```

```
    hold on
    plot(tv,PIsim,'k')

    cP = 20;      % Viscosity (cP)
    viscosity = cP/1000/4.448/39.37^2; % English units
%     SG = 0.75;   % Specific gravity of oil
%     density = SG*62.4/1728/386.1; % English units
    out = sim('Pump_Inlet_Circuit_V3');
    istart = 1000*tIC+1;
    tv = out.simout.Time(istart:end);
%     PIexp = out.simout.Data(istart:end,4);
    PIsim = out.simout.Data(istart:end,3);
    hold on
    plot(tv,PIsim,'g')

    cP = 10;      % Viscosity (cP)
    viscosity = cP/1000/4.448/39.37^2; % English units
%     SG = 0.70;   % Specific gravity of oil
%     density = SG*62.4/1728/386.1; % English units
    out = sim('Pump_Inlet_Circuit_V3');
    istart = 1000*tIC+1;
    tv = out.simout.Time(istart:end);
%     PIexp = out.simout.Data(istart:end,4);
    PIsim = out.simout.Data(istart:end,3);
    hold on
    plot(tv,PIsim,'m')


    legend('Experiment','40 cP','30 cP','20 cP', '10 cP')
%
end
```

Simulink Model

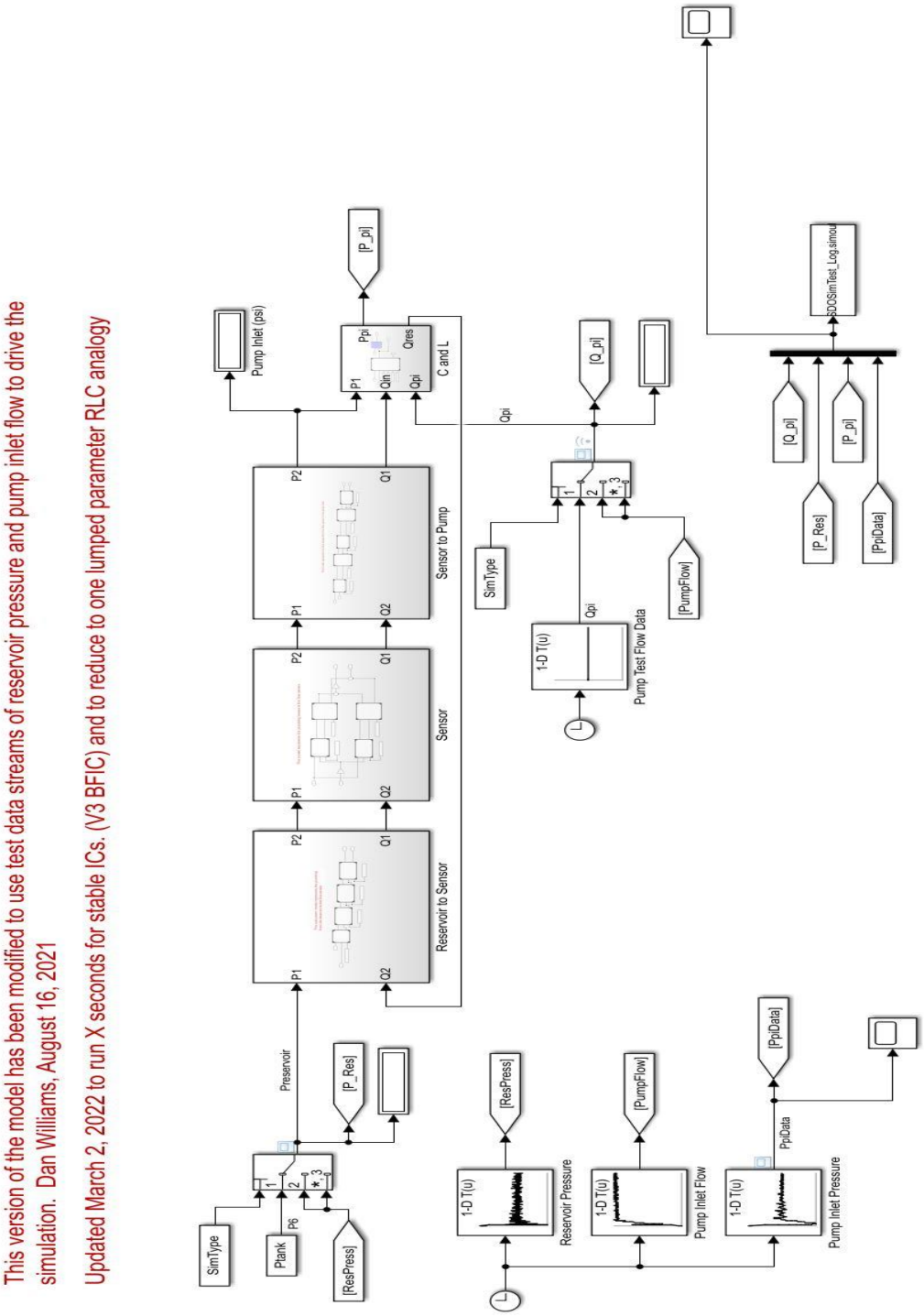

Figure G1 - Simulink Model of the Dynamometer Inlet.

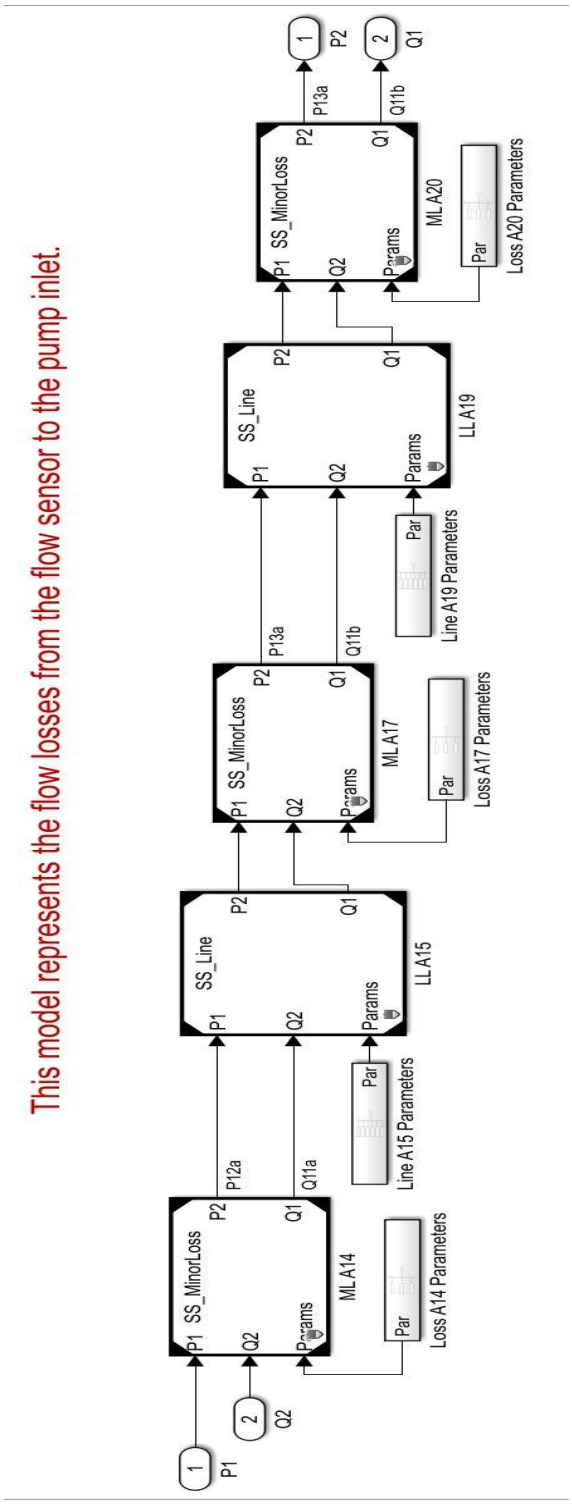

Figure G2 - Model Subsystem 1.

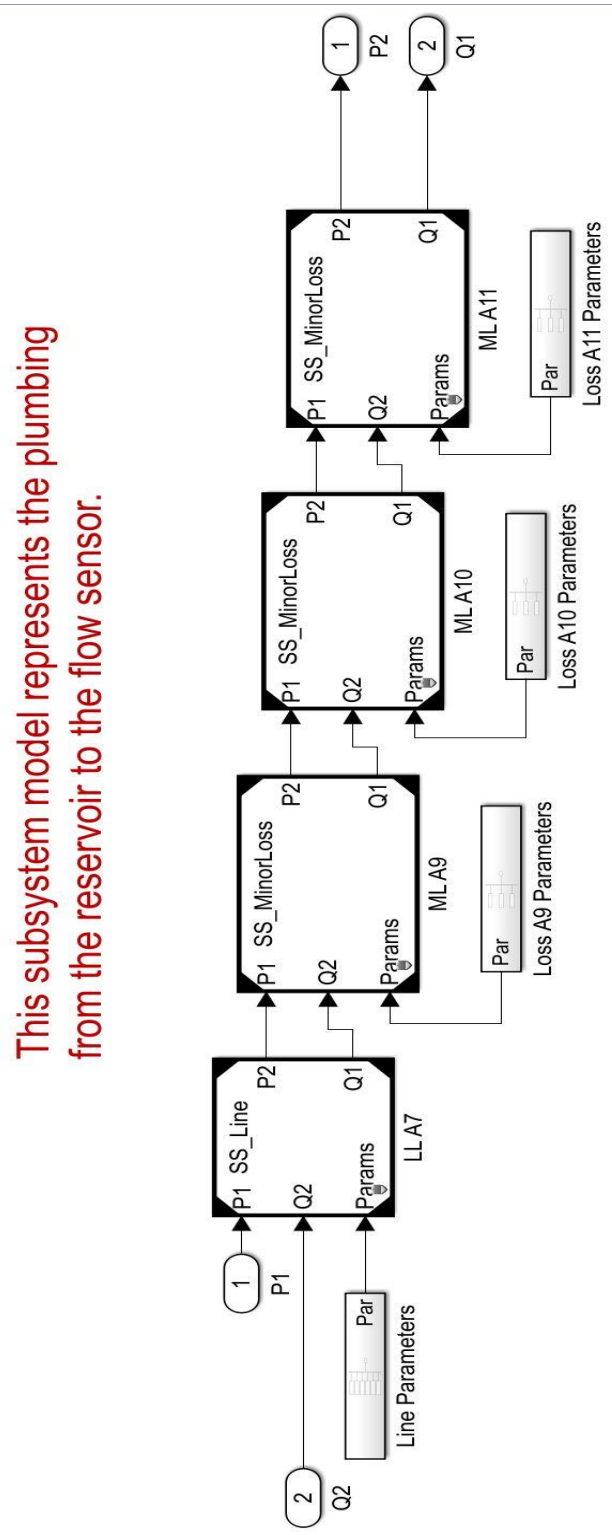

Figure G3 - Model Subsystem 2.

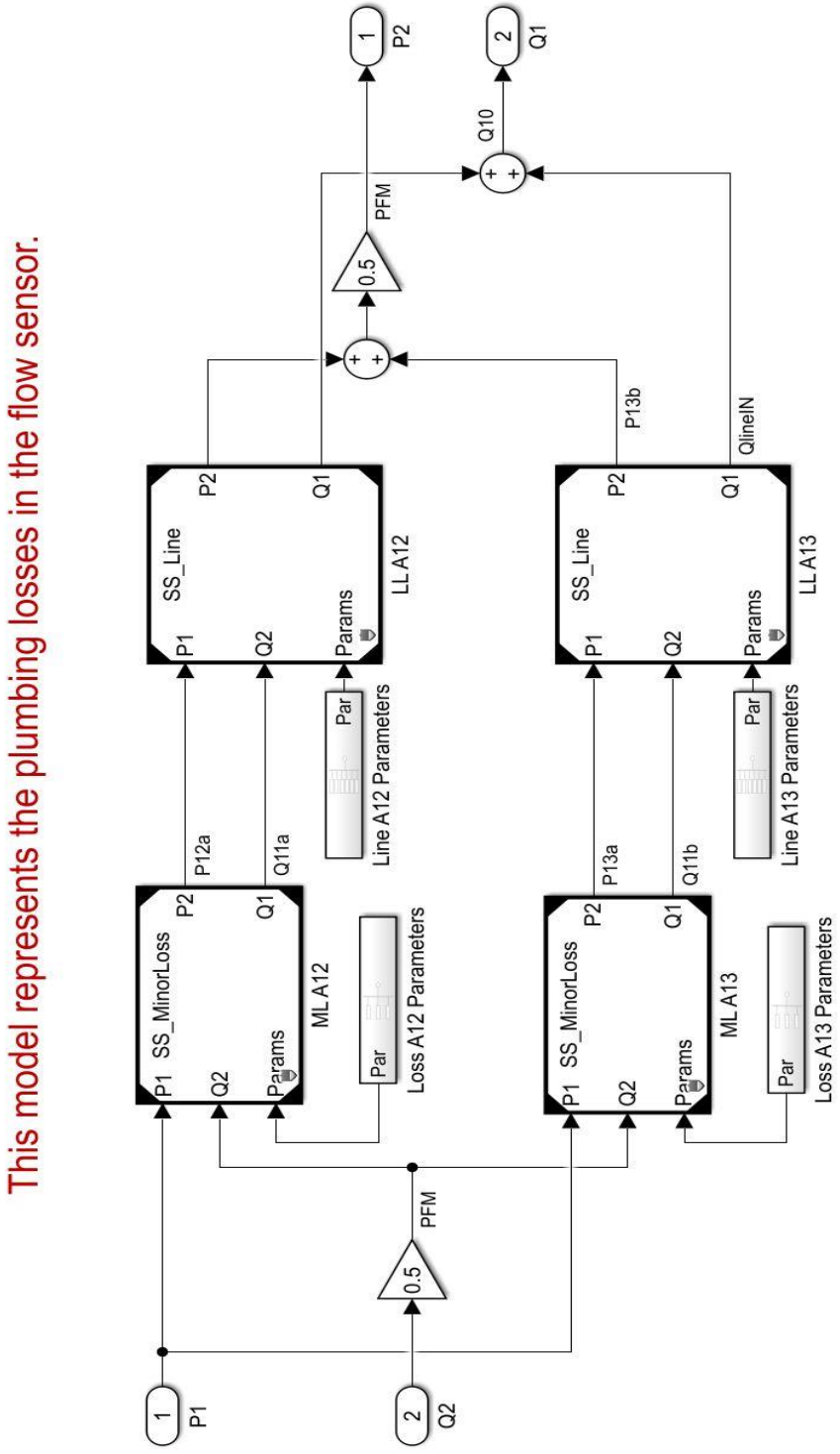

Figure G4 - Model Subsystem 3.

Engineering

Capstone Report Approval Form

Master of Science in Engineering – MSE

Milwaukee School of Engineering

This capstone report, titled "Dynamometer Testing of Hydraulic Fluids in an Axial Piston Pump Under Simulated Backhoe Loader Trenching Conditions," submitted by the student Muhammad Hassan Mansoor Malik, has been approved by the following committee:

Faculty Co-Advisor: _____ Date: _____

Dr. Subha Kumpaty, Ph.D.

Faculty Co-Advisor: _____ Date: _____

Paul Michael, B.S., M.B.A.

Faculty Member: _____ Date: _____

Gary Shimek, M.L.I.S.